Time-resolved Spectroscopy of Charge Transfer at the Interface of Nanomaterials and Porphyrins

Pınar Arpaçay

School of Physics

Trinity College Dublin

Supervisor: **Prof. Werner J. Blau**

A thesis submitted for the degree of

Doctor of Philosophy

July, 2018

Declaration of Authorship

I declare that this thesis has not been submitted as an exercise for a degree at this or any other University.

Except where otherwise stated, the work described herein has been carried out by the author alone.

I agree to deposit this thesis in the University's open access institutional repository or allow the library to do so on my behalf, subject to Irish Copyright Legislation and Trinity College Library conditions of use and acknowledgement.

I have read and I understand the plagiarism provisions in the General Regulations of the University Calendar for the current year, found at: http://www.tcd.ie/calendar.

I have also completed the Online Tutorial on avoiding plagiarism 'Ready, Steady, Write', located at http://tcd-ie.libguides.com/plagiarism/ready-steady-write.

Pınar Arpaçay

Date:

ABSTRACT

Time-resolved Spectroscopy of Charge Transfer at the Interface of Nanomaterials and Porphyrins

Pınar Arpaçay

In order to optimize performance in many light-harvesting systems such as photovoltaics and photocatalysis, a fundamental comprehension of interfacial electron transfer at the interfaces of donor (D)-acceptor (A) systems is quite important. The relevant parameters that are involved in charge transfer, charge separation, charge recombination, intersystem crossing, triplet state lifetime at porphyrin-based donor-acceptor interfaces are the main focuses in the discussions in this thesis. To investigate the charge transfer processes in various donor-acceptor systems, a combination of steady-state, time-resolved transient absorption (TA) and photoluminescence spectroscopies were used.

Furthermore, photophysical properties (absorption spectra, fluorescence spectra, singlet and triplet state lifetimes) of newly synthesized 5,10-disubstituted *push-pull* porphyrins (Am1 5,10-1 and SlpE029) and their 5,15-disubstituted isomers (Am1 5,15-1 and SlpE026) were studied in this thesis. While ground-state and excited-state properties are very similar for the Am1 5,10-1 and Am1 5,15-1 porphyrins, slight differences exist among the isomers of the SlpE029 and SlpE026. Clear correlations were also observed between the steady-state measurements and time-resolved spectroscopy results which can be explained by greater extent of intramolecular charge transfer between the D and A groups and this case was most observed in the SlpE029 porphyrin. Although the singlet state lifetime of all of the investigated porphyrins was almost the same, interestingly the longest triplet state lifetime was recorded in SlpE026 porphyrin, followed by SlpE029, and then Am1 5,15-1 and Am1 5,10-1 with the almost same triplet state lifetime. Additionally, the process of photoinduced electron transfer was investigated for the first time between methylammonium lead triiodide perovskite film and the porphyrin interface with a case study using the SlpE026 porphyrin.

Additionally, the interfacial charge transfer dynamics between two neutral porphyrins (Am1 5,15-1 and SlpE026) with different polymorph of nanocarbon (neutral fullerene, C_{60} and negatively charged graphene carboxylate, GC) were investigated using steady-state measurements and nanosecond (ns) and femtosecond (fs) TA spectroscopies. Static and a combination of static and dynamic quenching in the presence of GC and C_{60}, were studied through fs and ns-TA as well as being demonstrated by Stern-Volmer plots. Moreover, fs-TA spectroscopy revealed that both porphyrins presented strong ground state bleach corresponding to the depletion of the Soret band and excited state absorption due to presence of a long-lived triplet state. Lastly, the spectroscopic results showed that slightly changing the structure of the porphyrins from the *meso*-units does not change much the interaction with nanocarbon materials.

Keywords: Photoinduced electron transfer, charge transfer, donor-acceptor systems, photophysics, porphyrins, *push-pull* porphyrins, methylammonium lead triiodide ($MAPbI_3$) perovskite film, graphene carboxylate (GC), fullerene (C_{60}), ultrafast, time-resolved spectroscopy, solar energy conversion

DEDICATION

This thesis is dedicated to all who made the world a better place...

And also, to the all who made my world a better place:
Aynur Arpaçay, Hüseyin Arpaçay,
Selin Arpaçay Kuduğ, Fıstık
Öznur Ersever and Radiye Arpaçay…

ACKNOWLEDGEMENTS

Doing a PhD may only be known as a four-year process; however, it is very long and very tough. It has been a challenge for me, both in my academic life and personal life. Even if the author of this thesis is only one person, it is almost impossible to deny the contribution of the people who helped me to come to this stage materially and morally. Although time is categorized as past, present and future, I personally believe that everything is related to create one overall structure. It is just like the final version of this thesis and the hidden people who have made a great effort in each sentence of it.

Prof. Werner J. Blau, when looking back, I am very glad that my first email found you at the right place and time as you have become the right supervisor for me. I am very well aware that I was able to complete this thesis, because you were the first person who opened a door for me with lots of opportunities to move in further as well as your endless trust. You have lighted my way with your great science background, support and help in each moment during my PhD. While you have been changing the direction of my life in every way with your valuable contributions, you have also always been an excellent role model for me with your great personality.

Prof. Omar F. Mohammed, I believe that I have learned a tremendous amount from you in a short research time period, including how I could complete my PhD studies successfully and what steps I need to follow after my PhD. You have always been very patient while you are teaching me everything, using your great science knowledge and sharing your time generously. As well as being a well-known, successful scientist in your research area, you are also very good teacher. That's why you have become more than a supervisor to me.

Dr. Partha Maity, you have always been very helpful, smart and supportive in each step of my research journey. I have learned various aspects of science from you. My PhD thesis and paper publication process would have been more difficult without your generous effort and understanding all the time.

I would like to express my deep thanks to Prof. Mathias Senge for his valuable suggestions and his contribution to enrich my project with newly synthesized porphyrins. Many thanks also to PhD candidate Alina Meindl for her help.

Warm thanks to Dr. Emre Yengel for his help during my research.

Thanks to Science Foundation Ireland (SFI, 12/IA/1306) and King Abdullah University of Science and Technology (KAUST) Visiting Student Research Program (VSRP) for the financial supports to complete this study.

Thank you very much Helen O'Halloran for always being helpful and nice with your administrative solutions when I need.

Many thanks to my lovely friends Ayse and Afra for your help and the nice memories.

Big thanks to my dear friend Selmin Eren for her valuable support before and during my PhD journey.

My deepest and heartfelt thanks are extended to PhD candidate Sevilay Akca as you have always been very supportive and empathetic in each moment of both my academic and personal life as well as making my time in Dublin and in Trinity College more attractive and meaningful since the first day of my PhD until now. This thesis would not have been completed without your unconditional contributions which I will always remember.

Words are inadequate to express my special big thanks to my lovely family Aynur Arpaçay, Hüseyin Arpaçay, Selin Arpaçay Kuduğ as you have always supported me in every endeavour I have chosen and who I can always depend on, whatever the path I choose to go down. Thanks for making me what I am today. I would not be here without your endless love, sacrifice and motivation all the time. Finally, but not any less important, my grateful thanks are also go to my precious family members my second mother Öznur Ersever, Radiye Arpaçay with her moral support always, Güner Arpaçay Boran and Nurten Alpaslan for their contributions in my academic life and Halil Kuduğ for his support. Without them

and my parents' untiring efforts, encouragement and love, I would not have reached here on my own and this work would have only remained a dream.

Pınar Arpaçay

Dublin, July 2018

TABLE of CONTENTS

LIST of ABBREVIATIONS

A	Acceptor
α	Alpha
β	Beta
CR	Charge recombination
CS	Charge separation
CT	Charge transfer
DI	Deionized
DMSO	Dimethyl sulfoxide
D	Donor
DSSCs	Dye-sensitized solar cells
ET	Electron transfer
EU	European Union
ES	Excited state
ESA	Excited state absorption
fM	Femtomolar
fs	Femtosecond
S_1	First excited singlet state
T_1	First excited triplet state
F	Fluorophore
C_{60}	Fullerene
FWHM	Full width at half-maximum
GC	Graphene carboxylate
S_0	Ground electronic state
GS	Ground state
GSB	Ground-state bleach

HOMO	Highest occupied molecular orbital
IC	Internal conversion
PbI_2	Lead (II) iodide
LUMO	Lowest unoccupied molecular orbital
MA	Methylammonium
$MAPbI_3$	Methylammonium lead triiodide
μs	Microsecond
ns	Nanosecond
NIR	Near-infrared
DMF	N,N-dimethylformamide
NMP	N-methyl-2-pyrrolidone
PET	Photoinduced electron transfer
PL	Photoluminescence
PV	Photovoltaics
ps	Picosecond
PCE	Power-conversion efficiency
Q	Quencher
S_2	Second excited singlet state
SV	Stern-Volmer
SE	Stimulated emission
THF	Tetrahydrofuran
TRPL	Time-resolved photoluminescence
TRS	Time-resolved spectroscopy
TiO_2	Titanium oxide
TA	Transient absorption
UV-Vis	Ultraviolet-Visible
H_2O	Water

ZnTPP	Zinc tetraphenyl porphyrin
SlpE029	{5-[Bis(4-*tert*-butylphenyl)amino]-10-(4-carboxyphenylethynyl)-15,20-bis(2,6-dioctyloxyphenyl)porphyrinato}zinc(II)
SlpE026	{5-[Bis(4-*tert*-butylphenyl)amino]-15-(4-carboxyphenylethynyl)-10,20-bis(2,6-dioctyloxyphenyl)porphyrinato}zinc(II)
Am1 5,15-1	[10,20-Bis(3,5-di-*tert*-butylphenyl)-5-(4-carboxyphenylethynyl)-15-(N,N-dimethylanilinyl)porphyrinato]zinc(II)
Am1 5,10-1	[15,20-Bis(3,5-di-*tert*-butylphenyl)-5-(4-carboxyphenylethynyl)-10-(N,N-dimethylanilinyl)-porphyrinato]zinc(II)

LIST of SYMBOLS

A	Absorbance
ΔA	Absorbance change
c	Concentration
E	Energy
ν	Frequency
I	Intensity
Ø	Luminescence quantum yield
ε	Molar extinction coefficient
V_{OC}	Open-circuit voltage
OD	Optical density
d	Optical path length
h	Planck's constant
P_{in}	Power of the incident light
k_Q	Quenching rate constant
J_{SC}	Short-circuit current density
M	Spin multiplicity of an electronic state
K_{SV}	Stern-Volmer constant
S	Sum of electron spins populating
η	Sunlight-to-electric power conversion efficiency
t	Time
τ	Time constant or time delay
λ	Wavelength

LIST of FIGURES

LIST of TABLES

More than just a PhD, less than a life…

Pınar Arpaçay

CHAPTER 0: Objective and Outline of the Thesis

0.1 Objective

Understanding the charge transfer (CT) dynamics at donor (D)-acceptor (A) interfaces is important to enhancing the device performance since an efficient photovoltaics (PV) device requires fast CT and a long-lived charge separation (CS) state. Herein, ultrafast broadband time-resolved spectroscopy, which is a useful technique that provides direct information on the fundamental photovoltaic studies (charge carrier dynamics) at D-A interfaces, enabling monitoring of the evolution of CS states in D-A systems, was employed. More specifically, this work is aimed to investigate charge transfer interaction between newly synthesized *push-pull* porphyrins with different nanomaterials, such as nanocarbons (fullerene, C_{60} and graphene carboxylate, GC) and organic-inorganic hybrid halide perovskite such as methylammonium lead triiodide ($CH_3NH_3PbI_3$ or $MAPbI_3$) using steady-state measurements, time-resolved transient absorption and photoluminescence spectroscopies. In addition, this works explores the ultrafast photophysics including intersystem crossing of newly synthesized 5,10-disubstituted and 5,15-disubtituted *push-pull* porphyrins using the same spectroscopic techniques.

0.2 Outline

CT is an important process in PV devices. New nanomaterials allow flexible, easily processed devices with potentially high efficiencies, e.g. perovskites. Spectroscopy is a general technique to understand and optimise devices. It is important to cover a very wide time range to observe and quantify CT processes. With any new material system, this is necessary and my thesis provides a blueprint for what is required to test future new materials.

A detailed introduction will be given for porphyrins and photophysical processes in chapter 1 and 2, respectively in this thesis. After describing experimental details in chapter 3, a comprehensive introduction will be also given at the beginning of chapter 4 and chapter 5 to comprehend the background, perspective and aim of the studies reported, which are

photophysical characterization of newly synthesized *push-pull* porphyrins using spectroscopic techniques and a detailed research of photoinduced electron transfer in different D-A systems using the same spectroscopic techniques.

In chapter 1, an introduction into porphyrins and the materials used in the studies of this work are presented.

In chapter 2, the basis for ultrafast spectroscopies is discussed outlining and introducing the basic photophysical processes involved.

In chapter 3, materials, methods and experimental procedures for the all studies in this thesis are described in detail.

In chapter 4, photophysical characterization of newly synthesized unsymmetrically 5,15-disubstituted Am1 5,15-1 and SlpE026 *push-pull* porphyrins and their 5,10-disubstituted counterparts Am1 5,10-1 and SlpE029 *push-pull* porphyrins are explored using steady-state absorption and emission, time-resolved transient absorption and photoluminescence spectroscopies. Steady-state measurements and nanosecond (ns) transient absorption (TA) spectroscopy results indicate that the origin of the broadened and red-shifted spectral features, which are mostly observed in the SlpE029 and SlpE026 porphyrins, is likely due to the greater extent of intramolecular charge transfer between the D and A groups. Nanosecond time-resolved TA and time-resolved photoluminescence (TRPL) using a streak camera experiments indicate that the singlet state lifetime of the porphyrins is almost the same, but interestingly, the longest triplet state population is recorded in SlpE026 porphyrin, followed by SlpE029, and then Am1 5,15-1 and Am1 5,10-1 with almost the same triplet state lifetime. Moreover, to show the capability of these *push-pull* porphyrins to accept electron from $MAPbI_3$ perovskite in film phase, a case study is presented for the first time to demonstrate the process of charge transfer between the perovskite film and the porphyrin interface using steady-state emission, time-resolved transient absorption and photoluminescence spectroscopy.

In chapter 5, interfacial charge transfer between 5,15-donor-acceptor-subsituted newly synthesized porphyrin (Am1 5,15-1 and SlpE026) and nanocarbon in the form of fullerene, C_{60} and graphene carboxylate, GC is investigated using state-of-the-art femto second (fs) and ns laser spectroscopy with broadband capabilities. Steady-state photoluminescence (PL) quenching of the porphyrin indicates electron and/or energy transfer from photoexcited porphyrin to the nanocarbon. More interestingly, the Stern-Volmer plot of the PL quenching shows linear and non-linear patterns upon increasing concentration of GC and C_{60} into porphyrin, which clearly indicates static and a combination of static and dynamic quenching, respectively. Furthermore, fs-TA study reveals that the both porphyrins show strong ground state bleach (GSB) corresponding to the depletion of the Soret band and excited state absorption (ESA) due to presence of long-lived triplet state. Ultrafast electron transfer from singlet-excited porphyrin to the nanocarbon is identified by the fast bleach recovery. Rising of the excited state decay kinetics of porphyrins in the presence of GC attributes the formation time of porphyrin cation radical. Moreover, nanosecond transient absorption results illustrate, in presence of C_{60} fast recovery and decay of GSB and ESA, respectively of the porphyrins, which attributed long distance diffusion-controlled quenching process. However, no clear change for porphyrin/GC hybrids is monitored in ns-TA spectroscopy which confirms that the electron transfer here is only static nature. The results also showed that slightly changing the structure of the porphyrins from the *meso*-units does not change much the interaction with nanocarbon materials.

CHAPTER 1: Introduction to Porphyrins

1.1 Porphyrins: An Overview

The origin of the word porphyrin is derived from the Greek word porphura, which means purple colour. Porphyrins are the class of deeply coloured red or purple pigments whose molecules include a substituted aromatic macrocyclic ring comprising of four pyrole rings which is linked by four unsaturated methine groups (=CH-), and sometimes with a central metal atom.[1, 2]

Kuster first proposed the porphyrin macrocyclic structure over a century ago[3] and study in the area has risen dramatically since that time. The current series of the "Handbook of Porphyrin Science" introduced in 2010 contains 44 volumes including a total of 214 chapters[4] now and this can be shown as an indication of continuing to expand of the research in the field at a rapid pace. The award of several Nobel prizes for porphyrin-related research during the years[5], and much of the recent increase has been driven by the potential for applications in materials science & engineering[6, 7] are also the evidences to demonstrate purely scientific significance.

1.1.1 Natural Occurring Porphyrins

Porphyrins are an essential type of naturally occurring macrocyclic compounds found in biological materials, which are of vital importance for our green Earth and our red blood. They are a class of pigments and included in the earliest metabolic phenomena in the world. Porphyrins are made up of a macrocyclic ring of carbon and nitrogen atoms; one of the well-known examples is iron-containing porphyrins found as heme which is most prevalently known as components of haemoglobin, the red pigment in the blood. The other well-recognized example is the magnesium-containing reduced porphyrin (or chlorine) found in chlorophyll, the green pigment in plants. This biological substance absorbs sunlight and uses its energy to synthesize carbohydrates from carbon dioxide and water. This process is known as photosynthesis. In the light of this information, life would be impossible without porphyrins and their relative compounds and the knowledge about

these systems and their excited states is important in comprehending different kinds of biological process such as oxygen binding, catalysis, and electron transfer.[8]

1.1.2 General Structure of Porphyrin

Porphine ($C_{20}H_{14}N_4$), which forms a stable solid at room temperature, is the structure of the porphyrin parent compound as represented in Figure 1.1. According to the nomenclature suggested by IUPAC, Figure 1.2 indicates the several carbon and nitrogen positions.[9] In Figure 1.2a, the carbons of the macrocycle numerated from 1 to 20, and the four interior nitrogens are at locations 21-24. The nitrogen at locations 21 and 23 are linked to hydrogen, which project toward the interior of the macrocycle. As shown in Figure 1.2b, plenty sidearm substituents are feasible at the β and *meso* sites, however these substituents are missing in the basic porphine structure.[10]

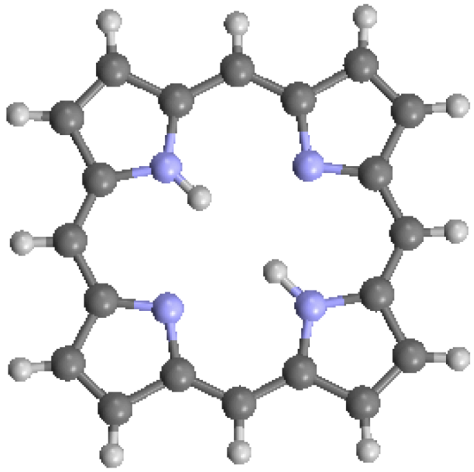

Figure 1.1: The porphine structure.[11, 12] Dark grey, light blue, and white colours are used to show carbon, nitrogen, and hydrogen atoms, respectively.

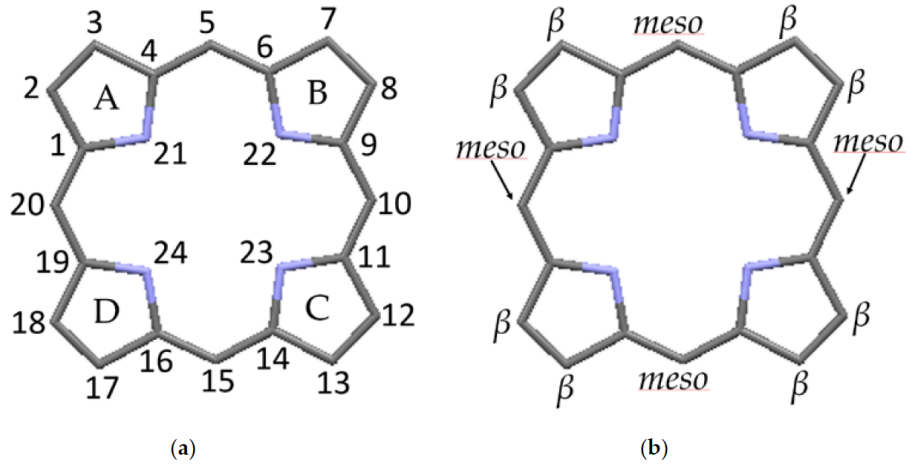

Figure 1.2: Nomenclature of macrocycle atomic locations[9]: (a) numerical demonstration, and (b) site demonstration.

The macrocyclic structure of porphyrins was first proposed by Küster in 1912, and later X-ray crystallography confirmed that porphyrins were essentially flat molecules. The porphyrin macrocycle, the chemical formula $C_{20}H_{14}N_4$, obeys Huckel's (4n+2) electrons rule (where n is a non-negative integer) and is thus an aromatic compound. The macrocycle contains 22 π electrons, but only 18 of them are included in any delocalization pathway. The six possible delocalization pathways (18 π electrons) are illustrated in bold in Figure 1.3. The other 4 non-delocalized electrons are placed on the two double bonds which are shown inside the circles at the C_4H_4NH rings (see Fig. 1.3). These two double bonds are easily oxidized or reduced utilizing several reactions because of the isolation of them from the delocalization pathway.[13]

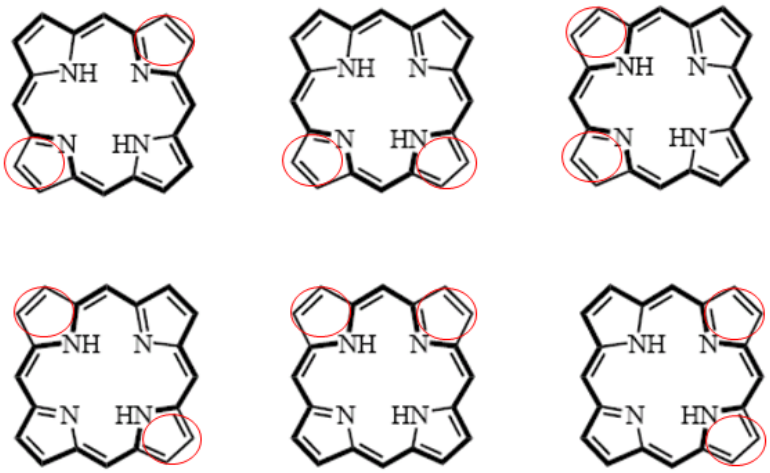

Figure 1.3: The six possible delocalization pathways of porphyrins.[14]

Porphyrins possess excellent chemical and thermal stability. Architectural flexibility is offered by their macrocyclic structure and chemical reactivity, and this makes for easy tailoring of chemical, physical and optoelectronic parameters.[15] They are versatile organic nanomaterials with a rich photochemistry and the excited state features of porphyrins can be arranged without difficulty *via* conformational design, molecular symmetry, metal complexation, orientation and strength of the molecular dipole moment, size and degree of conjugation of the π-systems, and suitable donor–acceptor substituents.[16-18]

1.1.3 Electronic Structure of Porphyrins

To answer the questions such as "Why is grass green and blood red", we need to know something about the chemical and physical features of porphyrins. We will require a knowledge of porphyrin electronic structure to comprehend those features. The electronic structure of porphyrins is based upon a skeleton of twenty carbon atoms surrounding a central core of four nitrogen atoms. A highly stable configuration of single and double bonds, named an aromatic π-system is supported by this atomic arrangement.[1]

Several types of models such as free electron theory (FET) and the cyclic polyene theory (CPT) were used to explain the electronic structures of porphyrins. However, in the 1960s, Martin Gouterman developed the four-orbital (two highest occupied π orbitals and two lowest unoccupied π^* orbitals) model that still serves as the best introduction to explain the electronic and spectroscopic properties of porphyrins.[19, 20] According to the model, the absorption bands in porphyrin macrocycles result from transitions between the two highest occupied molecular orbitals (HOMO-1, HOMO) and the two lowest unoccupied molecular orbitals (LUMO, LUMO+1). As shown in Fig. 1.4, the HOMOs are labelled as a_{1u} and a_{2u} orbitals, whereas the LUMOs are labelled as a set of degenerate e_g orbitals. Two excited states, both of ^1E_u character, occur due to the transitions from the HOMO to the LUMO. Orbital mixing splits these two excited states in energy giving rise to the two bands: Soret (B) band, and Q band. Soret band is a higher energy ^1E_u state with greater oscillator strength, while Q bands are a lower energy ^1E_u state with less oscillator strength.[8]

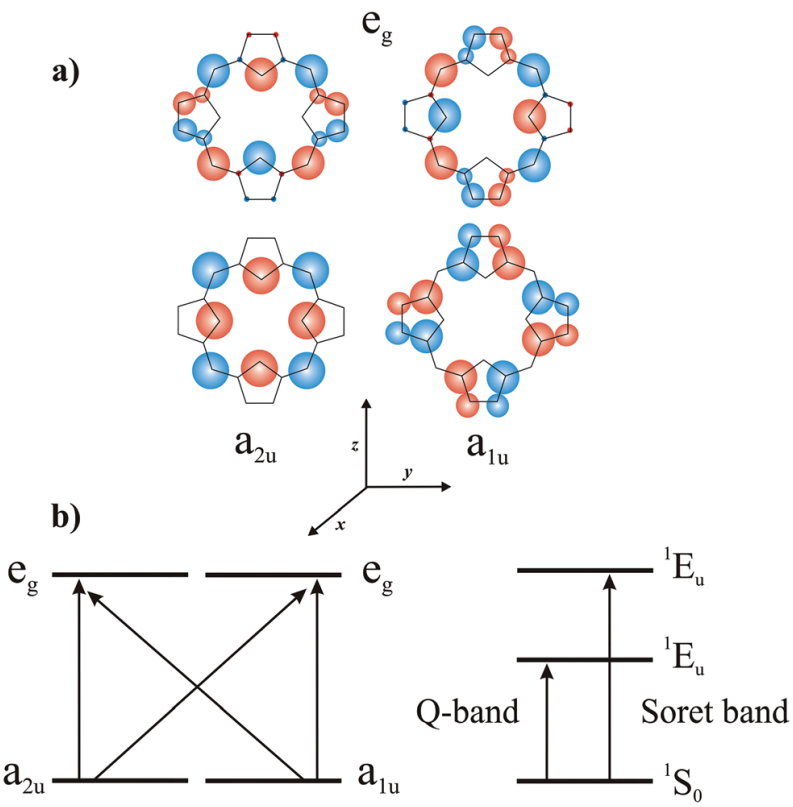

Figure 1.4: (A) The four-orbital model of Gouterman and (B) energy levels illustrating the transitions of a porphyrin system.[21]

1.1.4 Electronic Absorption Spectra of Porphyrins

It is known that porphyrins possess striking colours and strong absorption in the near ultraviolet and visible region due to the existence of highly conjugated π-electron systems in their structure.[22] An intense absorption band, called the B band or Soret band, exists in the wavelength range of 390-425 nm (depending on whether the porphyrin is β (beta)- or *meso*-substituted) and consists of the transition from the ground state to the second excited state ($S_0 \rightarrow S_2$). In the wavelength range of 480-700 nm, there is a weak transition to the first excited state ($S_0 \rightarrow S_1$), and the corresponding bonds are known as Q bands, which have between two and four weaker bands. The Soret band (B band) and Q bands both arise from $\pi \rightarrow \pi^*$ transitions. Figure 1.5 shows the typical Ultraviolet-Visible (UV-Vis) absorption spectrum of a porphyrin.[8] The number and intensity of these bands have a crucial importance in order to interpret the UV-vis spectra. By this means, it could be easy to understand the substitution pattern of the porphyrin and whether it has a metal in its centre or not.[1] Metal-free (free-base) porphyrins have four Q bands, while metalloporphyrins have two Q bands in the UV-Vis spectrum.

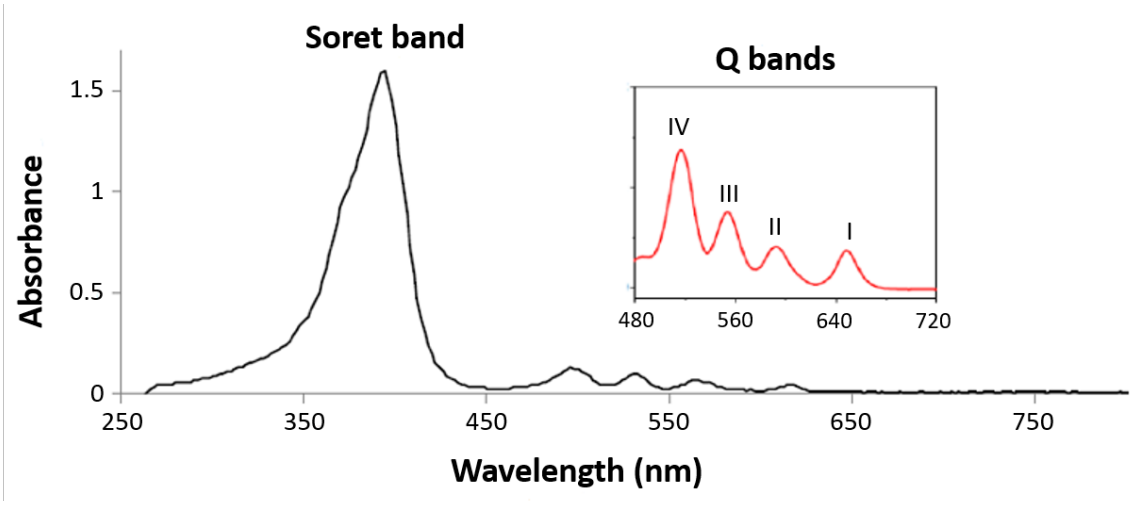

Figure 1.5: The typical UV-Vis absorption spectrum of a free-base porphyrin with showing an enlargement of Q region (modified from reference [8]).

Compared to free-base porphyrins, metalloporphyrins are more symmetrical macrocycles and there are only two bands in their Q bands spectra. These bands are known as α (alpha)- and β bands, the α band at a longer wavelength range than the β band. The relative intensities of these two bands give an idea about the stability of the metalloporphyrin.[1]

1.1.5 Porphyrins as Light Harvesters in the Dye-sensitized Solar Cell

1.1.5.1 Dye-sensitized Solar Cells

Fossil fuel depletion has been accelerated owing to the ever-increasing demand in energy supply. It is anticipated that the reserves of fossil fuels in the world can only last 40 years for oil, 60 years for natural gas and 200 years for coal.[23] The advancement of renewable energy technologies has been spurred because of the imminent depletion. For instance, a target has been agreed by the European Union (EU) that until 2030 renewable energy should account for at least 27% of EU's final energy consumption.[24] Accordingly, more than $90 billion has been invested by United State in clean energy development through the Recovery Act.[25] Photovoltaic (PV) technology is especially attractive for direct conversion of sunlight into high-quality electricity energy among all renewable energy technology. However, because of the reasons of high production and environmental costs, the existing silicon-based solar cells are restricted to the terrestrial PV market.

Dye-sensitized solar cells (DSSCs) are well known as a cost-effective photovoltaic device owing to affordable materials and easy fabrication process in comparison with high-cost conventional silicon solar cells. They are made up of titanium oxide (TiO_2) semiconductors which are generally utilized as a paint base in the pigment industry, and dye sensitizer that could be extracted from various resources with minimal expenditure. Additionally, instead of using platinum catalyst, carbonaceous materials can be preferred, by this way the material cost could be further decreased. As such, due to the fact that DSSCs are not sensitive to environment contaminants and processable at ambient temperature, they are easy to fabricate. In roll-to-roll process which is a continuous, low-cost manufacturing method to print dye-sensitized solar cells on flexible substrates, these unique properties are favoured. Moreover, the performance of DSSCs is better even during darker conditions e.g. in the dawn and dusk or in cloudy weather. DSSCs are a great choice for indoor applications such as windows and sunroof thanks to the capability of efficiently utilizing diffused light.[26]

O'Regan and Gratzel[27] initiated the seminal work on DSSCs in 1991, then the study has improved at a rapid pace and a significant number of researches have been made to increase the device efficiency from 7.1% in 1991 to 13% in 2014, a level considered as essential for commercial utilization.[28]

As can be seen in Figure 1.6, four main processes are normally taken into account in a DSSC: (i) a photon form sunlight is absorbed by the dye (sensitizer) and the sensitizer (S) is excited to an excited state. The HOMO-LUMO transition determines this process; (ii) an electron into the conduction band of the semiconductor electrode (i.e., TiO_2) is injected by excited state dye; (iii) an electron from a reducing agent present in the electrolyte (generally iodide (I) ions) is accepted by resulting oxidized dye and resulting oxidized dye goes back to the ground state; (iv) photogenerated electrons at the semiconductor anode flow via an external circuit and reach at the Pt counter electrode (cathode), and at the cathode, the oxidized redox mediator (I_3^-/I^-) is regenerated. The efficiencies of these four processes are quite critical in terms of the overall efficiency of a solar cell.[29] Based upon sunlight-to-electric power conversion efficiency (η) , the overall performance of the DSSC can be evaluated.

$$\eta = (V_{OC} J_{SC} FF/P_{in}) \times 100\% \quad \textbf{(1.1)}$$

Where V_{OC} is the open-circuit voltage (V), J_{SC} is the short-circuit current density (mA cm^{-2}), FF is the fill factor, and P_{in} is the power of the incident light.[26]

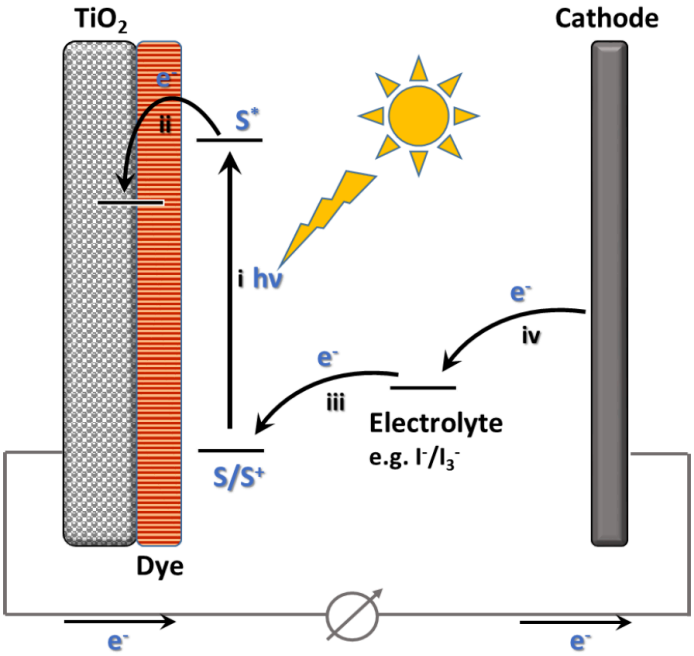

Figure 1.6: Schematic diagram of a dye-sensitized solar cell.[29]

1.1.5.2 Porphyrins as Dyes for DSSCs

The electron transfer reactions occurring at the photosynthetic reaction center of several bacteria and plants has a remarkable similarity to the electron transfer reactions occurring inside a DSSC device.[30, 31] When solar energy is captured by plants and bacteria, they can convert the solar energy efficiently into chemical energy by chromophores based upon porphyrins. Porphyrins are attractive candidates as light harvesters on a semiconductor, due to the primary role of them in photosynthesis.[32] Thanks to characteristic structural and photophysical features of porphyrins, they are well suited for adaptation into artificial designs, not only for solar energy conversion but also for applications in photodynamic therapy[33-38], enzyme mimics[39-41], catalysis[42-46], and molecular electronics devices[47, 48]. To develop highly efficient light harvesters, porphyrins have a great potential owing to their number of properties such as unusual high molar extinction coefficients (ε, ~ $4x10^5$), and multiple absorptions (Soret and Q bands) in the range of 400-

800 nm (the attractiveness of porphyrins in solar conversion schemes becomes obvious, because these bands result in the absorption of visible photons), as well as high thermostability that distinguish them from other organic/inorganic sensitizers.[49-51]

Moreover, the emission wavelengths of a given porphyrin may align with its Q-band absorption, by this way the spectral overlap which is needed for efficient energy migration is provided.[51]

Porphyrins have been used as sensitizers for DSSCs since 1993.[52] In spite of positive characteristics of porphyrins, the overall performance of ruthenium polypyridyl dyes had been much better than the overall performance of porphyrins (η<7.2%) until very recently. A solar to electricity conversion efficiency of 11% was demonstrated for a porphyrin possessing donor-acceptor properties installed at the porphyrin *meso*-positions via an ethynyl bridge in 2010.[53] Since that day, numerous DSSCs based upon *push-pull* porphyrins have been reported and a record high efficiency (η= ~13%) has been succeeded with *push-pull* porphyrins.[28]

1.1.5.2.1 *Push-Pull* Porphyrins

Push-pull chromophores having both an electron-donating group(s) (*push*) and an electron-withdrawing group(s) (*pull*) on their periphery have been the subject of intensive study for decades due to their feasible applications in organic electronics, opto-electronics and photonics.[50, 54-61] They are made up of an electron donor(s), an electron acceptor(s), and a conjugated bridge linking the donor(s) (D) and acceptor(s) (A) (D-π-A). Each component in D-π-A system is quite critical in tuning the HOMO-LUMO gap of the compounds, modulating their inter- and intra-molecular charge transfer (CT) and charge recombination (CR) features, as well as their nonlinear optical characteristics. To construct D-π-A systems, porphyrins have been broadly utilized as π-conjugated bridges. The first *push-pull* porphyrins were reported in 1992[62] by Suslick, Meredith and coworkers, and since that time a lot of effort has been made to design, synthesize and study them. For further functional group modification, porphyrins have four *meso*-positions and eight β-positions available. The functionalization of *push-pull* porphyrins is mostly done at the *meso*-

positions.[50, 54, 56, 57, 61] Due to the lack of suitable functionalization methods, functionalization at β-positions is harder. Until 2016, only three *push-pull* porphyrins carrying both a D and A group(s) at the porphyrin β-positions had been reported.[63-65] Several studies have also been made about the mix-functionalized *push-pull* porphyrins at both the *meso*- and β-positions.[66-68]

A significantly different effect on the electronic and optical characteristics of the porphyrins can be expected with substitution at different positions of the porphyrin and their substitution pattern owing to the different electron density and geometry at different positions.[29]

Several synthetic strategies are feasible; the classic being mixed condensations, which can result in different isomers.[69] Total synthesis[70-72], organolithium reactions or transition-metal-catalyzed coupling reactions are the other strategic methods.[73-76] By using these methods, stepwise functionalization of the porphyrin is enabled and nearly any *meso*-substitued porphyrin can be formed for studies on *push-pull* porphyrins.[77] *Meso*-substitued porphyrins possess the advantage of easy preparation and in light of the continuing improvement in synthetic porphyrin chemistry, they offer a suitable entry into industrially utilizable materials.[15] Strong intramolecular dipole moment is present in *meso*-substitued *push-pull* porphyrins, because electrons are transferred from an electron-donating group through a π-spacer to and electron-withdrawing group and different dipole moment orientations in them are exhibited in Figure 1.7. In this thesis, a dipole running along the *meso-meso* axis and β-β axis will be studied.

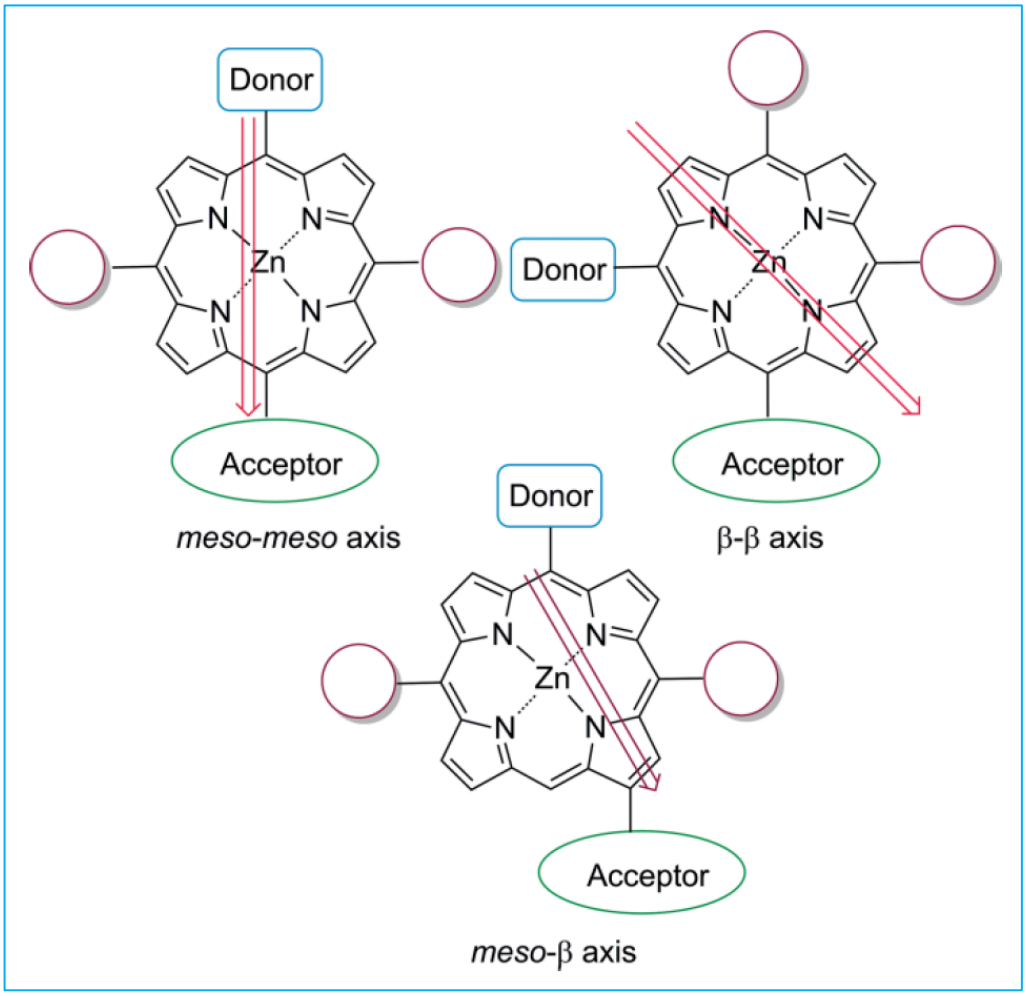

Figure 1.7: Three varied dipole moment orientations in *push-pull* porphyrins.[77]

1.1.5.3 Substrates

1.1.5.3.1 Methylammonium Lead Triiodide Perovskite

The emergence of solar cells based upon hybrid organic-inorganic perovskite materials is the most remarkable scientific milestone in photovoltaics in the last several years. Hybrid perovskite solar cells have already achieved a certified 22.1% power-conversion efficiency (PCE)[78, 79], matching conventional solar cell technologies in only a couple of years since their first device architecture was tested, as conventional silicon and thin-film solar cells have seen steady progresses in their PCEs spanning a few decades.[80] Winning the combination of characteristics of hybrid perovskite materials, by this way they can be able to set the stage for a disruptive technology in the area of photovoltaics: (i) high absorption coefficient and a tunable energy band gap in wavelengths ideal for solar cells, (ii) long diffusion lengths and lifetimes for photogenerated charge carriers, which readily separate into efficiently collected electrons and holes, (iii) Earth-abundant elemental composition,

and (iv) their compatibility with low-cost and low-temperature fabrication methods.[81-84]

Methylammonium lead triiodide perovskite materials have the general formula of ABX_3, where A: Methylammonium (MA) cation, B: lead (Pb) di-cation, and X: iodide (I); this is named as MA lead triiodide perovskite (see Figure 1.8). The band structure of these materials is made up of a conduction band consists of lead p orbitals, while the valence band dominated by ioide p orbitals, the optical transitions being from p-to-p orbitals.[85]

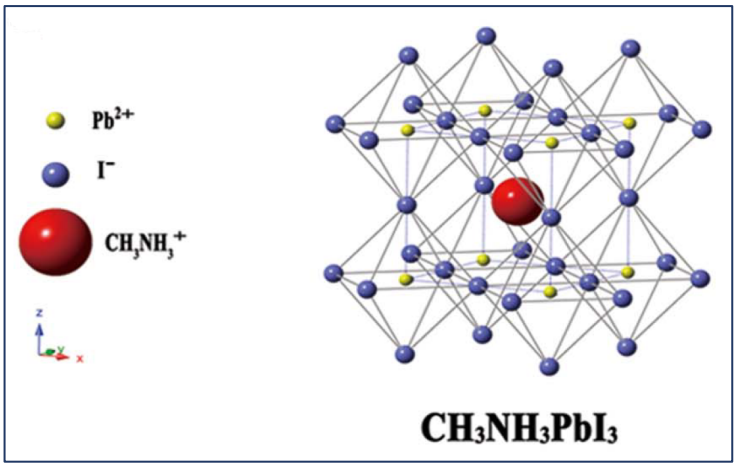

Figure 1.8: The crystal structure of methylammonium lead triiodide perovskite.[86]

A panchromatic absorption down to ca. 800 nm, direct bandgap of 1.57 eV, large absorption coefficient of 1.5 x 10^4 cm^{-1} at 550 nm[87], low exciton binding energy (<10 meV)[88], very high charge-carrier mobility (66 cm^2/Vs)[88], ambipolar charge transport[82], large electron and hole diffusion lengths (over 1 μm and potentially over 100 μm)[89], and low nonradiative recombination rates are the properties of MA lead triiodide ($CH_3NH_3PbI_3$) perovskite material.[90]

One-step solution coating[91, 92], sequential deposition[93], vapour phase deposition or any combination thereof[94] are the several techniques which have been developed for preparing methylammonium lead triiodide perovskite ($MAPbI_3$) perovskite thin films so far. Among these, as one-step solution relies on affordable deposition equipment and is versatile on controlling the deposition conditions and the composition of perovskite materials[95, 96], one-step solution coating (see Fig. 1.9) is relatively favourable. In this

thesis, to prepare the $MAPbI_3$ films, one-step precursor deposition will be used.

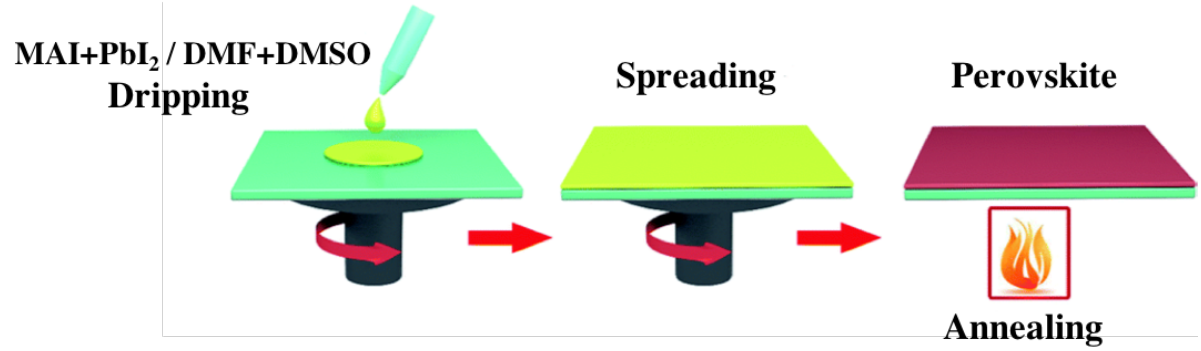

Figure 1.9: One-step precursor deposition method for perovskite film preparation.[97]

1.1.5.3.2 Fullerene (C_{60})

One of the most exciting nanocarbon materials is fullerene. Due to interesting physical, chemical and optoelectronic characteristics of fullerene, it has been extensively studied and has been used in several areas including device fabrication and drug delivery[98-100]. Before the discovery of fullerene, graphite and diamond occurring of extended networks of sp^3- and sp^2-hybridized carbon atoms, respectively presented the only know allotropes of carbon for a long time. The scenario was changed by Kroto et al.[101] with the discovery of functional molecule fullerene C_{60} in 1985, and it was marked the beginning of new period of synthetic carbon allotropes. The improvement of synthetic carbons then was in progress until 1991[102] with successful production of carbon nanotubes and rediscovery of graphene in 2004.[103] Although Canadian physicist Philip Russel Wallace[104] first explored the theory of graphene in 1947 as a first step to understand the electronic characteristics of 3D graphite, experimental discovery of graphene was done by Andre Geim and Konstantin Novoselov in 2004[103].

Zero-dimensional fullerene has been widely investigated nanomaterial in carbon family. The smallest, stable and most prominent molecular carbon allotropes which are made up of a spherical network of sixty structurally equivalent sp^2- hybridized carbon atoms in a cage lattice (diameter ~ 0.8 nm) in the shape of a soccer ball (see Figure 1.10) is fullerene C_{60}. It is consisted of 12 pentagons and 20 hexagons with alternative single and double bonds and has truncated icosahedron symmetry, I_h. Moreover, the curvature induced by

the cage structure rises the energy associated with the double bonds increasing the reactivity of the molecule. This makes fullerenes stable but not completely unreactive. To form the closed sphere, which produces angle strain, the sp^2-hybridized carbon atoms, which are at their energy minimum in planar graphite, must be bent. Electrophilic addition at 6,6-double bonds, which decreases angle strain by changing sp^2-hybridized carbons into sp^3-hybridized ones is the characteristic reaction of fullerenes. The electron accepting behaviour of fullerene C_{60}, i.e., it is an electron deficient molecule because of the existence of energetically unfavourable double bond in pentagonal rings is one of the most intriguing properties of it.[105] Molecular complexes of fullerenes with organic donors (such as porphyrins, phthalocyanines, pentacene) can be used in organic optoelectronic devices, e.g. as artificial photosynthesis systems and solar cells.[106-108] Fullerene-based structures can be important for the study of photoinduced electron transfer (PET) due to the fact that fullerene is an acceptor with strong π-electron accepting ability. Synthesis of dyad molecules with C_{60} covalently bonded to porphyrin[109] and developing the self-assembled non-covalent complexes[107, 110] are two basic approaches to the formation of such systems.

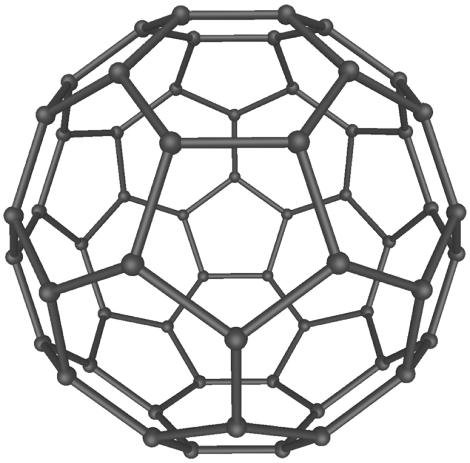

Figure 1.10: The molecular structure of C_{60}.

Porphyrins and fullerenes systems have been considered as one of the comprehensively organic donor-acceptor pairs investigated.[111-114] As a noncovalent complex, a zinc tetraphenyl porphyrin (ZnTPP) was linked to a C_{60} derivative via axial pyridine coordination to the metal for using as donor-acceptor systems in the literature.[115-119] Optical spectroscopy revealed that photoexcitation of the Zn-complex led to electron

transfer with very long lifetimes of the charge-separated pairs and this result was also supported by time-resolved electron paramagnetic resonance spectroscopy.[120]

In an another study in the literature, Sugunan et al.[121] examined the spectroscopy and dynamic behaviour of the self-assembled, Soret-excited zinc tetraphenylporphyrin (ZnTPP) plus fullerene (C_{60}) model system in solution using several spectroscopic techniques. Clear evidence of ultrafast quenching of the locally S_2-excited state of ZnTPP in the ZnTPP $\cdots$ C_{60} complex has been obtained from both steady-state and ps transient absorption measurements, despite the unavoidable complication of simultaneous excitation of uncomplexed and complexed ZnTPP in the experiments. Electron transfer in the excited complex as well as short-range electronic energy transfer have been also evaluated.

Recently, Stangel et al.[122] published a case study for artificial photosynthesis using C_{60} fullerene. To build an electron donor/acceptor (C_{60}-dipyr·ZnP_2), a new modified C_{60} derivative with an oPE/oPPV conjugated bridge bearing two pyridyl groups has been used in combination with a flexible porphyrin dimer (ZnP_2). Detailed photophysical experiments have been accomplished in order to explore the interactions between the electron donor and acceptor entities, both in the ground state and in the excited states. Especially, strong interactions between the electron donor and the electron acceptor within the hybrid have been confirmed by both absorption and fluorescence titrations. Moreover, intramolecular electron-transfer from the photoexcited porphyrin dimer (ZnP_2) to the fullerene derivative (C_{60}-dipyr), leading to a long-lived charge-separated state has been revealed by transient absorption measurements.

1.1.5.3.3 Graphene

We end up with a two-dimensional carbon structure, namely graphene, if we increase the dimensionality of nanocarbon even further. A zero-band-gap semiconductor characteristic of it makes graphene a rising star in materials science. It is made up of a honeycomb lattice of sp^2-hybridized carbon (see Figure 1.11) and since the first experimental evidence of the electronic properties of graphene in 2004[103], the studies revealed that it is very strong material as well as becoming atomically thin[123-126]. Remarkable electronic and

mechanical features and a considerable number of new optical effects make graphene unique compared with other materials[127, 128]. Its considerable high carrier mobility, broad absorption spectral range, and high optical transparency signify graphene as an economical and plentiful material that enables to use especially in solar cell applications as well as displays and light emitting diodes in optoelectronic devices[129-132]. Different approaches are possible to prepare graphene such as micromechanical[103] or chemical exfoliation of graphite[133], chemical vapour deposition (CVD) growth[134-136], and chemical, electrochemical, thermal, or photocatalytic reduction of graphene oxide and fluorographene[137-140]. In this thesis, negatively charged graphene carboxylate (GC) will be used.

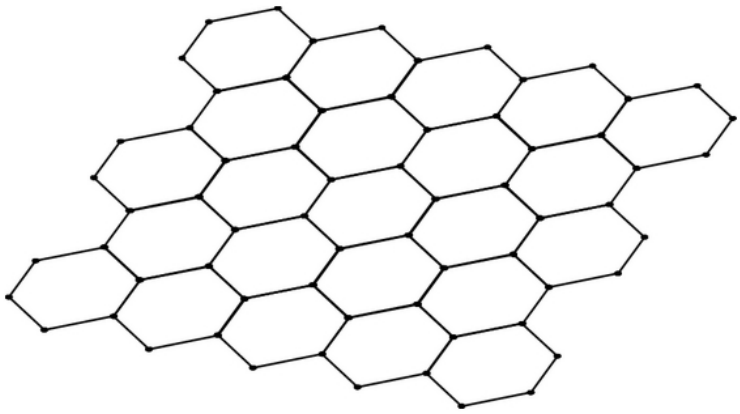

Figure 1.11: The molecular structure of graphene.[141]

The addition of photosensitizing molecules, e.g. porphyrins, phthalocyanines, etc., establishes electron donor-acceptor systems based upon graphene. Thus, the electronic interaction is either only in the excited state, or both in the ground state and excited state. Radical ion pair states occur in the excited state including in the radical cation of the electron donating phthalocyanines and/or porphyrins and electrons that are delocalized within the basal plane of graphene.[142] In point of fact, to afford functional nanographene based charge-transfer hybrids, aromatic macrocycles are highly versatile.[143-145] Like in the case of fullerene C_{60}, synthesis of dyad molecules with graphene covalently bonded to porphyrin[146] and developing the self-assembled non-covalent complexes[142] are two basic approaches to the formation of such systems.

Porphyrins and graphene systems have been also considered as organic donor-acceptor systems in the literature. Aly et al.[147] reported a study to help advancing the comprehension of GC interfaces for electronic and solar energy applications in 2014. Accordingly, three free-base porphyrin structures (5,10,15,20-tetra(4-pyridyl)-porphyrin (TPyP), 5,10,15,20-tetra(1-methyl-4-pyridino)porphyrin tetra(p-toluenesulfonate) (TMPyP) and 5,10,15,20-tetra(4-trimethylammoniophenyl)porphyrin tetra(p-toluenesulfonate) (TMAP)) with different charge localization of the *meso* unit and different redox properties of the porphyrin cavity were selected carefully to comprehend the ultrafast electron injection event at the GC-porphyrin interface from the molecular structure point of view. Then, the results demonstrated that charge transfer (CT) process can be tuned from zero to very efficient and ultrafast by changing the electronic structure of the porphyrin-*meso* unit with using steady-state absorption and fluorescence spectra, Raman spectroscopy, time-correlated single photon counting (TCSPC) and femtosecond (fs) transient absorption (TA) and fs fluorescence upconversion data. More specifically, their results showed that only positively charged porphyrin can approach closer after molecular flattening on the GC surface for ultrafast electron injection.

The same research group completed another work[148] in 2015 extending their study to non-covalent interaction between the metalated porphyrin meso tetrakis(4-N-methylpyridyl) zinc porphyrin (ZnTMPyP) and negatively charged GC. Here, the ultrafast electron transfer (ET) between the porphyrin and the GC using state-of-the-art femtosecond laser spectroscopy with broadband capabilities was presented. Other spectroscopic techniques were also utilized. Steady-state absorption and emission measurements confirmed ground-state complex formation. The high binding affinity between the porphyrin and GC via electrostatic and π-π stacking interactions and rotations of methylpyridinium moieties toward a coplanar conformation were revealed by absorption spectra changes. Due to the ET from the excited porphyrin to GC, the emission of the porphyrin was quenched by GC and it was demonstrated that the quenching mechanism was in the static nature based on the modified Stern-Volmer (SV) plot. Additionally, with the help of ultrafast TA spectroscopy it was clearly presented that excited state absorption (ESA) decayed rapidly in ps time scales attributed to ultrafast electron injection from the

excited ZnTMPyP* to GC, as indicated by the formation of a porphyrin radical cation.

The same research group continued their research with a new publication[149] in the same year (2015) using β-cyclodextrin (β-CD) as an external cage to control carefully of the charge localization on the 5,10,15,20-tetra-(1-methyl-4-pyridino)porphyrin (TMPyP) macrocycle. By this way, they were able to enhance electron injection efficiency from cationic TMPyP to negatively charged GC by 120% compared to TMPyP alone. Here, β-CD not only block intramolecular charge transfer between the macrocycle and the *meso* substituents of the porphyrin, but also restricts free pyridinium rotation. As a result, electron density is localized on the cavity of the porphyrin and its oxidation potential is decreased and also the ability to donate electrons to GC is increased. Interestingly, the interaction between TMPyP and GC is the mixed dynamic static mechanism, however the interaction of TMPyP- β-CD with graphene carboxylate is an efficient static mechanism as indicated by steady-state and TA spectroscopy measurements.

An introduction to the porphyrin molecules investigated (*push-pull* porphyrins) and the substrates ($MAPbI_3$ perovskite, C_{60} and GC) used to facilitate or observe CT behaviour are described in this chapter so far. The photophysical processes, their timescales and how these processes can be observed in action through the use of time-resolved spectroscopies containing combinations of steady-state and pump-probe techniques will be discussed in detail in chapter 2.

CHAPTER 2: Introduction to Photophysical Processes

2.1 Photophysical Processes: An Overview

The impact of energy in the form of photons on materials is investigated with photophysics. Physical changes such as absorption, momentum transfer and emission of electromagnetic energy result, without chemical change, when photons interact with matter.[150]

The photophysical processes found in electronically excited organic molecules include transitions from one state to another state via radiative and non-radiative transitions. The interaction of organic molecules with light is normally represented with a Jablonski diagram. As showed in Figure 2.1, a Jablonski energy diagram illustrates the essential electronic transitions included in the absorption and emission of light by a fluorophore after photoexcitation of the molecule.[151] In the Jablonski diagram, the ground electronic state (S_0), first excited singlet state (S_1), second excited singlet state (S_2), and first excited triplet state (T_1) are taken to be the most significant energy states. An electron is promoted from the highest occupied molecular orbital (HOMO) to the lowest unoccupied molecular orbital (LUMO), due to the electronic excitation by a photon of light. The electrons in the molecule have their spins paired in the singlet states, while one set of electron spins will be unpaired in the triplet states. The vibration levels of each electronic state are indicated by the horizontal lines. Although retaining the same electronic configuration, the vibrational levels originate due to a molecule in a given electronic structure state absorbing small increments of energy equalling to changes in vibrational modes.[152] Complete arrows show radiative transitions, while non-radiative transitions are demonstrated with dashed arrows. Several different pathways in the Jablonski energy diagram such as absorbance, vibrational relaxation & internal conversion, fluorescence, phosphorescence & intersystem crossing, and delayed fluorescence show how an electron could absorb and then dissipate photon energy of a certain wavelength, which will be described in detail below.

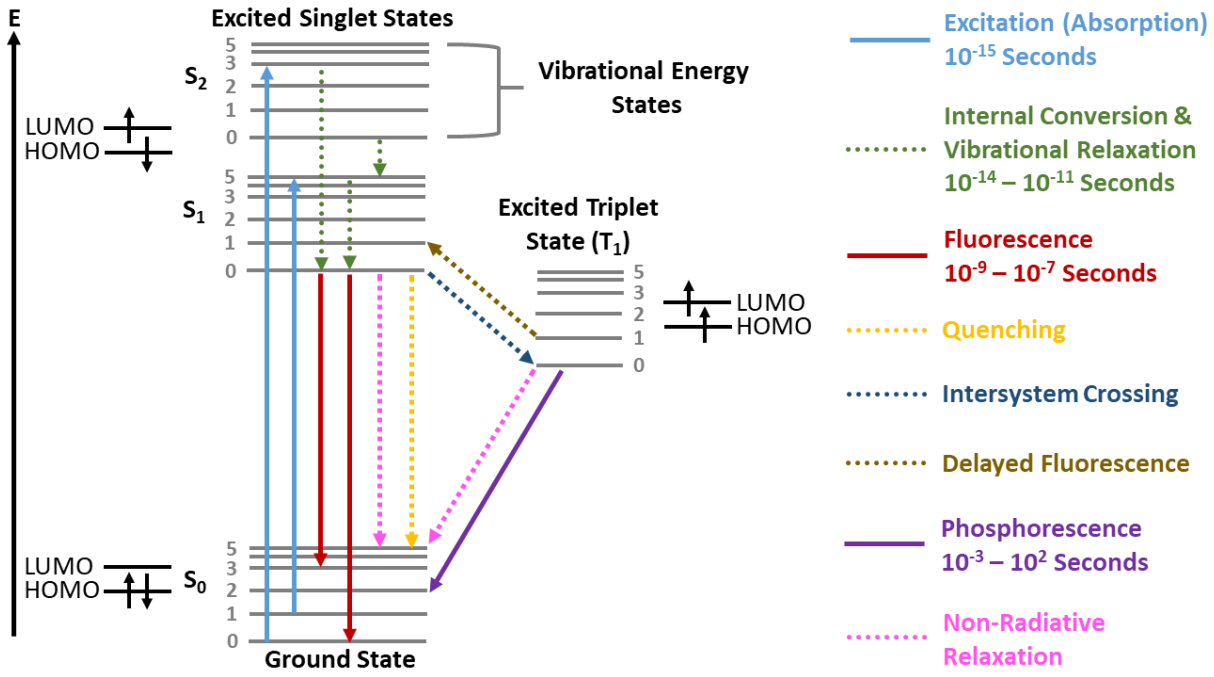

Figure 2.1: An illustration of Jablonski energy diagram.

2.1.1 Absorbance

As indicated by a straight arrow pointing up in Fig. 2.1, the absorption of a photon of a particular energy by the molecule of interest is the first transition in the Jablonski diagram. An electron is excited from a lower energy level to a higher energy level in the absorption process, firstly the energy of the incident photon is transferred to the electron, secondly this is followed by the transition of that electron to an unexcited eigenstate whose difference in energy equals to the amount of energy transferred. Absorption of light is possible only at particular wavelengths, for example those which imply a photon energy equal to that of an electronic transition. These transitions occur on the order of 10^{-15} seconds.[151, 153] As the transition is very fast, no chemical process can compete with it. The absorption process only covers the electrons movement. Electronic transitions occur faster than nuclear motion, according to the Condon approximation. These transitions are then of vibronic nature.[154] It means that when the geometries of the initial and final states are identical, electronic transitions are most favourable.

The energy (E) of photons absorbed is corresponded by the energy difference between the excited state (ES) and ground state (GS) and the relationship is shown with Equation 2.1

below. In the equation, h represents the Planck's constant and frequency of the absorbed photon is illustrated with ν.

$$E_{ES} - E_{GS} = h\nu \quad \textbf{(2.1)}$$

Lambert-Beer Law explains the light absorption by materials, as shown in Equation 2.2.[155] According to the formula, Absorbance (A) or optical density (OD) is linearly dependent on the concentration (c) and the optical pathlength of the beam of light through the sample (d). The efficiency of light absorption is expressed by the molar absorptivity (ε) which depends mainly on the intrinsic characteristics of the molecules.

$$A = \log (I_0/I) = \varepsilon dc \quad \textbf{(2.2)}$$

In Equation 2.2, I_0 represents the intensity of the incident light and I show the intensity of the transmitted light.

Absorption and subsequent luminescence such as reflection, scattering, diffraction or refraction can be dramatically affected by other types of light-matter interactions.

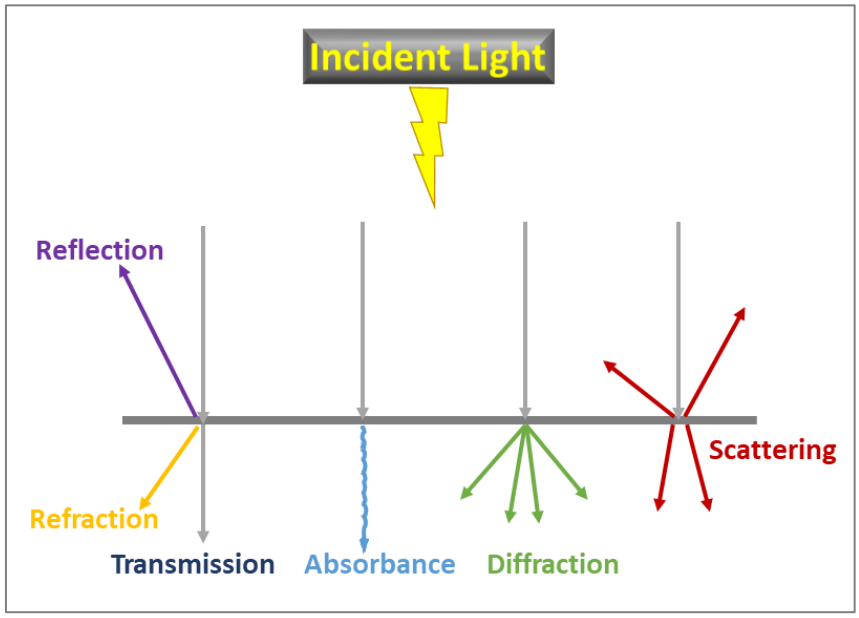

Figure 2.2: A schematic representation of light-matter interaction.

Normally, an electron is promoted from an occupied molecular orbital (usually a non-bonding (or lone pairs) n or bonding π orbital) to an unoccupied molecular orbital (an antibonding π^* or σ^* orbital) by absorption of light. As shown in Eq. 2.1, the energy needed for electron transition depends on the molecular orbitals included and these are listed in order of increasing energy below:

$$n\rightarrow\pi^* < \pi\rightarrow\pi^* < n\rightarrow\sigma^* < \sigma\rightarrow\sigma^*$$

$\sigma\rightarrow\sigma^*$ (in saturated hydrocarbons such as methane, ethane etc.) and $n\rightarrow\sigma^*$ (in saturated compounds which containing one hetero atom has unshared pair electron e.g. alcohols and ethers) transitions occur in the far ultraviolet region or weakly in the region between 180 nm and 240 nm and these transitions need a great deal of energy. $\pi\rightarrow\pi^*$ and $n\rightarrow\pi^*$ transitions require less energy and occur at longer wavelength than transitions to σ^* orbitals as these two types of transitions occur in molecules with unsaturated centres and thus these transitions are high relevance for spectroscopic applications.[156]

If the spin multiplicity stays unaltered, electron transitions are dipole allowed and the relative equation is illustrated below:

$$M = 2\left|S\right| + 1 \qquad \textbf{(2.3)}$$

M represents spin multiplicity of an electronic state and sum of electron spins or total spin populating that is exhibited with *S* in Eq. 2.3.

As a result, singlet-singlet and triplet-triplet transitions are both dipole-allowed, however singlet-triplet and triplet-singlet transitions are quantum mechanically forbidden and dipole-forbidden.[157] Because of the forbidden and thus highly improbable transitions, there is no arrow indicating a transition from the ground state to the triplet state in the Jablonski diagram in Fig. 2.1.

2.1.2 Vibrational Relaxation and Internal Conversion

Photon absorption occurs on the timescale of 10^{-15} seconds. Energy may be dissipated in several ways, after the excitation of an electron. Vibrational relaxation is the first one through a non-radiative process in the Jablonski diagram. As it was in the S_0, immediately after excitation a molecule has the same geometry and is in the same environment. Two processes can happen in this case: (i) a photon emission from the same vibrational level to which it was excited at first, and (ii) changes in vibrational levels just before a radiative emission. Depending on the environment of the molecule, one of these two things will be dominant. Thermal relaxation of a vibrationally excited molecule is pretty fast thanks to transfer of excess vibrational energy from the solute molecule to the solvent in a solution. This efficient process where all the excess vibrational energy of the excited state is lost occurs in 10^{-14} to 10^{-11} seconds. It means that an excited molecule in a solution will undergo vibrational relaxation, before it can emit a photon, and consequently photon emission will always occur from the lowest vibrational level of an excited state.

If a molecule is excited to the second excited singlet state, the molecule will undergo vibrational relaxation as described above. The destiny of the molecule as it arrives into the zeroth vibrational level of second excited singlet state depends on the energy separation between the excited singlet states. Internal conversion (IC) can occur when the lowest vibrational level of S_2 overlaps with higher vibrational levels of the S_1 state, that do not include large variations in configuration from the lowest vibrational level of the S_1 state. As a consequence, an extremely effective path for crossing from the S_2 state to the S_1 state is provided, because of a high degree of coupling between the vibrational levels of the S_2 and S_1 states. This efficient process occurs in 10^{-14} to 10^{-11} seconds.[152]

2.1.3 Fluorescence

Photon emission is an alternative pathway for molecules to deal with energy gained from photons. This is referred to as fluorescence and is indicated by a solid line going down on the energy axis between electronic states in the Jablonski diagram. A molecule is metastable, when it finally reaches the lowest vibrational level of the S_1 electronic state after ~ 10^{-12} seconds and generally stays there for at most 10^{-8} seconds (it can be more, depending on

the molecular species) or less (depending on the rate constants of de-excitation through all the other available pathways for de-excitation). Fluorescence is emitted from this state. Depending on the environment of the chromophore, the existence of dynamic quenching, or energy transfer, fluorescence normally occurs in 10^{-9} and 10^{-7} seconds. Fluorescence is a spin-allowed process which obeys the dipole selection rule $\Delta S=0$. A molecule comes back to one of many different higher vibrational levels of the S_0 state if it fluoresces. Thus, the excitation photons have a higher energy than an emitted photon; this is named as the Stokes shift. This is the main reason why the fluorescence spectrum is "red-shifted" relative to the absorption spectrum, although the transitions are both between the S_0 and S_1 states.[158]

2.1.4 Phosphorescence and Intersystem Crossing

A more effective process exists for population of triplet states from the lowest excited singlet state in many molecules, even though population of triplet states by direct absorption from the ground state is improbable. This process is known as a spin-dependent internal conversion and it is known as intersystem crossing. One may be startled that a singlet-triplet transitions e.g. intersystem crossing can take place within the lifetime of an excited singlet state (10^{-8} seconds), as singlet-triplet transitions are normally less probable than singlet-singlet transitions. Vibrational coupling between the excited singlet state and triplet state is included in the mechanism for intersystem crossing. Singlet-singlet transitions are more probable than singlet-triplet transitions by a factor of 10^{+5} to 10^{+6}, and the non-radiative vibrational process e.g. internal conversion take place in ~ 10^{-13} seconds, the time needed for a spin-forbidden vibrational process would be ~ 10^{-8} to 10^{-7} seconds and this is the identical order of magnitude as the lifetime of an excited singlet state. Thus, intersystem crossing could compete with photon emission from the lowest vibrational level of an excited singlet state, however could not compete with vibrational deactivation from higher vibrational level of a singlet state.

Molecules undergo the standard internal conversion process within the time window of 10^{-13} to 10^{-11} seconds when intersystem crossing has occurred and drops to the lowest vibrational level of the triplet state. Repopulation of a singlet state from a triplet state is pretty much improbable, as thermal energy is small compared to the variation in energy

between the lowest vibrational level of the triplet state and the zeroth vibrational level of the lowest excited singlet state. To improve tendency of a non-radiative transition between the lowest triplet state and the ground state, there are two elements: (i) the energy variation between the lowest singlet state and the ground state is bigger than the variation between the triplet state and the ground state. This can improve vibrational coupling between these two energy states, and thus, this also tends to improve internal conversion. (ii) More importantly, loss of excitation energy by collisional transfer is normally improved, because of the lifetime of a triplet state is much longer than that of an excited singlet state (~ 10^{-4} to 10 seconds). The second process is frequently the effective pathway for the loss of triplet state excitation energy and is significant in solution at room temperature.

A radiative transition between the zeroth triplet state and the ground state is observed if a molecule is put in a rigid environment where collisional processes are reduced. This emission process is named as phosphorescence. Effective spin-orbit coupling is enabled by using organometallic heavy-metal complexes and in this way, phosphorescence can be favoured. Phosphorescence will have a decay time almost equal to the lifetime of the triplet state (~ 10^{-4} to 10 seconds), as it originates from the lowest triplet state. Thus, an afterglow (with durations of fractions of a second up to hours) which is not monitored for in fluorescence (the glow of fluorescence stops right after the source of excitatory radiations is switched off) frequently characterizes phosphorescence.[152, 159, 160]

Phosphorescence represents longer lifetimes than fluorescence. The variation between the lifetimes of the fluorescence and phosphorescence is linked with the reality which it includes a spin-forbidden electronic transition. As displayed in Figure 2.3, compared with the fluorescence bands, phosphorescence bands are always red-shifted, due to the relative stability of the triplet state in comparison with the singlet manifold.[161]

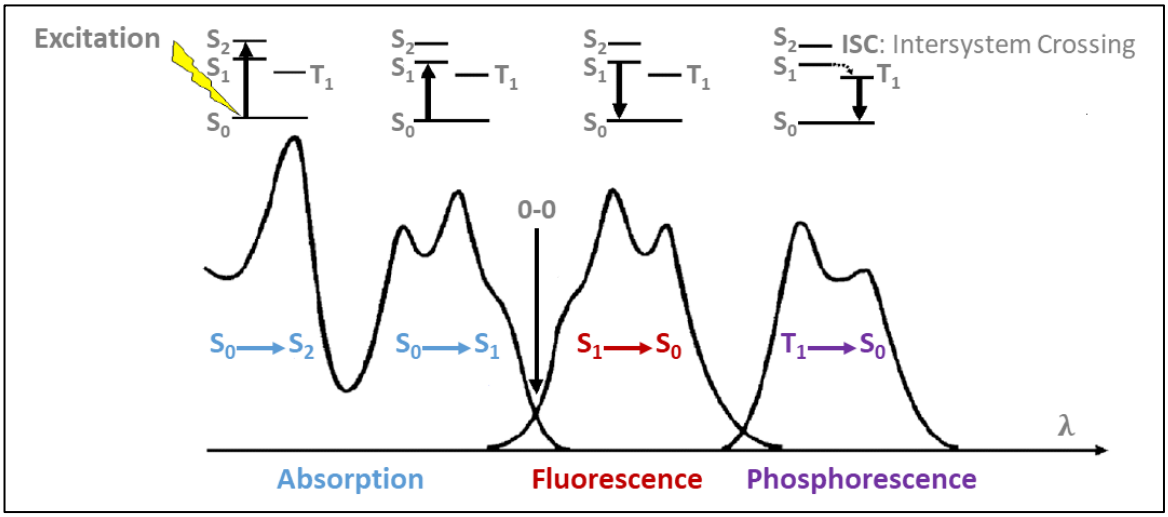

Figure 2.3: Illustration of absorption, fluorescence, and phosphorescence with relative positions (re-arranged from reference[161]).

Multiplicity of the singlet state is one, and all electron spins are paired antiparallel in the singlet states. However, multiplicity is three and two electrons are no longer antiparallel in the triplet states. The triplet state is usually lower in energy than the corresponding singlet state, because the electrons with opposite spin can stay further apart (Hund's rule).[162]

2.1.5 Delayed Fluorescence

Delayed fluorescence can occur, when the energy gap between S_1 and T_1 is small and the lifetime of T_1 is long enough. The obtained emission spectrum is the same as fluorescence spectrum; however, the decay time constant is longer in this case.

There are two types of delayed fluorescence: (i) E-type, and (ii) P-type.

Thermally activated E-type delayed fluorescence which has higher temperature and efficiency was first monitored in eosin. Because of the large energy gap between S_1 and T_1, aromatic hydrocarbons generally do not represent this process, however E-type fluorescence can be highly effective in fullerenes.

Concentrated solutions are required for P-type delayed fluorescence and this type of process was first recorded with pyrene. Enough energy for going back to the S_1 state can be provided by collisions between other molecules and those in T_1 states.[157]

2.2 Intermolecular Deactivation Process (Quenching)

Intrinsic de-excitation in excited molecules was described so far above. Intermolecular de-excitation phenomena will be taken into account now. In this case, the interaction of an excited fluorophore F* with another molecule Q will be explained. This process is known as quenching.

A reduction of fluorescence intensity, fluorescence quantum yield and/or decay occurs, because of quenching which cause a bimolecular process. Here, several potential fluorescence quenching mechanisms such as energy, electron or proton transfer, formation of excimer or exciplex, collision with a heavy atom (e.g. halogenids) or paramagnetic species (e.g. O_2) can be included.

A few situations could be distinguished when fluorescence quenching is in competition with intrinsic de-excitation:

(i) The concentration to the quencher [Q] is in excess. In this way, it can be possible that F* and Q are close to one another that interaction can be formed within time of excitation. The probability of finding Q within the encounter distance with F* is less than 1 in the case of static quenching. [Q] can be taken as constant if this probability is equal to 1.

(ii) [Q] is not in excess. Throughout the excited-state lifetime (e.g. lifetime is very short, highly viscous medium), interaction of F* and Q is not probable, but if the interaction is significant at distances longer than the encounter distance, quenching is formed in the case for long-range energy transfer.

(iii) [Q] is not in excess, however interaction of F* with Q is probable throughout the excited-state lifetime. This is known as dynamic quenching (diffusion-controlled).

Dynamic, static and simultaneous static and dynamic quenching will be described below. [157, 163]

2.2.1 Dynamic Quenching

The experimental quenching rate constant k_Q is supposed to be time-independent in dynamic quenching. Dynamic quenching exhibits decreased fluorescence intensity, and reduced decay times which is showed in Equation 2.4 below:

$$\tau_0 / \tau = 1 + k_Q \tau_0 [Q] \quad \textbf{(2.4)}$$

where τ_0 is the luminescence decay time in the absence of the quencher (s), τ is the luminescence decay time at variable quencher concentration (s), k_Q is the quenching rate constant ($M^{-1}\ s^{-1}$), and [Q] is the quencher concentration.

When k_Q is multiplied by τ_0, Stern-Volmer constant K_{SV} is obtained and introducing K_{SV} into Equation 2.5 causes to the Stern-Volmer relation by the following equation:

$$Ø_0/Ø_Q = \tau_0/\tau_Q = I_0/I_Q = 1 + K_{SV} [Q] \quad \textbf{(2.5)}$$

where I_0 is the luminescence intensity in the absence of the quencher, I_Q is the luminescence intensity at a variable quencher concentration, $Ø_0$ is the luminescence quantum yield in the absence of the quencher, $Ø_Q$ is the luminescence quantum yield at a variable quencher concentration, and K_{SV} is the Stern-Volmer constant.

Normally, plotting I_0/I against [Q] gives a basic linear dependence and from its slope, the Stern-Volmer constant can be obtained.

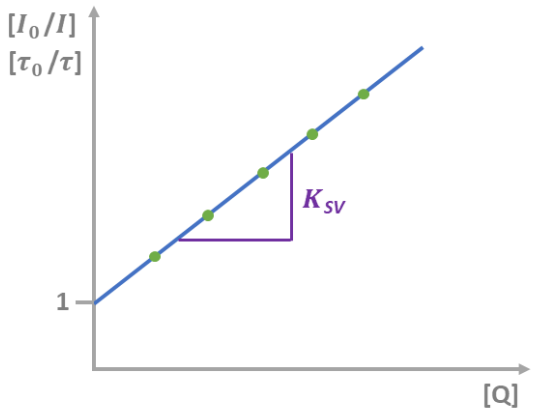

Figure 2.4: An illustration of dynamic quenching in Stern-Volmer plot.

2.2.2 Static Quenching

In contrast to the case of dynamic quenching, static quenching is not dependent on molecular transport from Q to F* within the excited state lifetime. The formation of a non-fluorescent complex in the ground state frequently induces static quenching. Typically, I_0/I versus [Q] plots are of the identical shape as Stern-Volmer plots, while the ratio of τ_0/τ stays same over [Q].

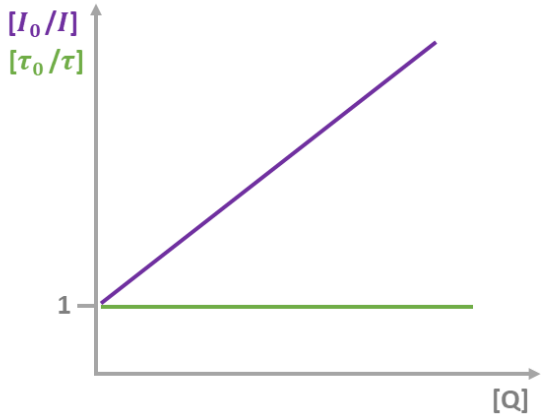

Figure 2.5: An illustration of static quenching in Stern-Volmer plot.

The quencher cannot collide with an excited fluorophore within its lifetime in a highly viscous medium. In this way, a model with the title of 'sphere of effective quenching' has been suggested.[157] This model indicates that quenching only is formed, if Q is placed inside an encounter sphere of F*, as showed in Figure 2.6.

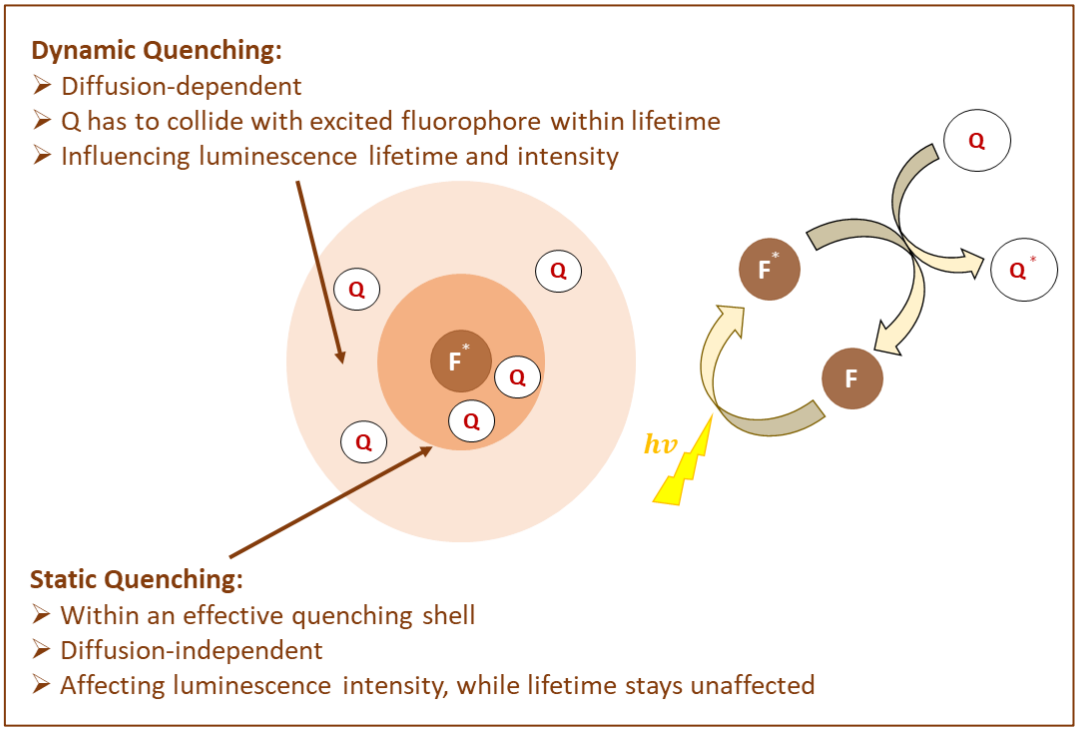

Figure 2.6: The difference between dynamic and static quenching (modified from reference[164]).

2.2.3 Simultaneous Static and Dynamic Quenching

Static and dynamic quenching can act at the same time, when [Q] is constantly rising. This is particularly observed when the quencher is in tendency to generate complexing agents which do not emit photons. At high [Q], this causes a deviation of linearity of the Stern-Volmer plot.

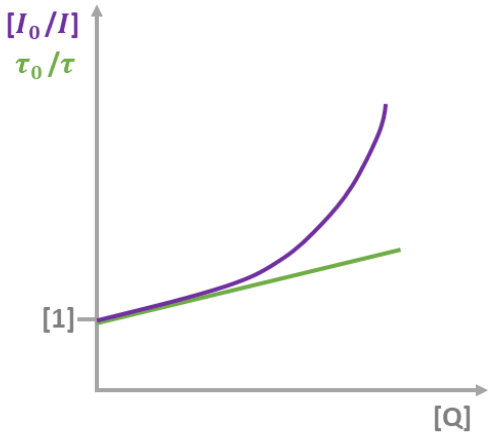

Figure 2.7: An illustration of simultaneous static and dynamic quenching in Stern-Volmer plot.

2.2.4 Photoinduced Electron Transfer

Photoinduced electron transfer (PET) occurs between a donor (D) and an acceptor (A) with the absorption of visible (Vis) or ultraviolet (UV) light from the donor. A conversion of the light energy into the electrochemical energy is followed by electron transfer. The process results in the generation of a charge transfer state, which is a dipolar species: the radical cation of the donor ($D^{+\bullet}$) and the radical anion of the acceptor ($A^{-\bullet}$) as can be seen in Figure 2.8.[165, 166] D and A coexist in the same molecule in an intramolecular PET process, whereas they correspond to different molecules in an intermolecular PET.[167] One of the most essential elements to enable electron transfer (ET) is the energy level arrangement of the highest occupied molecular orbital (HOMO) and lowest unoccupied molecular orbital (LUMO) of the D and the A, respectively. In this way, to facilitate the PET, the D-A systems should be chosen meticulously.

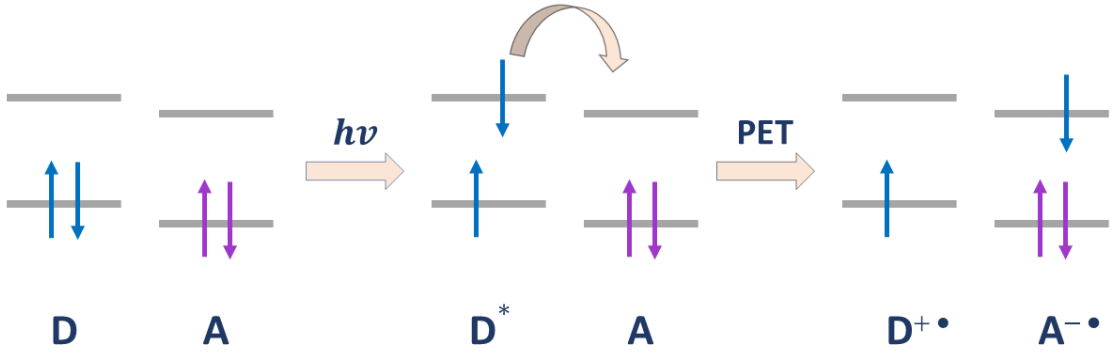

Figure 2.8: Illustration of the PET process at a donor-acceptor system.

The foundations of vital natural functions, e.g. photosynthesis, vision, and DNA damage repair is made up by PET phenomena.[168-170] PET is an important research field in bimolecular systems, due to the need for solar energy conversion. There have been enormous publications on PET illustrated in the literature in the 20th and 21st centuries, because of its ability to cover the global demand for energy.[171-174] Besides the potential of optimizing and controlling of PET reactions in solar energy conversion, they also propose the opportunity to figure out high impact technological and social challenges in the applications of artificial photosynthesis, photocatalysis, molecular electronics, photodynamic therapy, etc.[175, 176]

Since the great contribution of Marcus[177, 178] in 1950s and Weller[179] in 1960s with their researches, the kinetics and thermodynamics principle for the intermolecular PET process are known. The electrochemical and excited state features of the A and D moieties modulates PET. Intramolecular and/or intermolecular PET is in direct competition with several other radiative and radiationless deactivation processes found in the excited states of molecular systems.[180] In general, PET causes reduction of both lifetimes and emission quantum yields. But, it is frequently disregarded that other mechanisms may be responsible of the fluorescence quenching, such as from internal conversion and intersystem crossing mechanisms to energy transfer processes. To clearly evidence the presence of PET and quantify its rate, the finding of radical ions with time-resolved spectroscopies are needed. Therefore, laser flash photolysis experiments, which measure the transient absorption of the radical anion and cation species, can probe charge separation or recombination (back electron transfer).[181, 182] Information about charge separation or recombination can also be provided by other techniques, e.g. time-resolved resonance Raman, electron spin resonance and infrared spectroscopies.[183, 184] As compared to intermolecular processes, intramolecular PET processes have less thoroughly been investigated with these techniques[182, 185, 186], despite their enormous interest.

Bimolecular electron transfer process is significant, because to quench an electronically excited state, for example to block its luminescence and/or reactivity, and to sensitize other species, i.e. to give rise to chemical changes of, or luminescence from, species that do not absorb light.[187]

2.2.4.1 How Is the Electron Transferred from Donor to Acceptor?

When electron transfer processes are investigated, some questions can arise such as "how are we supposed to monitor the real transfer of the electron?" and "what happens?". Electrons are frequently said to be jumping from D to A, to hop around or to be injected into an acceptor. We have to take into account the fact that we can only discuss the probability of detection an electron in a particular region.

Figure 2.9 illustrates the ground state, excited state and charge separated state of D-A

system with three positions on the potential energy surface. D possesses the lowest excitation energy as represented in Fig. 2.9. Three positions on the potential energy curves showing the excited state (D*-A) and the charge separated state ($D^{+\cdot}$-$A^{-\cdot}$) are demonstrated with numbers (1, 2 and 3).

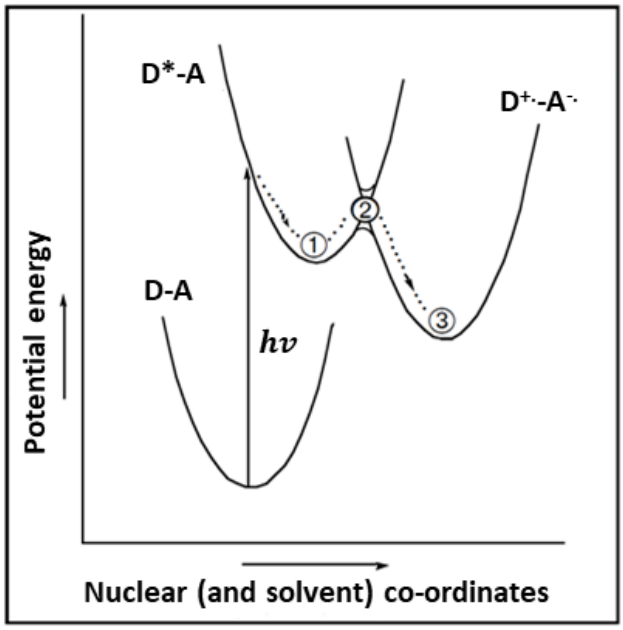

Figure 2.9: The ground state, excited state and charge separated state of a donor-acceptor system is illustrated with three positions on the potential energy surface.[166]

(1) A situation (D*-A) occurs upon excitation of D that we can express with harmonic potential approximation. An electron is promoted from a low-lying state to a state in which most of the electron probability density is placed on D. But, there is also a small probability of detecting the electron on the acceptor place, as electronic coupling is existent. Relaxation to the bottom of the first potential energy well occurs and the electron experiences a potential barrier.

(2) When the barrier is achieved, there are two possible scenarios which are crossing to the product state or staying on the initial state. At this stage, there is a 50% probability of detecting the electron on the acceptor site at the top of the barrier: the orbital that is intrinsically connected with this situation possesses 50% electron probability density on the D site and 50% electron probability on the A site.

(3) An orbital coefficient evolution which implies a decrease of electron probability density on the D site and a rise of electron probability density on the A site is caused by a crossing, going from the top of the barrier to the bottom of the potential energy well of the product state.[166]

2.3 Fast Processes and Time Scale

A big effort and research are devoted to understanding the dynamics of diverse processes in biology, physical chemistry, and material science. Scientists are interested to observe system parameters changing over time. The time scales on which the changes happen can be different from slow to highly rapid (from a human's perspective), depending on the size of the object being investigated. Various processes are represented in the order of decreasing time taken in Figure 2.10.

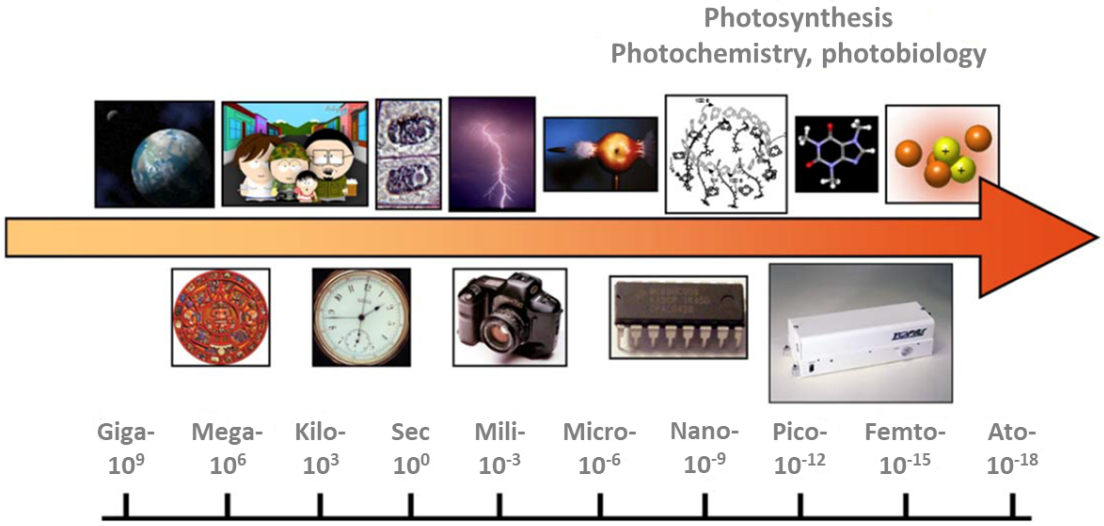

Figure 2.10: Several natural processes with their time period and instruments for tracking them.[188]

It is clear that biological processes have lifetimes spanning 26 orders of magnitude. As this dynamic area is huge, it is impossible to cover it with a single instrument. Thus, in order to track various processes, different tools are needed. A calendar is probably the slowest tool we have, the more scientifically oriented of us will choose radioactive dating procedures. Processes stretched over centuries and millennia is followed by them. When the time scale is more closely relatable to that of human life, a newspaper or a chronicle would be used to

represent them. Fast film cameras or photographic cameras with short exposure times such as down to 0.001 seconds can be used to record even faster events. To access the domain of microseconds, nanoseconds, down to hundreds of picoseconds, electronic devices can be utilized. In the case of even more rapid processes, the durations of which are tens of picosecond and less, need the most rapid tool available in nature – light itself. ~ $3x10^8$ m/s is the constant speed of the travel of light in vacuum.

It is quite clear that some natural processes occur very rapid that even light manages to cover a distance of some microns during the whole event.[188] Figuring out the time scales of each electronic transitions in the Jablonski diagram is also important to comprehend the feasibility of these processes (see Fig. 2.1).

Ultrafast processes take place on timescales place faster than 1 μs. Time-resolved or ultrafast spectroscopy is the field of science that investigates ultrafast processes in atoms, molecules, crystals and glasses utilizing light-based spectral systems. Ultrafast spectroscopic test techniques are required to obtain information about the charge migration via the materials to track the transient processes in real time.[188]

2.3.1 Time-resolved Spectroscopy

A wide range of applications in several fields of research including physics, chemistry, material science, and nanotechnology is offered by time-resolved spectroscopy (TRS). To probe in real time the very early dynamical events (e.g. excitons and charge carriers created by photoexcitation) taking place in the femtosecond (1 fs=10^{-15} s) and picosecond (1 ps=10^{-12} s) time domains is allowed us by TRS. The present TRS techniques have been improved dramatically by the progress of modern spectroscopic tools. Norrish and Porter,[189, 190] were awarded Nobel Prize in Chemistry in 1967 for their discovery[191] and design of the (flash) photolysis technique, which has millisecond resolution. The application of time-resolved optical spectroscopy has been further developed since that time. A new world of study in the microsecond (μs) time range, providing an opportunity for the direct detection of short-lived transients was opened up with their discovery.

Afterwards, further advancement of this technique came due to the development of short-pulsed lasers with temporal resolution of femtoseconds. The Nobel Prize in Chemistry was given to Zewail in 1999 for his research on the transition states of chemical reactions using fs spectroscopy.[192]

2.3.1.1 Time-resolved Photoluminescence Spectroscopy

Optical materials can be characterized with time-resolved photoluminescence (TRPL) spectroscopy to comprehend the dynamics of excitonic transitions in the materials using temporal information as well as spectral information. Understanding the competition between radiative and non-radiative energy transfer processes can be contributed by analysis of TRPL.[193] The additional information to uniquely identify a material and distinguish isomers or very similar materials from one another can often be provided by photoluminescence (PL) lifetime, when steady-state PL is not enough. Additionally, information about the dynamics of a material process, information that is not easily acquired from steady-state PL can be provided by PL lifetime.[194]

In the TRPL technique, electron-hole pairs that decay to lower energy levels of the samples are generated by the short pulse of light. Afterwards, these electron-hole pairs can recombine and emit light which is consisted of a set of wavelengths corresponding to transition energies of the sample. Consequently, a means to measure the transition energies and their lifetimes is provided by the measurement of the optical spectrum as a function of time. A conventional spectrum analyser cannot provide the resolution needed, as these decay times are on the order of picoseconds or nanoseconds, and the intensity of light emitted can be very weak. For this reason, it is essential to utilize a device called as a streak camera which is an ultra-high-speed detector which captures light emission phenomena taking place in highly short time ranges.[195] Around 180 fs is the time-resolution of the best optoelectronic streak cameras.[196]

2.3.1.2 Pump-Probe Spectroscopy: Transient Absorption Measurements

Pump-probe spectroscopy is one of the most powerful techniques for detecting transient species and obtaining direct measurements of the charge carrier dynamics by observing the

evolution of charge-separated states in donor-acceptor systems.[197] Charge transfer (CT), charge separation (CS), and charge recombination (CR) processes are significant to comprehend the photophysical and photochemical processes in donor-acceptor systems, because of the fact that they could assist the development of solar device performance by providing main information needed for device optimization and fabrication.[198]

Transient absorption (TA) tests have a simple idea which is based on two ultra-short laser pulses. To excite a system into an excited state from S_0 to S_n, one laser pulse is used as a pump, and afterwards, the second one serves as a probe light. Figure 2.11 represents a schematic illustration of the fundamental design of all pump-probe tests. With observing CT, CS and CR dynamics in real time, necessary information about the mechanistic and kinetic details of the important events that take place in very short time regions can be provided by TA measurements. The durations of the ultrafast pump and probe pulses and the resolution of the time delay created between them have a significant role in terms of the time resolution of the ultrafast pump-probe tests.[199]

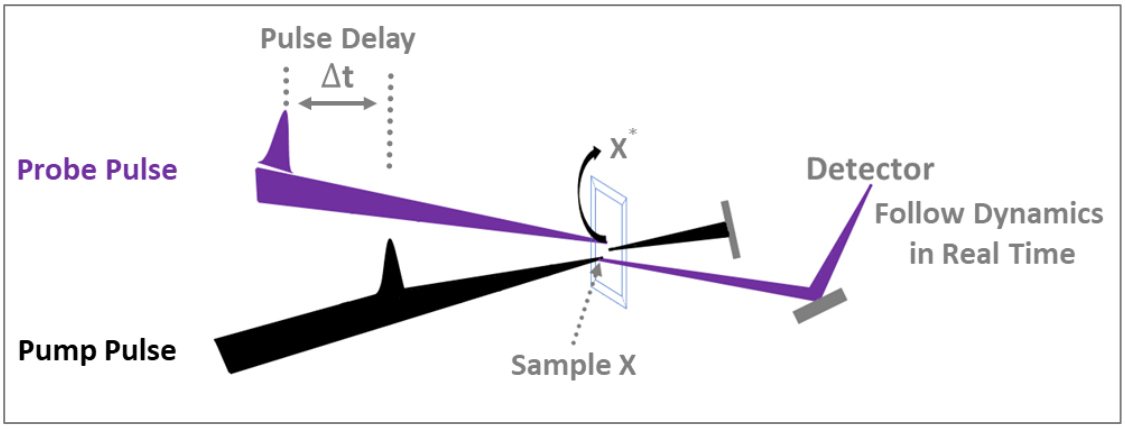

Figure 2.11: Illustration of fundamental pump-probe experimental system.

As exhibited in Figure 2.11, pump pulse is used to excite the sample, and probe measures transmittance. The time dependence of the difference absorption signal is provided by the variable delay between the pump and probe pulses. The time delay can be known by calculating the extra distance travel by the probe pulse (0.3 μm travel in 1fs).

To generate the differences in the molecules, the pump pulse should be more intense than the probe pulse, while the probe only interrogates them, so the probe should not have any impact on the studied material for ideal tests.[200]

2.3.1.2.1 Femtosecond and Nanosecond Transient Absorption Spectroscopy

Femtosecond (fs) and nanosecond (ns) TA spectroscopies, which are designed to study with highly amplified laser resolutions, are matchless broadband pump-probe TA techniques. HELIOS and EOS setups (Ultrafast Systems), respectively, are used to operate fs-TA and ns-TA tests. Remarkable spectral and kinetic data, which is desirable for studies of photoexcitation events with ultrafast time resolutions (such as fs-TA experiments), is generated by the HELIOS system throughout its broad spectral coverage and long-time window. The EOS setup operates over a greatly extended time range starting from a few ns to hundreds of ms after photoexcitation for the ns-TA measurements. It uses almost any ~ 1 kHz repetition rate laser to enable the gathering of broadband TA spectra. In chapter 3, the HELIOS and EOS instrumental setups will be explained in detail. The pump and probe beams are adjusted to overlap spatially and temporally on the investigated sample in this technique. The probe beam after passing through filters that decrease the white light around the Spitfire fundamental at 800 nm, is gathered by the selected spectrometer. Until achieving the ideal signal-to-noise ratio, the TA spectra are generally averaged. Only the total absorption signals gained are recorded for both the fs- and ns-TA. Lastly, to extract the kinetics of dynamical processes from the TA spectra, global analysis fitting procedures are used.[200]

2.3.1.2.2 Transient Absorption Spectrum

A fraction of the molecules are promoted to an electronically excited state through an excitation (or pump) pulse in transient absorption spectroscopy. This fraction usually ranges from 0.1% to tens of percent depending on the kind of experiment. A weak probe pulse is transferred through the sample with a delay τ with respect to the pump pulse. Then, a difference between the absorption spectrum of the excited sample and the absorption spectrum of the sample in the ground state is calculated, thus a ΔA is obtained.

A ΔA profile as a function of the time delay τ and wavelength λ in other words, a ΔA (λ,τ) is obtained by changing the τ between the pump and the probe and recording a ΔA spectrum at each time delay. Information on the dynamic processes that happened in the investigated system, e.g., excited state energy migration, electron and/or proton transfer processes, isomerization, and intersystem crossing is contained by ΔA (λ,τ). The evolution of non-emissive states and dark states can be studied with ultrafast transient absorption spectroscopy and this is one superiority of the TA spectroscopy over time-resolved fluorescence technique. Normally, a ΔA spectrum has contributions from four processes as follows.[201]

- **Ground-State Bleach**

Ground-state bleach (GSB) is the first contribution. The number of molecules in the ground state has been reduced, as a fraction of the molecules has been promoted to the excited state thanks to the influence of the pump pulse. Therefore, in the excited state sample, the ground-state absorption is less than the absorption in the non-excited sample. As a result, as can be seen in Figure 2.12, in the region of ground-state absorption, a negative signal in the ΔA spectrum is monitored.

- **Stimulated Emission**

Stimulated emission (SE) is the second contribution in TA spectrum. The Einstein coefficients for absorption from the ground to the excited state and stimulated emission from the excited to the ground state are same for a two-level system. Therefore, when the probe pulse passes through the excited volume, upon population of the excited state, stimulated emission to the ground state will occur. SE will occur only for optically allowed transitions and will possess a spectral profile that follows the fluorescence spectrum of the excited chromophore, i.e., it is Stokes shifted with respect to the GSB. Throughout the physical process of SE, a photon from the probe pulse induces emission of another photon from the excited molecule, which returns to the ground state. SE produces the photon which is emitted in the exact same direction as the probe photon, and thus both will be detected. It is worth to mention that the excited-state population is not influenced

significantly by this process, because the intensity of the probe pulse is so weak. As schematically indicated in Fig. 2.12, SE results in an increase of light intensity on the detector, corresponding to a negative ΔA signal. The Stokes shift could be very small that the SE band spectrally overlaps with GSB and merges into one band in numerous chromophores.

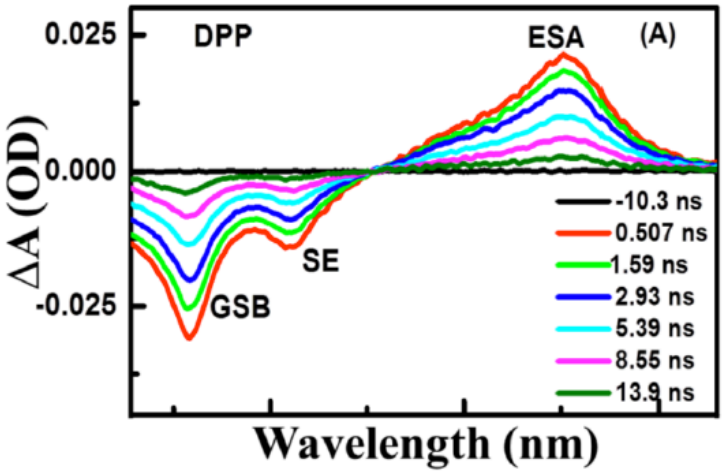

Figure 2.12: An illustration of the three important processes (GSB, SE, and ESA) in the TA spectrum of diketopyrrolopyrrole (DPP).[202]

- **Excited State Absorption**

Excited-state absorption (ESA) provides the third contribution. Optically allowed transition from the excited states of a chromophore to higher excited states may exist in specific wavelength regions upon excitation with the pump beam, and absorption of the probe pulse at these certain wavelengths will occur. As a result, a positive signal in the ΔA spectrum is observed in the wavelength region of ESA. The excited-state population is also not influenced significantly by this process, because the intensity of the probe pulse is so weak.

- **Product Absorption**

Product absorption gives a fourth possible contribution to the ΔA spectrum. Reactions may occur that result in a transient or a long-lived molecular state e.g., triplet states, charge-separated states, and isomerized states, after excitation of the photosynthetic or

photobiological or photochemical system. The absorption of such a product (transient) will become clear as a positive ΔA signal in the spectrum. A GSB will be monitored at the wavelengths where the chromophore on which the product state resides has a ground-state absorption.

The intensity of the probe light transmitted through a sample is detected before *(I_0)* and after *(I)* the photoexcitation in the TA experiment. From the intensity ratio, the following equation gives the absorbance change:

$$\Delta OD = \log (I_0/I) \quad \textbf{(2.6)}$$

From this relation, positive signals in the ΔOD is provided by photoproducts, whereas photobleaching results in negative signals in the ΔOD, because of the reduction in the GS as showed in Fig. 2.12. Detection of absorbance changes in the order as small as 10^{-5} to 10^{-6} depending on the measuring time domain after appropriate accumulation is possible using time-resolved spectroscopy techniques. As illustrated with Equation 2.2, based on Lambert-Beer's law, it is therefore technically difficult to detect a small absorbance change of 10^{-5}, in which the photoactive layer is typically as thin as 100 nm.[203]

CHAPTER 3: Experimental Section

3.1 Materials, Methods and Experimental Procedures

3.1.1 Porphyrins in the Project

As can be seen in Figure 3.1, four different types of neutral zinc centred *push-pull* porphyrins (abbreviated as Am1 5,15-1, Am1 5,10-1, SlpE029 and SlpE026) are used in this thesis. Each *meso*-positions of the porphyrin (5, 10, 15, and 20) are shown in purple colour below.

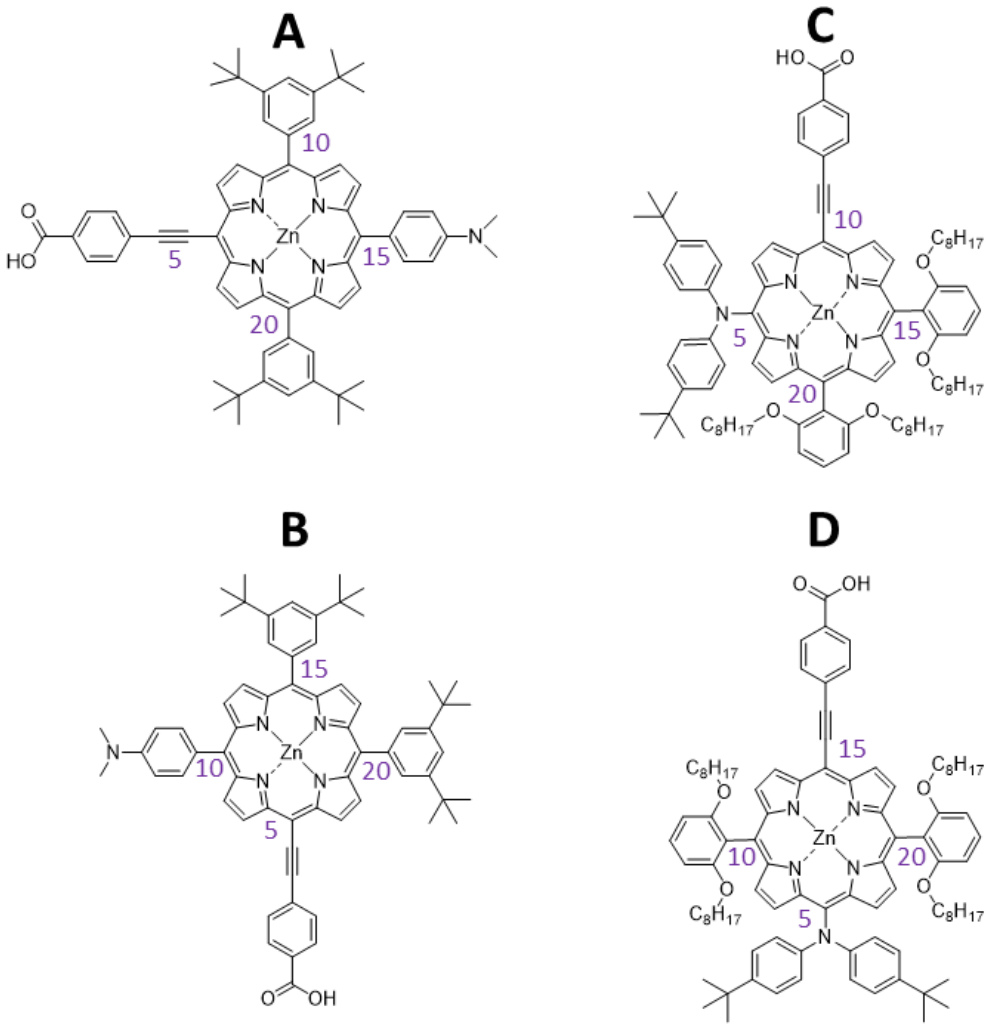

Figure 3.1: The chemical structures of the (A) Am1 5,15-1, (B) Am1 5,10-1, (C) SlpE029, and (D) SlpE026 porphyrins. *Meso*-positions are shown in colour for each porphyrin.

They are all *push-pull* porphyrins which have donor-π-acceptor (D-A) systems. By this way, the porphyrins have a strong intramolecular dipole moment, because electrons are transferred from an electron-donating group through a π-spacer to electron-withdrawing group. Am1 5,15-1 and Am1 5,10-1 porphyrins are the isomers of each other and SlpE029 and SlpE026 porphyrins are also isomers of each other.

For Am1 5,15-1 and Am1 5,10-1 isomers, *N,N*-dimethylanilinyl and 4-carboxyphenylethynyl are used as electron donor and electron acceptor groups, respectively. For Am1 5,15-1 porphyrin, the electron donor and acceptor moieties are attached at the 15-*meso*-position and at the 5-*meso*-position, respectively, however in the case of Am1 5,10-1 porphyrin, the electron donor group is placed at the 10-*meso*-position as well as with the same *meso*-position of electron acceptor group like in Am1 5,15-1. By this way, the dipole runs along the *meso-meso* axis for Am1 5,15-1 porphyrin and the dipole is along the β-β axis for Am1 5,10-1 porphyrin. Regarding to SlpE029 and SlpE026 isomers, the same electron acceptor group is used and located at the 10-*meso* position for SlpE029 porphyrin and at the 15-*meso* position for SlpE026 as well as the bis(4-*tert*-butylphenyl)amino group as electron donor at the 5-*meso* position for two porphyrins. Therefore, different dipole moment orientations in them are formed. As the dipole is along the β-β axis in the case of SlpE029, the dipole runs along the *meso-meso* axis for SlpE026 porphyrin. In Table 3.1, each chemical group name on the each *meso*-position of the Am1 5,15-1, Am1 5,10-1, SlpE029, and SlpE026 are represented with the systematic name of each porphyrin.

Table 3.1: Systematic name and name of chemical groups on the each *meso*-position of Am1 5,15-1 and Am1 5,10-1, SlpE029, and SlpE026 porphyrins, respectively.

Porphyrin Name	Systematic Name	Chemical Group on the *Meso*-Position			
		5	10	15	20
Am1 5,15-1	[10,20-Bis(3,5-di-*tert*-butylphenyl)-5-(4-carboxyphenylethynyl)-15-(*N*,*N*-dimethylanilinyl)porphyrinato]zinc(II)	4-carboxyphenylethynyl	3,5-di-*tert*-butylphenyl	*N*,*N*-dimethylanilinyl	3,5-di-*tert*-butylphenyl
Am1 5,10-1	[15,20-bis(3,5-di-*tert*-butylphenyl)-5-(4-carboxyphenylethynyl)-10-(*N*,*N*-dimethylanilinyl)-porphyrinato]zinc(II)	4-carboxyphenylethynyl	*N*,*N*-dimethylanilinyl	3,5-di-*tert*-butylphenyl	3,5-di-*tert*-butylphenyl
SlpE029	{5-[Bis(4-*tert*-butylphenyl)amino]-10-(4-carboxyphenylethynyl)-15,20-bis(2,6-dioctyloxyphenyl)porphyrinato}zinc(II)	Bis(4-*tert*-butylphenyl)amino	4-carboxyphenylethynyl	2,6-dioctyloxyphenyl	2,6-dioctyloxyphenyl
SlpE026	{5-[Bis(4-*tert*-butylphenyl)amino]-15-(4-carboxyphenylethynyl)-10,20-bis(2,6-dioctyloxyphenyl)porphyrinato}zinc(II)	Bis(4-*tert*-butylphenyl)amino	2,6-dioctyloxyphenyl	4-carboxyphenylethynyl	2,6-dioctyloxyphenyl

3.1.2 Materials

Am1 5,15-1, Am1 5,10-1, SlpE029, and SlpE026 porphyrins were synthesized by Mathias O. Senge's group in School of Chemistry at Trinity College Dublin according to a procedure reported in the literature[77].

In the measurements in chapter 4 and chapter 5, tetrahydrofuran (THF, 99%) was supplied from Alfa Aesar.

In the measurements in chapter 4, lead iodide (PbI_2, 99.999% trace metal basis), N,N-dimethylformamide (DMF, anhydrous, 99.8%), dimethyl sulfoxide (DMSO, anhydrous, ≥99.9%), toluene (anhydrous, 99.8%), and chloroform (anhydrous, ≥99%) were purchased from Sigma-Aldrich. Methylammonium iodide (CH_3NH_3I) was bought from Dyesol Limited. Microscope glass slides were provided from Fisherbrand.

In the measurements in chapter 5, fullerene (C60) and N-methyl-2-pyrrolidone (NMP, anhydrous, 99.5%) were purchased from Sigma-Aldrich. Graphene carboxylate (GC) was obtained from ACS material. Deionized (DI) water was used during the experiments.

3.1.3 Methods

3.1.3.1 Preparation of $MAPbI_3$ Perovskite Solution

$MAPbI_3$ perovskite solution and the perovskite film preparation were done according to a literature procedure[204]. Briefly, 461 mg of lead iodide and 159 mg of methylammonium iodide powders were dissolved in 71 μL DMSO and 635 μL DMF in a glass vial. The solution was stirred with a magnetic bar overnight at 70°C.

3.1.3.2 Preparation of $MAPbI_3$ Perovskite Thin Film

Glass microscope slides were cleaned with soap/DI water mixture, acetone and isopropyl alcohol (IPA), respectively in an ultrasonic bath for 10 minutes each followed by oxygen plasma treatment for 10 minutes. In a glovebox, 100 μL $MAPbI_3$ perovskite solution was spin coated on the glass substrate at 4000 rpm for 15 seconds and 300 μL toluene was dripped on the rotating glass substrate in 9 seconds. After that, the glass substrate was

heated at 100°C on a hot plate for 10 minutes in order to obtain a $CH_3NH_3PbI_3$ perovskite thin film.

3.1.4 Spectroscopic Investigations

3.1.4.1 Steady-state Measurements

Absorption spectra were recorded on a Cary 5000 UV–Visible spectrometer (Agilent Technologies), whereas the steady-state photoluminescence spectra were obtained using a Fluoromax-4 spectrofluorometer (Horiba Scientific) for the steady-state absorption and emission spectra data in chapter 4 and 5 in this thesis.

In chapter 4, $MAPbI_3$ perovskite film was placed on a sample holder and the steady-state absorption data was collected. After that, successive addition of SlpE026 porphyrin onto the perovskite film using a drop-casting method was studied. The fluorescence spectra were recorded after excitation at 675 nm.

Rectangular quartz cells with a 1 cm optical path were used for the steady-state and ultrafast spectroscopy TA and TRPL measurements in chapter 4 and chapter 5.

In chapter 5, the cuvette was filled with 2 mL fixed volume of the starting solution of donors (Am1 5,15-1 and SlpE026) in the corresponding solvent (NMP for the C_{60} and (THF:H_2O) [1:1 v/v for GC], while aliquots of the acceptors (C_{60} and GC) dissolved in solvent were added consecutively. The concentration of the porphyrin donor was kept constant throughout all of the tests. Sequential addition of a fixed volume of the quenchers into the donors' solution was investigated. The fluorescence spectra were collected after excitation at 625 nm and 600 nm for the porphyrin/C_{60} and porphyrin/GC hybrids, respectively.

3.1.4.2 Time-resolved Transient Absorption Spectroscopy

HELIOS and EOS setups (Ultrafast Systems, Florida, USA) were employed for fs- and ns-TA spectroscopy tests with the time resolutions of 120 fs and 100 ps and detection limits of 5.5 ns and 400 μs, respectively. Femtosecond broadband pump-probe spectroscopy was

used to excite and detect the wavelengths around a specific exciton absorption peaks of the donor. Figure 3.2 depicts a schematic of the experimental setup operated in this thesis for the ultraviolet (UV)/visible (vis) pump/NIR (near-infrared) probe tests. A fundamental laser, which is provided by a home built Ti:Sapphire using a chirped pulse amplification scheme, generating 35 fs pulses at 800 nm with 4 mJ of energy/pulse and a repetition rate of 1 kHz operates as the pump. Thanks to a pump-probe setup, the absorption decays were measured. In the setup, a white-light continuum probe pulse produced by a 2-mm-thick sapphire plate and spectrally tunable pump fs pulses (240–2600 nm; a few μJ pulse energy) formed in an optical parametric amplifier (TOPAS-C stage) selectively excite specific electronic transitions within an investigated sample. The probe beam is routed with a computer-controlled delay line, adjustable pinholes, focusing lens, and variable neutral density filter to a crystal for white light continuum (WLC) formation. Then, the probe beam is directed to the sample through a focusing mirror. To allow TA measurements within 5.5 ns (HELIOS) and 400 μs (EOS) time windows, the delay between the pump and probe pulses can be varied.

The pump and probe beams are arranged to overlap spatially and temporally on the sample. Following interaction with the sample, the probe beam is directed towards a near-infrared spectrometer (InGaAs-NIR) covering the range of 800-1600 nm with 3.5 nm resolution at 7900 spectra/s or a visible spectrometer (CMOS VIS) including the range of 350-800 nm with 1.5 nm resolution at 9500 spectra/s. The chosen spectrometer collects the probe beam after passing it through notch filters that attenuate the white light around the Spitfire fundamental at 800 nm. A two-channel probe (probe-reference) technique is used for both the HELIOS and EOS systems. The probe pulse is transferred via a beam-splitter before arriving at the sample to split the beam into two-channels (sample and reference). A part is directed to the detector to treat as a reference, the other is sent directly to the sample.

This technique allows us to dividing out any fluctuations in the probe beam intensity throughout the test. All spectra were averaged over a time period of 2 s for each time delay.[200]

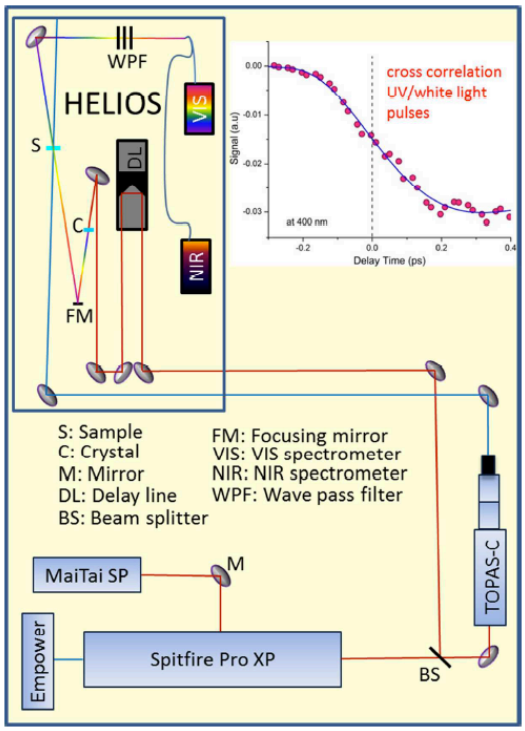

Figure 3.2: The schematic illustration of the fs laser system setup and broadband TA spectroscopy (see supporting information of the reference [205]).

Pulse width is ~ 35 fs for all fs-TA measurements in the thesis.[206] The ns-TA measurements were conducted same excitation pump (as fs-TA) with 100 ps time resolution in chapter 5. The electronic delay is used in ns-TA not mechanical delay like fs-TA.

In the photophysical characterization of the porphyrins in chapter 4, EOS detection system with the time resolution of 100 ps and the detection limits of 400 µs were operated to cover the transient spectra after excitation. For ns-TA measurements, a 2 mm-thick cell was filled with 0.02 mM porphyrin samples and excited at 532 nm. To monitor the change in the transient absorbance, the transmitted probe light from the solution was collected and focused on a broadband UV-Vis detector.

In chapter 4, in the absence and presence (using a drop-casting method) of 80 femtomolar (fM) SlpE026 solution, the pump and probe beams were focused on the $MAPbI_3$ perovskite film on a glass substrate. To monitor the change in the transient absorbance, the transmitted probe light from the film was collected and focused on a broadband UV-Vis detector.

In chapter 5, in the absence and presence of 1 mg/mL nanocarbon (C_{60} and GC) materials, the pump and probe beams were overlapped on 0.03 mM porphyrin (Am1 5,15-1 and SlpE026) solutions. To monitor the change in the transient absorbance, the transmitted probe light from the solution was collected and focused on a broadband UV-Vis detector.

All TA tests were operated at room temperature. To guarantee a fresh volume was available for each laser shot, the sample solutions were continually stirred with a magnetic stirrer in the tests in chapter 4 and 5. To avoid any degradation, the absorption spectrum of each sample was also tested before and after the TA measurements. To extract the kinetics of dynamical processes from the TA spectra, global analysis fitting procedures were used.

3.1.4.3 Time-resolved Photoluminescence Spectroscopy Using a Streak Camera

A Hamamatsu C10910 streak camera system with 1 picosecond temporal resolution was used to conduct time-resolved photoluminescence measurements.[207-209] Streak camera details can be read in reference[210]. Using a Spectra-Physics MaiTai HP and Inspire HF-100 OPO with a repetition rate of 4 MHz, the pump beam was centred at 532 nm for the photophysical characterization tests of porphyrins in chapter 4, and at 650 nm for investigating the electron transfer process from $MAPbI_3$ perovskite film to SlpE026 porphyrin in same chapter. These measurements were carried out with an excitation fluence of 10 nJ/cm^2.

CHAPTER 4: Charge Transfer Process at the Interface of Methylammonium Lead Triiodide Perovskite and *Push-Pull* Porphyrins

4.1 Introduction

A large number of photophysical studies on porphyrin derivatives have been performed during the past few decades[147, 198], due to their remarkable optical and electronic properties. These make them excellent candidates for a variety of potential applications including solar energy conversion[211], photodynamic therapy[212], oxygen sensor[213], nonlinear optics[15] and many others[214]. In general, these investigations have the aim of correlating the porphyrin molecular structure to some photophysical characteristic that can be modulated through conformational design, molecular symmetry, metal complexation, orientation and strength of the molecular dipole moment, size and degree of conjugation of the π-systems, and appropriate donor-acceptor substituents.[16-18, 215, 216] Recently, new porphyrin dyes are carefully designed as specific donor-π conjugated bridge-acceptor structures (simplified as D-π-A), these are known as *push-pull* porphyrins. This new class of porphyrins is used as light-harvester in dye-sensitized solar cells (DSSCs) due to their broad and strong absorption features.[50, 56, 57, 61, 217] More specifically, a remarkable solar power conversion efficiency (~ 13%) of porphyrin-based DSSCs[28] has been achieved with the help of introducing a push (electron-donating) and a pull (electron-withdrawing) group at the porphyrin periphery.[28, 218-223]

Grätzel and co-workers have been carefully employing variations of donor-acceptor systems including 5,15-disubstituted *push-pull* porphyrin as an absorber layer and very high power conversion efficiencies were achieved.[28, 53, 219, 224, 225] Unlike 5,10-disubstituted counterparts with the dipole moment along the β-β axis[226-228], unsymmetrically 5,15-disubstituted porphyrins, which have a dipole running along the *meso-meso* axis, are the most widely studied examples in literature. To understand differences between these two classes (see Fig. 1.7 for the illustration of *meso-meso* axis and β-β axis

dipole moment orientations in *push-pull* porphyrins), systematic studies on the relation between photo-physical properties and molecular structure are necessary.[229]

Additionally, hybrid perovskites, one of the most promising class of materials, have gained a leading role in the semiconductor research area, specifically in optoelectronics e.g. solar cells and light emitting diodes, which is primarily due to their unprecedented properties such as high absorption cross section, low trap density, tunable band gap and ultralong carrier lifetimes and diffusion lengths.[80, 81, 230, 231] These unique properties make them excellent absorber layers in solar cell devices, as proved by the realization of over 22% certified power conversion efficiency (PCE) within only six years of investigation.[232]

Moreover, by introducing high-valent metal ions,[233, 234] and strongly electron withdrawing substituents[235, 236] to the macrocycles, the electron-donating properties of porphyrins and metalloporphyrin complexes can be tuned as electron acceptors.[237, 238] To conclude, porphyrins and perovskites together can create a donor (D)–acceptor (A) system that can be used for energy conversion applications. Being in this regime, understanding the change transfer and recombination at their interface will be very beneficial for optimizing their optoelectronic devices.

In this work, we explore the ultrafast photophysics including intersystem crossing of newly synthesized *push-pull* porphyrin systems namely: [10,20-bis(3,5-di-t*ert*-butylphenyl)-5-(4-carboxyphenylethynyl)-15-(N,N-dimethylanilinyl)porphyrinato]zinc(II) (Am1 5,15-1), [15,20-bis(3,5-di-*tert*-butylphenyl)-5-(4-carboxyphenylethynyl)-10-(N,N-dimethylanilinyl)-porphyrinato]zinc(II) (Am1 5,10-1), {5-[bis(4-*tert*-butylphenyl)amino]-10-(4-carboxyphenylethynyl)-15,20-bis(2,6-dioctyloxyphenyl)porphyrinato}strezinc(II) (SlpE029) and {5-[bis(4-*tert*-butylphenyl)amino]-15-(4-carboxyphenylethynyl)-10,20-bis(2,6-dioctyloxyphenyl)porphyrinato}zinc(II) (SlpE026) using steady-state absorption and emission spectroscopy, time-resolved transient absorption spectroscopy and time-resolved photoluminescence (TRPL) spectroscopy using a streak camera. In addition, as a case study, we demonstrate the capability of one of these porphyrins to act as an electron

acceptor (porphyrin has vacant π^* orbital to accept the electron) at the interface of $MAPbI_3$ perovskite polycrystalline film using the same spectroscopic techniques. It is worth to mention that the porphyrins were chosen based on their different substituent pattern and the presence of donor-acceptor groups related to porphyrins currently in use in contemporary DSSCs studies. Here, all porphyrins studied have a zinc metal ion in their centre as its simple closed-shell d^{10} electronic configuration makes zinc a convenient metal. As well as zinc porphyrins are stable[239], zinc in porphyrins favour the production of long-lived triplet states[240].

4.2 Results and Discussion

4.2.1 Photophysical Studies of *Push-Pull* Porphyrins

4.2.1.1 Steady-state Measurements

The UV-Vis absorption and emission spectra of all the 5,15- and 5,10- substituted *push-pull* porphyrins are recorded while in THF solution and normalized with respect to the maximum absorption peak (see Fig. 4.1); the electronic absorption and emission spectroscopic data are summarized in Table 4.1.

All the porphyrin dyes display the typical characteristics of a metal-centred porphyrin ring, with a very strong Soret or B band ranging from 400 to 500 nm and quite strong Q bands in the range 550-700 nm (see Fig. 4.1A and B, respectively). The Soret band involves the transition from the ground state to the second excited state ($S_0 \rightarrow S_2$), while the Q bands correspond mainly to the transition from the ground state to the first excited state ($S_0 \rightarrow S_1$).[28] Additionally, as can be seen in Fig. 4.1C, upon excitation at 532 nm, the porphyrins exhibit a fluorescence band centred in the range of 644 nm and 669 nm, which corresponds to the transition from the first excited state to the ground state ($S_1 \rightarrow S_0$).

Overall, the trend observed in the UV-Vis and emission spectral features of Am1 5,15-1 (λ=446, 578, 629 and 645 nm) was similar to that of Am1 5,10-1 (λ=446, 577, 629 and 644 nm). On the other hand, SlpE029 (λ=448, 585, 637 and 669 nm) porphyrin represented

the most broadened and redshifted spectral features, which was followed by SlpE026 (λ=448, 580, 643 and 665 nm). As the aggregation effect was minimized at this ten times diluted 0.002 mM concentration value (See Fig. A.1 for data comparison in 0.02 mM concentration), the origin of the broadened and red-shifted spectral features is likely due to the greater extent of intramolecular charge transfer between the donor and acceptor groups.[241] It is worth to mention here that the broadening and red-shifting of the absorption bands can be explained as an indication of mixing with the intramolecular CT character in π-π^* absorption bands.[242] As reflected by the full width at half-maximum (FWHM) data, upon shifting to much stronger bis(4-*tert*-butylphenyl)amino electron donor group, the SlpE029 and SlpE026 porphyrins exhibited a greater extent of charge-transfer from the D to the A moiety. This results in broader Soret and emission bands of SlpE029 (FWHM= 50 and 60 nm) and SlpE026 (FWHM= 33 and 42 nm) porphyrins compared with those for Am1 5,15-1 (FWHM= 16 and 35 nm) and Am1 5,10-1 (FWHM=17 and 35 nm). Moreover, although the Q band intensities of Am1 5,15-1 and Am1 5,10-1 porphyrins were almost the same, the overall variations in the Q band intensities of all investigated porphyrins are reflecting the change of the molar absorption coefficient values of each porphyrin.

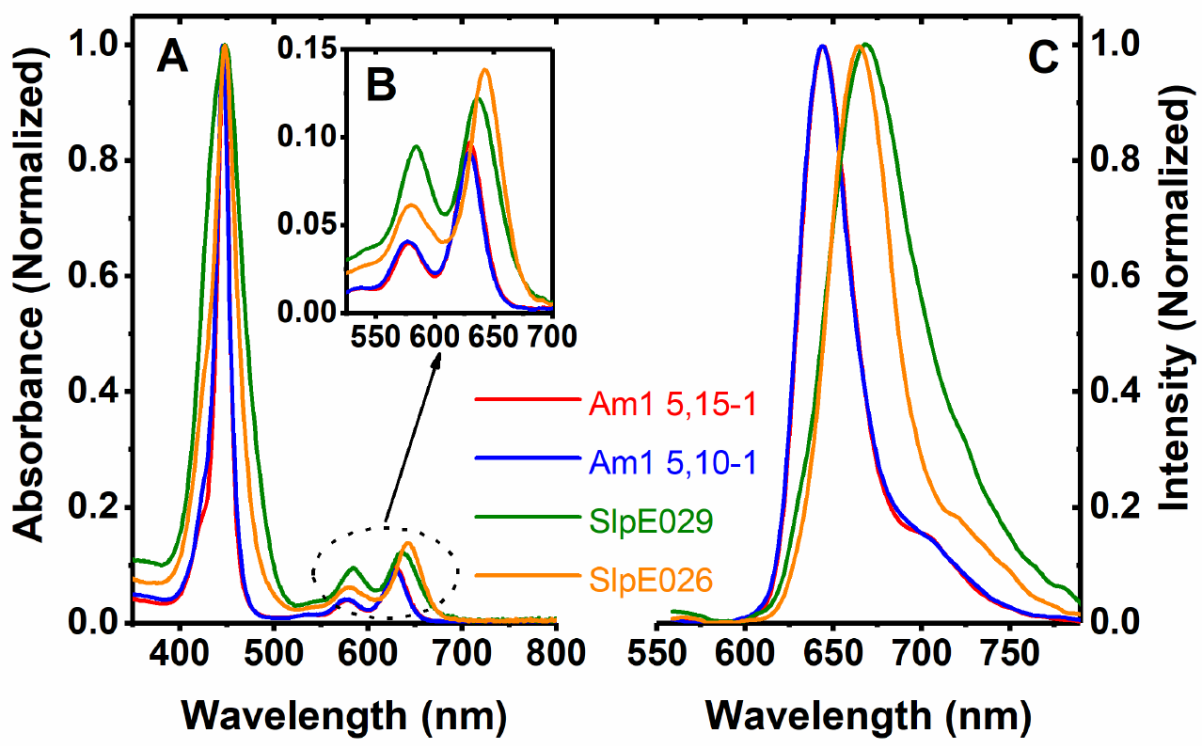

Figure 4.1: Normalized steady-state (A) absorption, (C) emission (λ_{Ex}= 532 nm) spectrums of 0.002 mM Am1 5,15-1 (red), Am1 5,10-1 (blue), SlpE029 (green) and SlpE026 (orange) porphyrins in THF solution. The Q bands region of each porphyrin in the absorption spectrum is enlarged in (B) for clarity purposes.

Table 4.1: Steady-state absorption and emission data of 0.002 mM Am1 5,15-1, Am1 5,10-1, SlpE029, and SlpE026 in THF solution.

Porphyrin	Absorption			Emission	
	Soret Band		Q bands		
	$\lambda_{Excitation}$ (nm)	FWHM (nm)	$\lambda_{Excitation}$ (nm)	$\lambda_{Emission}$ (nm)	FWHM (nm)
Am1 5,15-1	446	16	578, 629	645	35
Am1 5,10-1	446	17	577, 629	644	35
SlpE029	448	50	585, 637	669	60
SlpE026	448	33	580, 643	665	42

4.2.1.2 Excited-state Measurements

The photophysical properties concerning the fate of the excited states of the 5,10- and 5,15-substituted *push-pull* porphyrins were obtained from time-resolved photoluminescence (TRPL) studies carried out using a streak camera as presented in Fig. 4.2. A solution of Am1 5,15-1, Am1 5,10-1, SlpE029 and SlpE026 in THF at 0.02 mM concentration was excited at 532 nm and global analysis yielded monoexponential decay components with lifetime of 1.54±0.15 ns, 1.58±0.13 ns, 1.83±0.17 ns and 1.57+0.14 ns, respectively. These values can be attributed to the singlet state lifetime of the porphyrins and are consistent with the literature.[243] Accordingly, although the dipole moment orientation of each porphyrin isomer and the chemical structure of the *meso* units of the porphyrins are different, singlet state lifetime of the porphyrins investigated including the error bars are almost same.

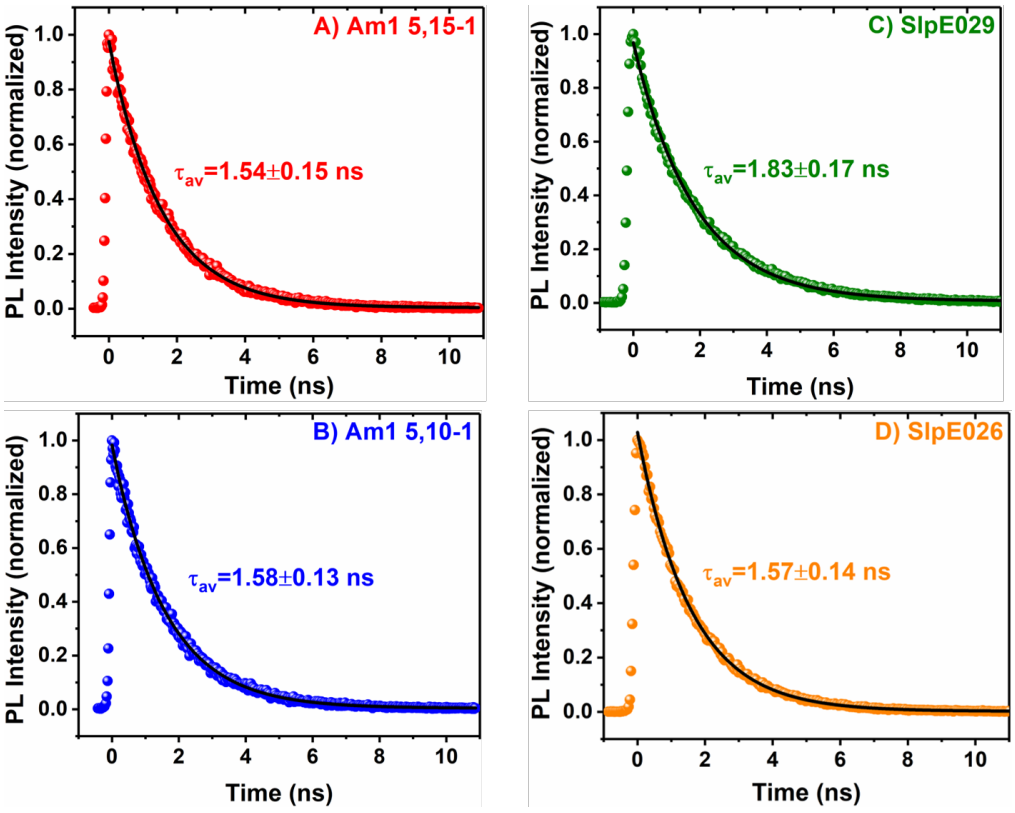

Figure 4.2: Time-resolved photoluminescence decay of the (A) Am1 5,15-1), (B) Am1 5-10-1, (C) SlpE029, and (D) SlpE026 recorded after 532 nm excitation. The time constants extracted at 650 nm for (A) and (B) and at 687 nm for (C) and (D).

Additionally, as can be seen in Fig. 4.2, the time constants extracted at 650 nm for (A) and (B) and at 687 nm for (C) and (D). These values are generally averaged based on 4-5 nm surrounding of $\lambda_{maximum}$ according to each graph or each data. Highly noisy graph can be obtained if only one wavelength value is considered. That's why it is necessary to take the average of the surroundings of the peak wavelength.

In order to determine the lifetime of the triplet state of the four porphyrins, nanosecond transient absorption spectroscopy was performed. Normally, depending on the solvent/electrolyte environment, triplet state lifetimes range from nanosecond to milliseconds for porphyrin molecules.[244] Fig. 4.3 shows the ns-TA spectra of the 5,10- and 5,15-substituted *push-pull* porphyrins after 532 nm excitation. A negative signal indicative of ground-state bleach (GSB) in the range of ~ 400 to 475 nm, as well as a positive signal as excited state absorption (ESA) in the range of ~ 475 nm to 550 nm are formed instantaneously upon excitation. In the case of the Am1 5,15-1 and Am1 5,10-1 porphyrins, we observed ~ 94% recovery in the GSB, whereas the recovery was about ~ 82% for SlpE029 and ~ 79% for SlpE026 within the same time window. These recovery values are based on percentage of peak GSB intensity. ns-TA spectroscopic results of the porphyrins supported the similar findings as already indicated in the steady-state absorption and emission spectroscopy measurements in Fig. 4.3. Accordingly, the greater extent of intramolecular charge transfer from the D group to the A moiety was monitored in the SlpE029 and SlpE026 porphyrins, due to the broadened and red-shifted GSB and ESA spectral features in Fig. 4.3C and D. These spectral features were observed mostly in the SlpE029 porphyrin, which was followed by SlpE026 and then Am1 5,15-1 and Am1 5-10-1 porphyrins with a similar trend behaviour as shown in Fig. 4.3A and B.

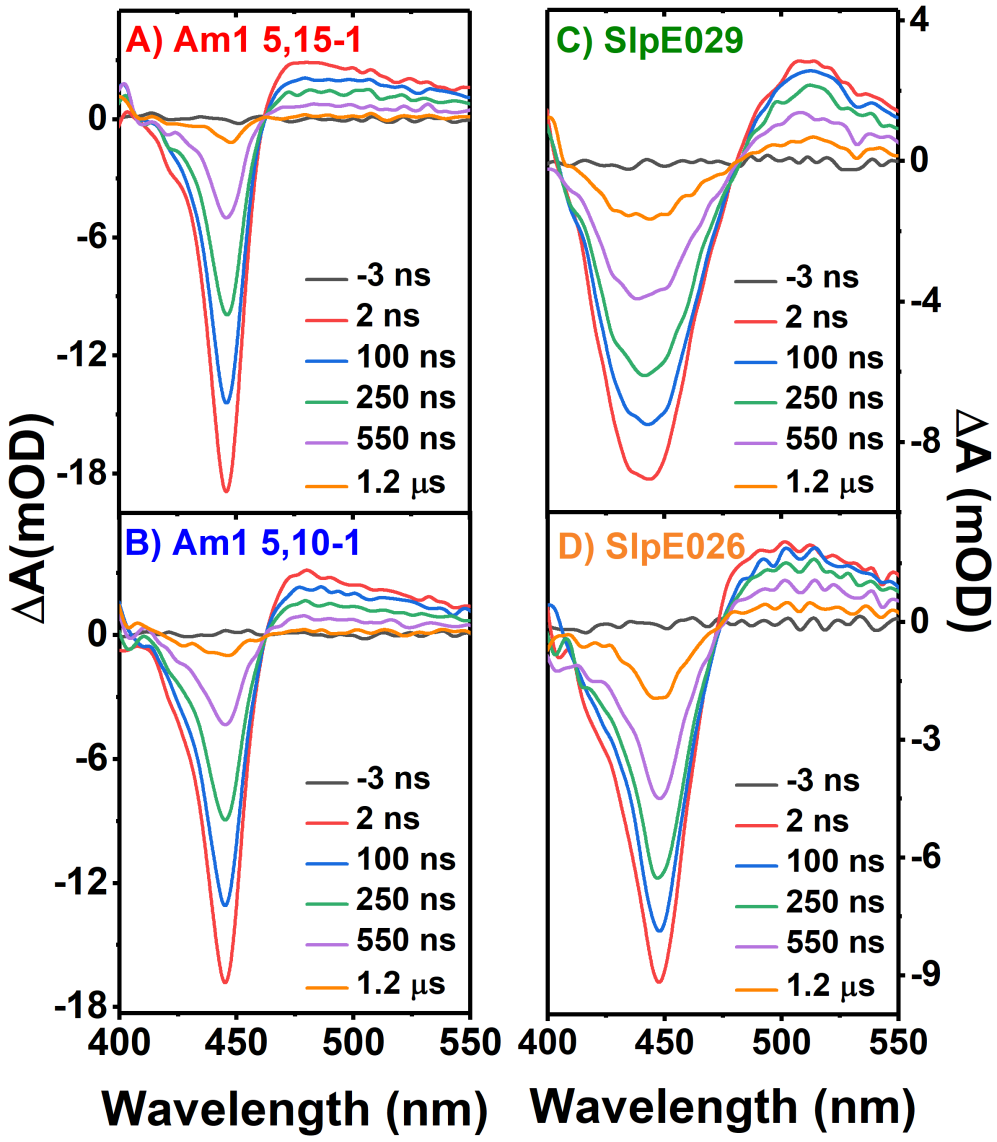

Figure 4.3: Nanosecond transient absorption spectra of the (A) Am1 5,15-1, (B) Am1 5-10-1 (C) SlpE029, and (D) SlpE026 recorded after 532 nm excitation.

Kinetic profiles collected from ns-TA of both GSB at 447 nm and ESA at 500 nm of the 5,10- and 5,15-substituted *push-pull* porphyrins are presented in Fig. 4.4. Applying the global fit to each porphyrin provides a fit described by single exponential decays with time constants (τ) of 450±41 ns, 450±39 ns, 660±55 ns and 750±72 ns for Am1 5,15-1, Am1 5,10-1, SlpE029 and SlpE026, respectively. Accordingly, SlpE026 has the longest triplet state population, followed by SlpE029, and then Am1 5,15-1 and Am1 5,10-1 porphyrins with the almost same triplet state lifetime. It is worth mentioning that the photophysical

characterizations of the porphyrins were done in the present of oxygen using the spectroscopies of steady-state absorption and emission and time-resolved PL using a streak camera and ns-TA so far. Oxygen, possessing a triplet state as ground state, is a very effective quencher of this excited triplet state. Energy is transferred to oxygen in the process of quenching and this leads to the formation of singlet oxygen. The lifetime of the porphyrin is quenched (reduced) in the presence of oxygen.[245] Therefore, as molecular oxygen is known as an efficient quencher of phosphorescence, TA spectroscopy was performed for only one type of porphyrin, SlpE026 to confirm the triplet nature of the porphyrins. The ns-μs TA signal in the absence of oxygen exhibited much slower dynamics (see Fig. A.2) with a time constant of 148±10 μs compared to the signal in the presence of oxygen (Fig. 4.4) with a time constant of 750±72 ns, fully supporting the triplet nature of the long-lived SlpE026 porphyrin.

It is worth to mention that the solid line for the fit has a downwards component is the part of the fitting in Fig. 4.4. This reflects total amplitude of an exponential function. The GSB rise time is more than the temporal resolution of both pump and probe pulses. Step size is earlier 1-5 ns and latter 50 ns up to few μs, then 500 ns for the measurement of ms lifetime.

The TRPL and ns-TA results showed that the singlet state lifetime of the Am1 5,15-1, Am1 5,10-1, SlpE029 and SlpE026 porphyrins were almost the same, but interestingly the longest triplet state population was recorded in SlpE026 porphyrin, followed by SlpE029, and then Am1 5,15-1 and Am1 5,10-1 with almost the same triplet state lifetime. These highly interesting results must obviously be correlated to some extent to different geometries and spin populations in the excited state versus ground state between the porphyrins. In order to conclusively this, high level theoretical calculations, for example using density functional theory (DFT) plus dipole moment calculations will be highly necessary for the paper publication process in the near future working in collaboration with the Ultrafast Laser Spectroscopy and Four-dimensional Electron Imaging research group in KAUST. Due to time constraints, these calculations were not undertaken in this thesis.

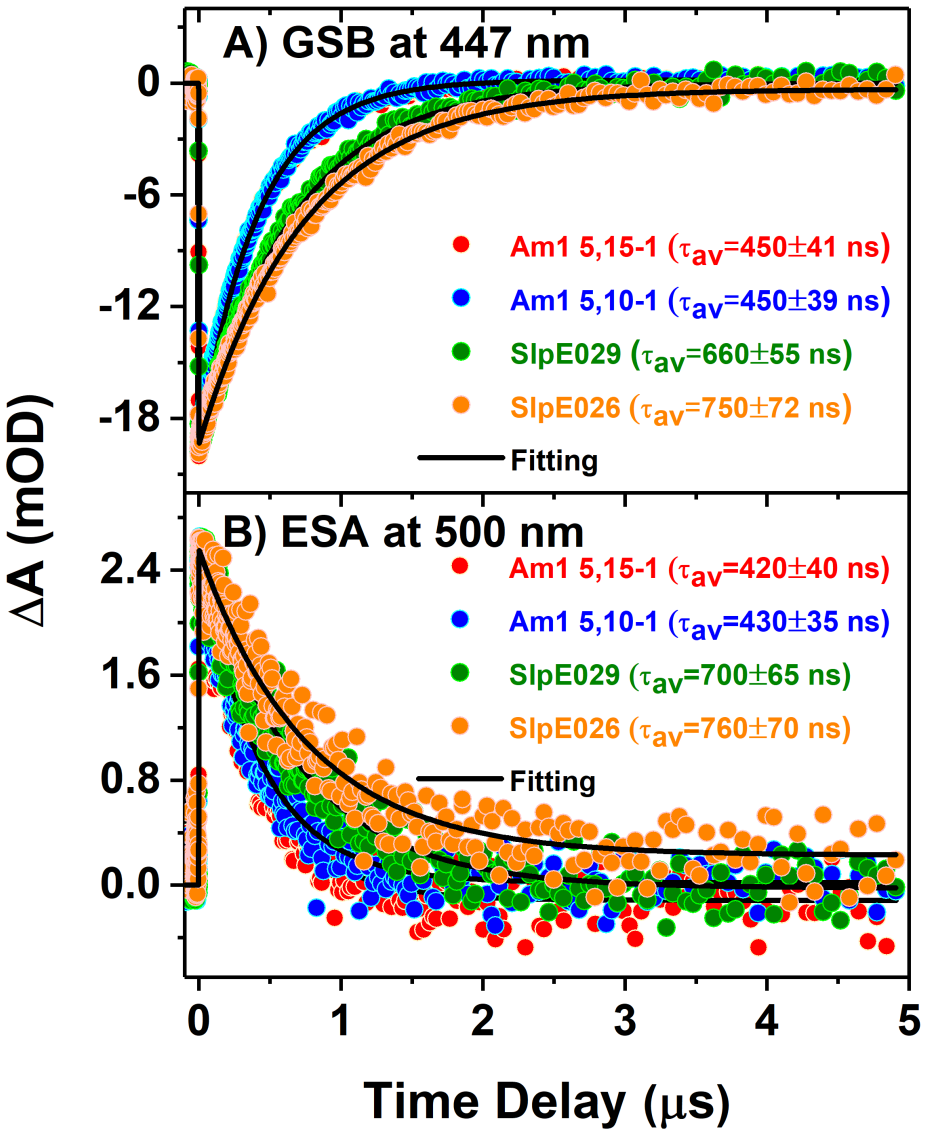

Figure 4.4: Normalized ns-TA kinetics of (A) GSB at 447 nm of the Am1 5,15-1 (red), Am1 5,10-1 (blue), SlpE029 (green), and SlpE026 (orange), respectively, and (B) ESA at 500 nm of the Am1 5,15-1 (red), Am1 5,10-1 (blue), SlpE029 (green), SlpE026 (orange) with the average triplet state lifetimes after 532 nm laser excitation. The black solid lines show the best fits to the acquired data.

4.2.2 Charge Transfer Study between $MAPbI_3$ Perovskite and Porphyrin

Although significant progress has been made in charge transfer (CT) study of various porphyrin-based[237], methylammonium lead triiodide ($CH_3NH_3PbI_3$ or $MAPbI_3$) perovskite-based[246] donor-acceptor systems, CT compounds containing both $MAPbI_3$ and porphyrins have not been reported yet. To investigate whether the present types of

push-pull porphyrins can also act as an electron acceptor in any donor-acceptor systems for the applications of solar energy conversion, we decided to investigate electron transfer (ET) process from $MAPbI_3$ perovskite in film phase to the porphyrin. For this, a case study was conducted with the SlpE026 porphyrin as model system. Based on the longest triplet state lifetime reflected from ns-TA kinetics results and one of the greater extent of charge transfer between D and A groups reflected from spectroscopic results and due to the reason that a classic 5,15-substituted *push-pull* porphyrins, which are used widely as many contemporary porphyrins in DSSCs studies, the SlpE026 porphyrin were chosen.

4.2.2.1 Steady-state Measurements

In order to understand the ground state and excited state interaction between $MAPbI_3$ film and the SlpE026 porphyrin, steady-state absorption and photoluminescence (PL) spectra of $MAPbI_3$ perovskite film were recorded with successive addition of the SlpE026 as shown in Fig. 4.5. As can be seen, the $MAPbI_3$ perovskite film displayed strong absorption from the visible wavelengths down to the near infrared (NIR) range.[247] As illustrated by the absorption spectra in Fig. 4.5(left), no spectral shifts or intensity change were observed on the $MAPbI_3$ film up to SlpE026 (80 fM) concentration. On the other hand, the PL spectra of the $MAPbI_3$ perovskite film was recorded around 775 nm in Fig. 4.5(right) which was also in agreement with the literature value.[248] Note that the $MAPbI_3$ film was selectively excited at 675 nm excitation wavelength, where the absorption of SlpE026 porphyrin can be neglected. It is worth mentioning that there is no spectral overlap between the absorption of the SlpE026 porphyrin and the PL spectrum of the perovskite film. Therefore, ~ 53% PL quenching of perovskite upon addition of SlpE026 porphyrin cannot be attributed to energy transfer in this system. Instead it indicates that the observed PL quenching should be attributed to photoinduced electron transfer (PET) from the $MAPbI_3$ perovskite film to the SlpE026. Here, probability of aggregation of the porphyrin can be excluded as low concentration of the porphyrin was used. It is worth to mention that we monitor the PL quenching of the perovskite film not the porphyrin.

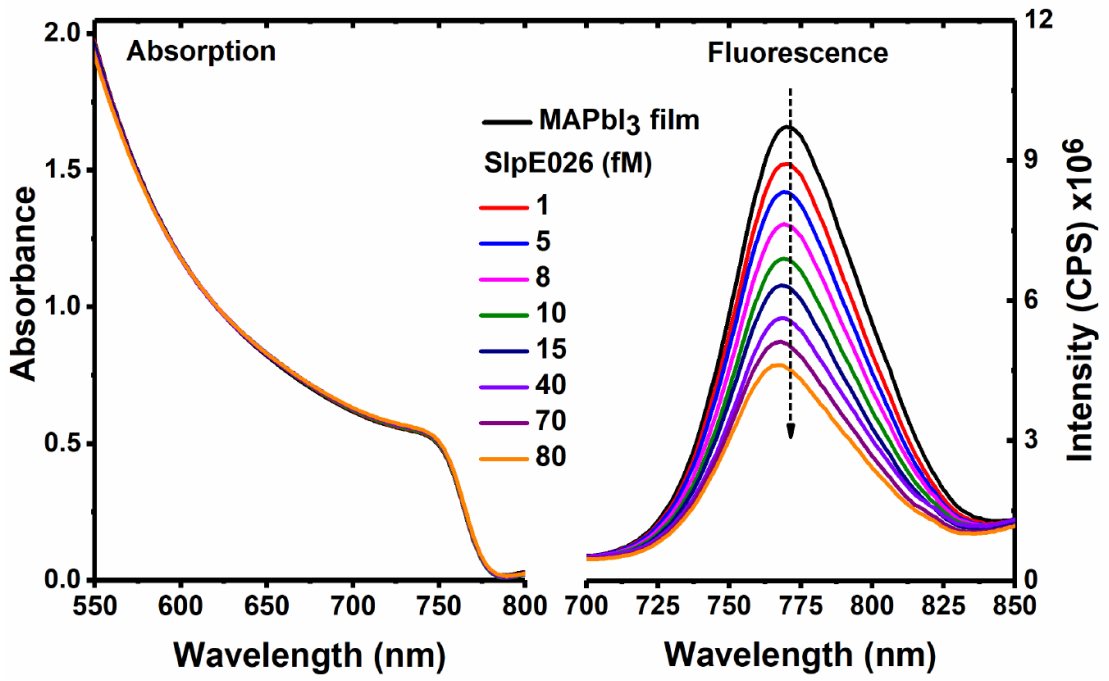

Figure 4.5: Steady-state absorption (left) and emission spectra (λ_{Ex}=675 nm) (right) of $MAPbI_3$ films recorded at different SlpE026 porphyrin concentrations (in fM) in chloroform solution as indicated.

4.2.2.2 Excited-state Measurements

Time-resolved fluorescence experiments using a streak camera with picosecond resolution were carried out in order to obtain physical insight into the reaction mechanism of the PET from the $MAPbI_3$ perovskite film to the SlpE026. Fig. 4.6 shows that the average photoluminescence decay lifetime of the $MAPbI_3$ film was changed from 1.69±0.15 μs to 0.52±0.05 μs after 80 fM addition of the SlpE026. Considering the apparent change in lifetime on the μs time scale with the addition of the SlpE206, we can conclude that there was an electron injection from the $MAPbI_3$ perovskite film to the SlpE026 porphyrin on the ns time scale. Considering the PL decays time durations of the $MAPbI_3$ perovskite film in the absence and presence of the SlpE026, repetition rate of the measurement is adjusted to 100 KHz leading to the suppressing of the background effects as shown for the time before <0 s in Fig. 4.6. It is also worth to mention that red and blue data show the photoluminescence decays of the perovskite film in the absence and presence of the SlpE026, respectively taken at λ=770 nm (this value is averaged based on 4-5 nm

surrounding of λ_{max} according to the data to prevent highly noisy graph) in Fig. 4.6C. Also, the PL decays were fitted with single exponential function where the chi-square values are found as >0.99 for both cases. The PL lifetimes for these fittings are shown as τ_{av}.

To elucidate the behaviour of the charge carrier lifetime, femtosecond transient absorption measurement has been performed in 725-875 nm spectral region after 640 nm optical excitation. The fs-TA spectra at different time delay of only $MAPbI_3$ perovskite film and $MAPbI_3$ perovskite film with 80 fM concentration of the SlpE026 porphyrin are plotted in Figure 4.7A and B, respectively. The TA spectra of $MAPbI_3$ film shows different transient features: a photo induced transient bleach in the spectral range of 765-815 nm. The feature at 778 nm can be assigned to transient bleaching of the band edge transition and laser-induced fluorescence. A wide size distribution is responsible for the broadening of the TA bleach signal. In addition to that a broad photoexcited absorption is noticed below 765 nm which can be attributed to excited state absorption of free lead(II) iodide (PbI_2) [249]. The fs-TA spectra of $MAPbI_3$/SlpE026 show similar pattern like $MAPbI_3$ perovskite film however, their attributions are different. Upon addition of SlpE026 on the $MAPbI_3$ film, the bleach (band edge as well as the stimulated PL) recovers at a faster rate. Femtosecond TA normalized kinetics can easily be distinguished by comparing the TA dynamics which are discussed in the next figure. The faster bleach recovery of the $MAPbI_3$ in presence of SlpE026 clearly indicates photoinduced electron transfer (PET) from perovskite film to the acceptor porphyrin molecule (the perovskite film gives its electron to the porphyrin via its conduction band). It is worth mentioning that there is no signal coming from the SlpE026 porphyrin (no intrinsic response of the porphyrin) at this excitation wavelength. fs-TA spectra of 80 fM SlpE026 in chloroform solution onto the glass substrate are shown in Fig. A.3.

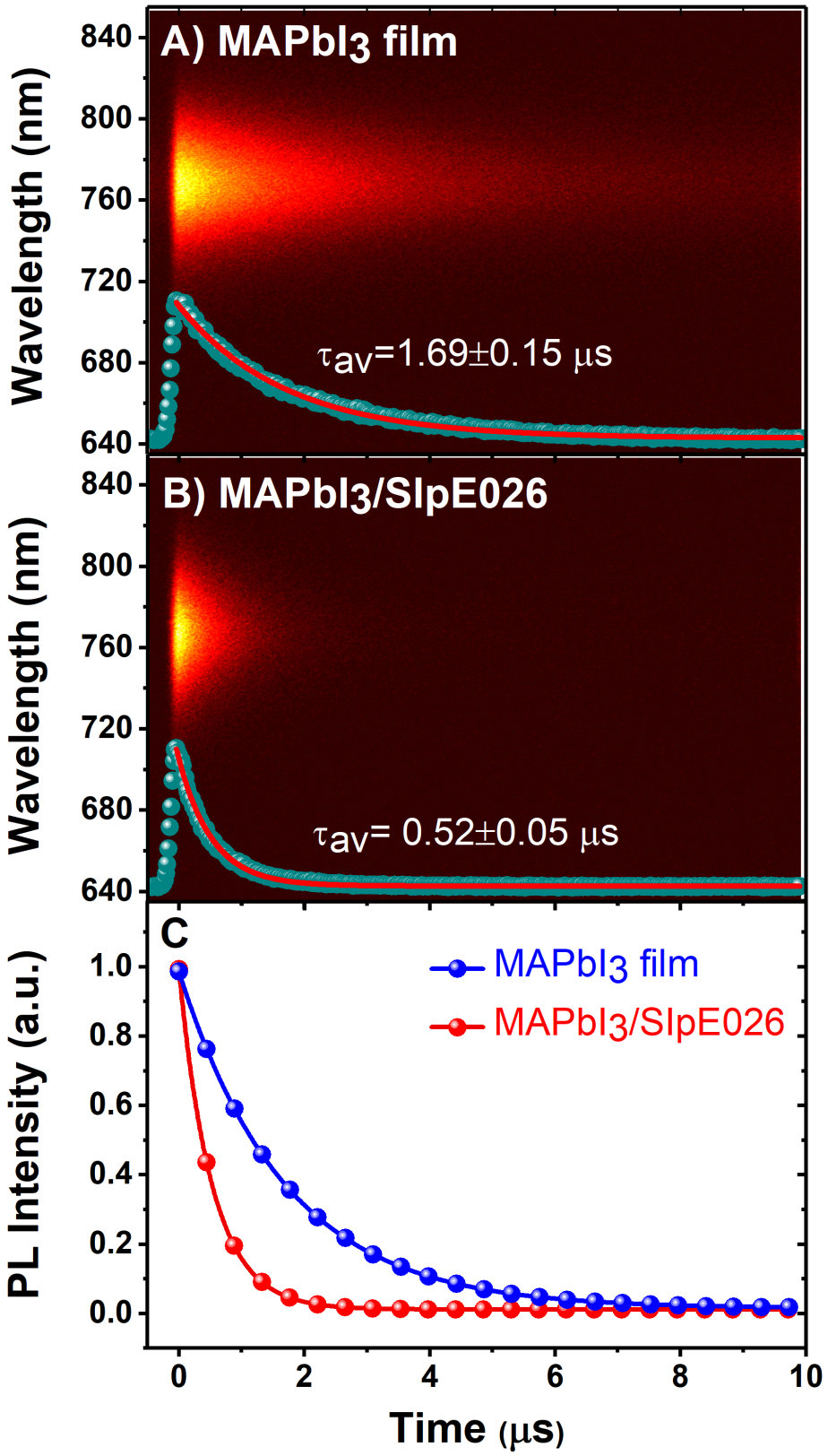

Figure 4.6: Time-resolved photoluminescence decay of the (A) $MAPbI_3$ film, and (B) $MAPbI_3$/SlpE026 with the average time constants recorded after 650 nm excitation. The time constants extracted at 770 nm.

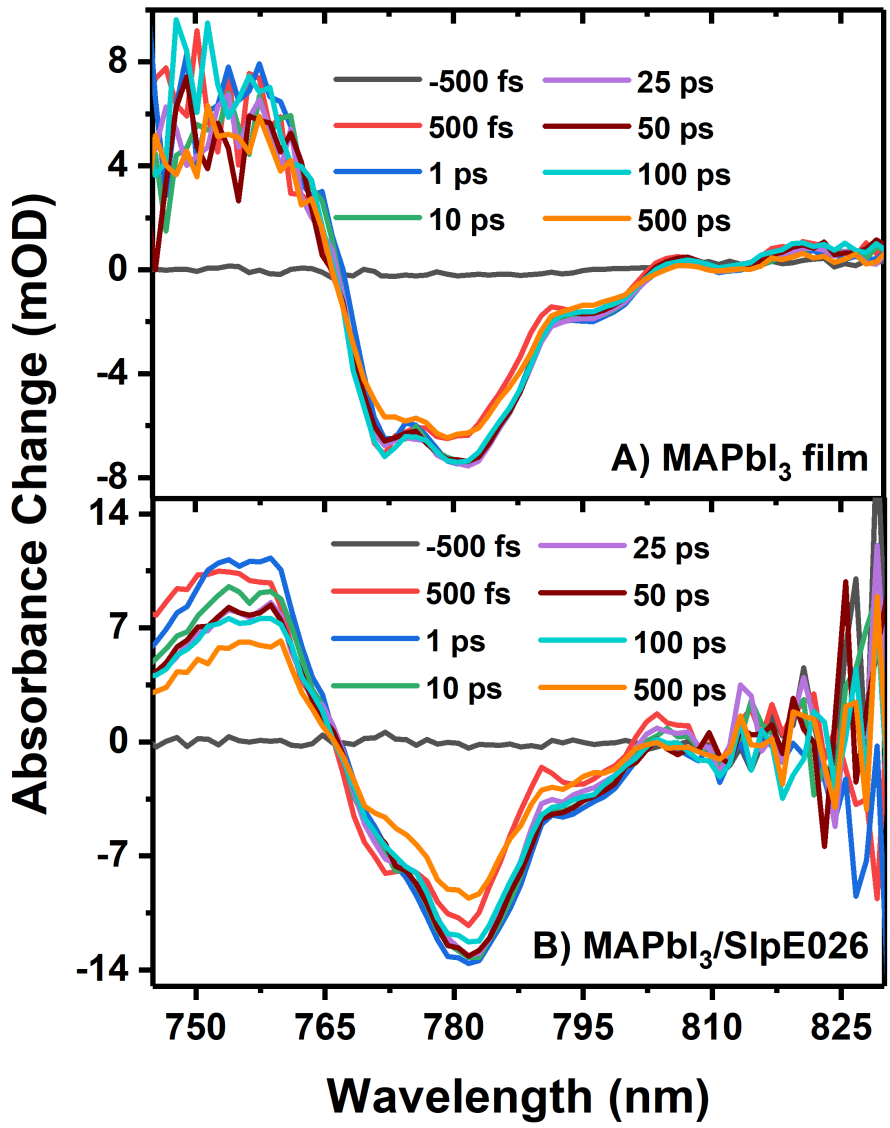

Figure 4.7: Femtosecond transient absorption spectra recorded after 650 nm pulsed-laser 120 fs excitation for (A) the $MAPbI_3$ film, and (B) $MAPbI_3$ film with 80 fM the SlpE026 in chloroform solution.

Femtosecond (fs) transient absorption kinetics are also presented to investigate the reaction mechanism of the PET from the $MAPbI_3$ perovskite film to the SlpE026 in Fig. 4.8. Fig. 4.8A shows the bleach recovery kinetics normalized at t= 0 ps time delay. The bleach probed at 778 nm has a growth component up to 3.5±0.3 ps time window represented as τg. The kinetics of the perovskite film can be fit exponentially with a time constant of 1.9±0.1 ns. Upon addition of 80 fM SlpE026 the growth component has completely disappeared also. GSB recovers at a faster rate than only $MAPbI_3$ film alone. Similarly, the

GSB recovery of $MAPbI_3$/SlpE026 fits an exponential function with a time constant of 1.1±0.1 ns. Absence of the growth components and fast bleach recovery can be attributed to electron transfer from the $MAPbI_3$ perovskite film to the SlpE026 porphyrin. We also monitored the kinetics at 794 nm (Fig. 4.8B; due to stimulated emission) of the same system. Both kinetics can be fit single exponentially with time constants of 1.6±0.1 ns and 0.9±0.08 ns, respectively for $MAPbI_3$ film and $MAPbI_3$/SlpE026.

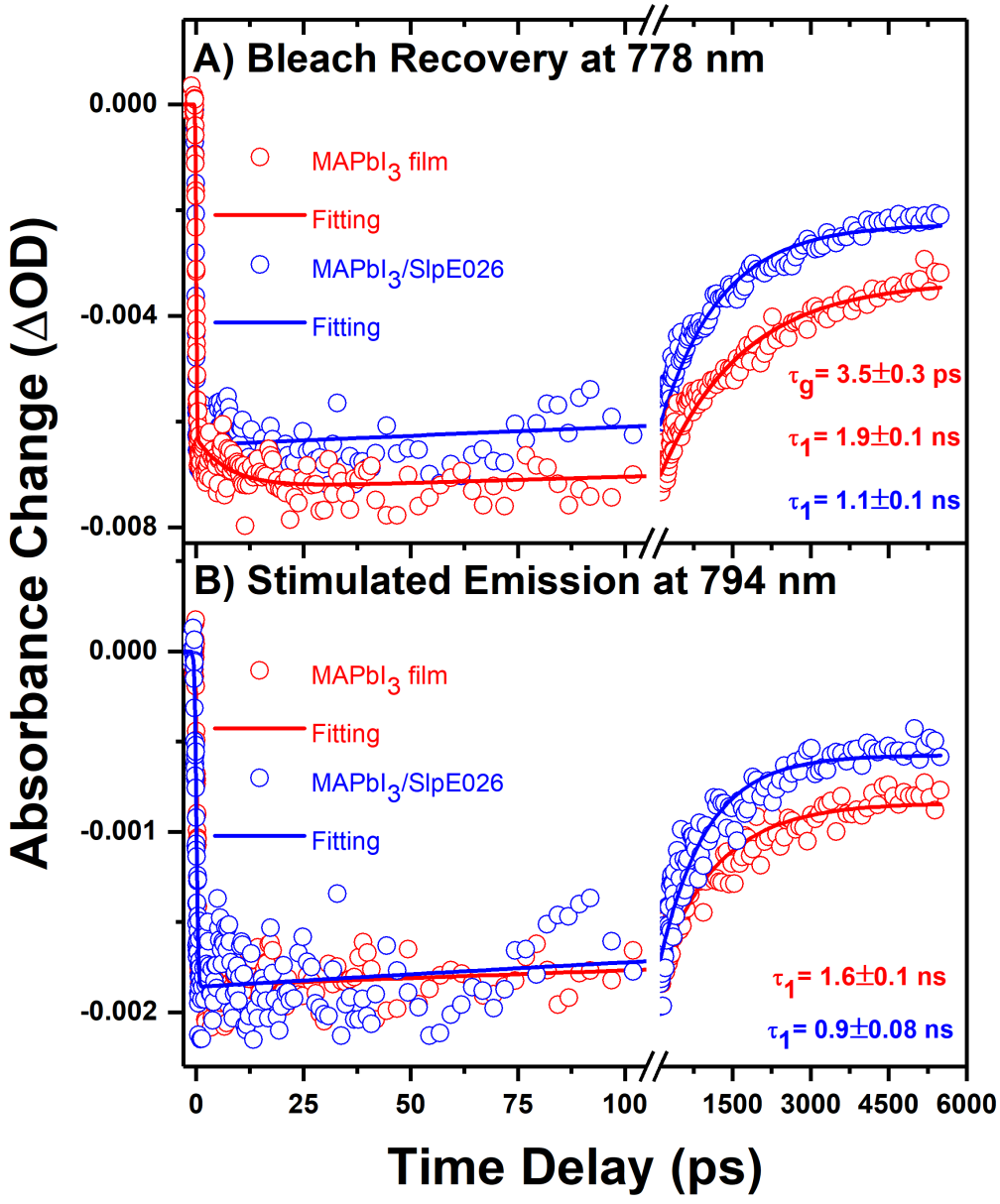

Figure 4.8: Normalized fs-TA kinetics of (A) bleach recovery at 778 nm of the $MAPbI_3$ film (red) and $MAPbI_3$/SlpE026 (blue) and (B) stimulated emission at 794 nm of the $MAPbI_3$ (red) and $MAPbI_3$/SlpE026 (blue) after 650 nm laser excitation.

4.3 Conclusion

In summary, ultrafast photophysics including intersystem crossing of newly synthesized unsymmetrically 5,15-disubstituted porphyrins (Am1 5,15-1 and SlpE026), which have a dipole running along the *meso-meso* axis, and their 5,10-disubstituted counterparts (Am1 5,10-1 and SlpE029) with the dipole moment along the β-β axis was explored using time-resolved transient absorption and photoluminescence spectroscopy. The greater extent of intramolecular charge transfer between the electron donor and acceptor moieties was most observed in the SlpE029 porphyrin, which was followed by SlpE026 and then Am1 5,15-1 and Am1 5,10-1 porphyrins using steady-state absorption and emission spectroscopy and ns-TA spectroscopy results of the porphyrins were also supported by similar findings due to the broadened and red-shifted GSB and ESA spectral features. Similar singlet state lifetime was monitored for all of the porphyrins using TRPL spectroscopy, but interestingly the longest triplet state population was recorded in SlpE026 porphyrin, followed by SlpE029, and then Am1 5,15-1 and Am1 5,10-1 with almost the same triplet state lifetime using ns-TA spectroscopy. Additionally, a case study was conducted with the SlpE026 porphyrin as a model system to investigate the capability of the present types of *push-pull* porphyrins to accept the electron from the $MAPbI_3$ perovskite film. Electron transfer process from $MAPbI_3$ perovskite in film phase to the porphyrin was demonstrated for the first time using steady-state emission, time-resolved transient absorption and photoluminescence spectroscopy. Here, the probability of energy transfer can be excluded as there is no spectral overlap between the absorption spectra of the porphyrin and PL spectrum of the $MAPbI_3$ perovskite film.

CHAPTER 5: Ultrafast Charge Transfer Interaction between Nanocarbon Materials and Porphyrins

5.1 Introduction

Investigation of interfacial charge transfer between the donor (D) and acceptor (A) is one of the major topic of research interest in photovoltaic and light emitting application due to its direct relation in photocurrent conversion efficiency.[27, 28, 250-254] Especially, sheer endless chemical and physical features are provided with the structural diversity of organic building blocks. The toolbox for building a wide palette of carbon allotropes is offered by changing the periodic binding motifs in sp^3-, sp^2-, and sp hybridized networks.[142] For this purpose, to investigate the physicochemical characteristics of nanocarbons in reduced dimensions starting with the advent of 0D fullerenes, followed by 1D carbon nanotubes and by 2D graphene, the past quarter century has served as a test-bed.[255-257] Due to the fact that the probabilities of arranging electronic and structural features of carbon-based materials are limitless, their function in charge-transfer systems is gaining importance.[258] As carbon nanostructures are easily acquired from natural products, they can maintain to contribute toward future energy supply in terms of sustainability.[259-261] Costly rare-earth metals and/or toxic materials existent in contemporary electronic devices can be replaced with carbon nanostructures thanks to their rich electrochemical characteristics.[262]

There has been significant interest to study of molecular-scale carbon-based hybrid materials that could be used in optoelectronic applications.[122, 142, 147, 148, 263, 264] Porphyrins possess good light-harvesting features owing to high molecular extinction coefficient of their Soret and Q-bands in the UV/Vis spectra. They exhibit unique photophysical and electrochemical characteristics that are tuneable by changing the *meso*-functional groups and via interactions with metal atoms[28, 265] and they have been broadly used to decorate carbon materials such as fullerene and graphene[266].

Furthermore, photoinduced electron transfer processes with carbon-based materials for the

development of optoelectronic devices can be supported by the electron-donor character of porphyrins.[267-269] Porphyrins and nanocarbon structures are one of the most promising components in terms of constructing new materials for future electronic devices.[270-272] To form a donor (D)-acceptor (A) system, hybrid materials based on these two classes of materials together can be used in energy conversion applications.[269, 273, 274] The D-A system performs through π-π interactions, and porphyrin structure and the charge on the surface of the nanocarbon material have an important role in this system.[275, 276]

In the present work, two different 5,15-donor-acceptor-subsituted *push-pull* porphyrins selected were: [10,20-bis(3,5-di-*tert*-butylphenyl)-5-(4-carboxyphenylethynyl)-15-(N,N-dimethylanilinyl)porphyrinato]zinc(II) (Am1 5,15-1) and {5-[bis(4-*tert*-butylphenyl)amino]-15-(4-carboxyphenylethynyl)-10,20-bis(2,6-dioctyloxyphenyl)porphyrinato}zinc(II) (SlpE026) (see Fig. 3.1). It is worth noting that these two porphyrins have same electron acceptor group (4-carboxyphenylethynyl), but they possess different electron donor (*N,N*-dimethylanilinyl for Am1 5,15-1 and bis(4-*tert*-butylphenyl)amino for SlpE026), and chemical groups on the *meso* units of the porphyrin cavity. Here, the dipole is along the *meso-meso* axis for both porphyrins. Molecules of this type are in contemporary use in dye-sensitized solar cells (DSSCs) studies, nonlinear optics and more, and further allow a comparison of the impact of different orientations of the molecular dipole moment on photophysical properties.[77] We investigated the ground-state and excited-state interactions of non-covalent association between these neutral porphyrins and nanocarbon materials (neutral C_{60} fullerene and negatively charged graphene carboxylate (GC)) using steady-state spectroscopy and state-of-the-art transient absorption (TA) spectroscopy with broadband capabilities. The affinity of each porphyrin on each nanocarbon surface was indicated by steady-state absorption and emission spectroscopies, and the efficiency of quenching of the porphyrin fluorescence was monitored. Stern-Volmer plots demonstrated a combination of diffusion-controlled (dynamic) and static mechanisms for porphyrin/C_{60} hybrids and static mechanism for porphyrin/GC hybrids. Time-resolved femtosecond (fs) and nanosecond (ns) TA measurements also performed to validate the electron transfer

process in this porphyrin/nanocarbon hybrid interface.

5.2 Results and Discussion

5.2.1 Steady-state Measurements

The main aim of the present study was to investigate the charge transfer interaction between two newly synthesized porphyrins (Am1 5,15-1 and SlpE026) with different polymorph of nanocarbon (fullerene, C_{60} and graphene carboxylate, GC). Studies on the porphyrin nanocarbon interactions using C_{60} and GC were carried out in NMP (N-methyl-2-pyrrolidone) and THF:H_2O mixture [1:1 v/v], respectively, owing to better solubility. Figure 5.1 and 5.2 represent steady-state absorption and emission spectrum changes for the investigated porphyrins (Am1 5,15-1 and SlpE026) at 0.002 mM fixed concentration with successive additions of C_{60} in NMP and GC in THF:H_2O mixture [1:1 v/v], respectively. In the absence of nanocarbons the two characteristic bands, Soret and Q-bands, of Am1 5,15-1 and SlpE026 are clearly depicted. The Soret and two Q-bands of Am1 5,15-1 in NMP and THF:H_2O mixture [1:1 v/v]mixture appear at 449 nm and 583 and 634 nm; and 446 nm and 579 and 630 nm, respectively (Figure 5.1A and 5.2A left panels, respectively). Similarly, for SlpE026 the Soret and two Q-bands in NMP and THF:H_2O mixture [1:1 v/v] appear at 452 nm and 582 nm and 645 nm; and 449 nm and 581 nm and 641 nm, respectively (Figure 5.1B and 5.2B left panels, respectively). Increasing the amount of added studied nanocarbon materials (C_{60} and GC) successively into the both Am1 5,15-1 and SlpE026 solutions caused the absorption to increase in the region, due to the absorption of the C_{60} and GC in the same spectral region. Upon addition of C_{60} and GC, the intensity of the Soret band of both porphyrin/nanocarbon mixtures are decreased significantly, while the Q bands in the same solutions become almost unnoticeable. The formation of the Am1 5,15-1/C_{60}, SlpE026/C_{60}, Am1 5,15/GC and SlpE026/GC nanohybrids and interactions between each hybrid are supported based on the ground-state absorption spectrums of porphyrin/nanocarbon solutions contain characteristics of both porphyrin and nanocarbon material[277]. The background to lower wavelength all cases is the increased absorbance due to scattering. Because, with successive addition of C_{60} and GC separately until reaching the final concentration, a monotonically decreased broad signal from the UV to the visible

region is observed which refers to the signal of the tested nanocarbons (see Fig. A.4). In the meantime, the characteristic peaks of the studied porphyrins in the Soret and Q bands region are still visible in less intensities. The intensity of the Soret and Q bands are slightly more distinctive in Am1 5,15-1/C_{60} and Am1 5,15-1/GC solutions at saturated concentration in Fig. 5.1A and 5.2A as compared to the SlpE026/C_{60} and SlpE026/GC hybrids in Fig. 5.1B and 5.2B. It is worth noting that the neutral porphyrin could not form any ground-state charge transfer (CT) complex with the nanocarbon due to weak electrostatic interaction. However, we noticed in the earlier work[147] the positively charged porphyrin could form CT complex with GC owing to strong electrostatic interaction and π-π stacking interactions[275].

To further investigate the non-covalent interactions between the novel porphyrins and nanocarbon materials, steady-state photoluminescence (PL) measurements were performed. Fig. 5.1A and 5.1B (right panels) illustrate the emission spectra of Am1 5,15-1 and SlpE026 measured after excitation at 625 nm in the presence of C_{60} at different concentrations, while the emission spectra of the same porphyrins are tested after excitation at 600 nm upon increasing the concentration of GC as illustrated in Fig. 5.2A and B (right panels). The emission of both porphyrins is successively quenched with the addition of C_{60} and GC specified a strong excited state association resulting in the generation of weak or non-luminescent hybrids. At a C_{60} concentration of 0.346 mg/mL, the quenching efficiencies are estimated to be 84% and 73% as well as 2 nm and 5 nm redshift for Am1 5,15-1 and SlpE026, respectively. On the other hand, the estimated efficiencies of quenching are 96% and 91% with 4 nm and 7 nm redshift for Am1 5,15 and SlpE026, respectively at a GC concentration of 0.750 mg/mL. On the basis of this information, slightly larger red shifts are examined in the emission spectrums of porphyrin/GC hybrids compared to the porphyrin/C_{60} hybrids. The shifts in the emission spectra are reflected in the degree of complexation or interaction. In the case of Am1 5,15-1/GC and SlpE026/GC, the interaction is slightly larger than the interaction between the same porphyrins and C_{60}. We also observed that the fluorescence quenching of Am1 5,15-1 is slightly more efficient than SlpE026. Regarding to the small variation in the fluorescence

quenching efficiency of the investigated porphyrins can be related to differences in the intermolecular contacts between porphyrin and nanocarbon. Steady-state measurements show that slightly changing the structure of the porphyrins from the *meso*-units does not change much the interaction with nanocarbon materials.

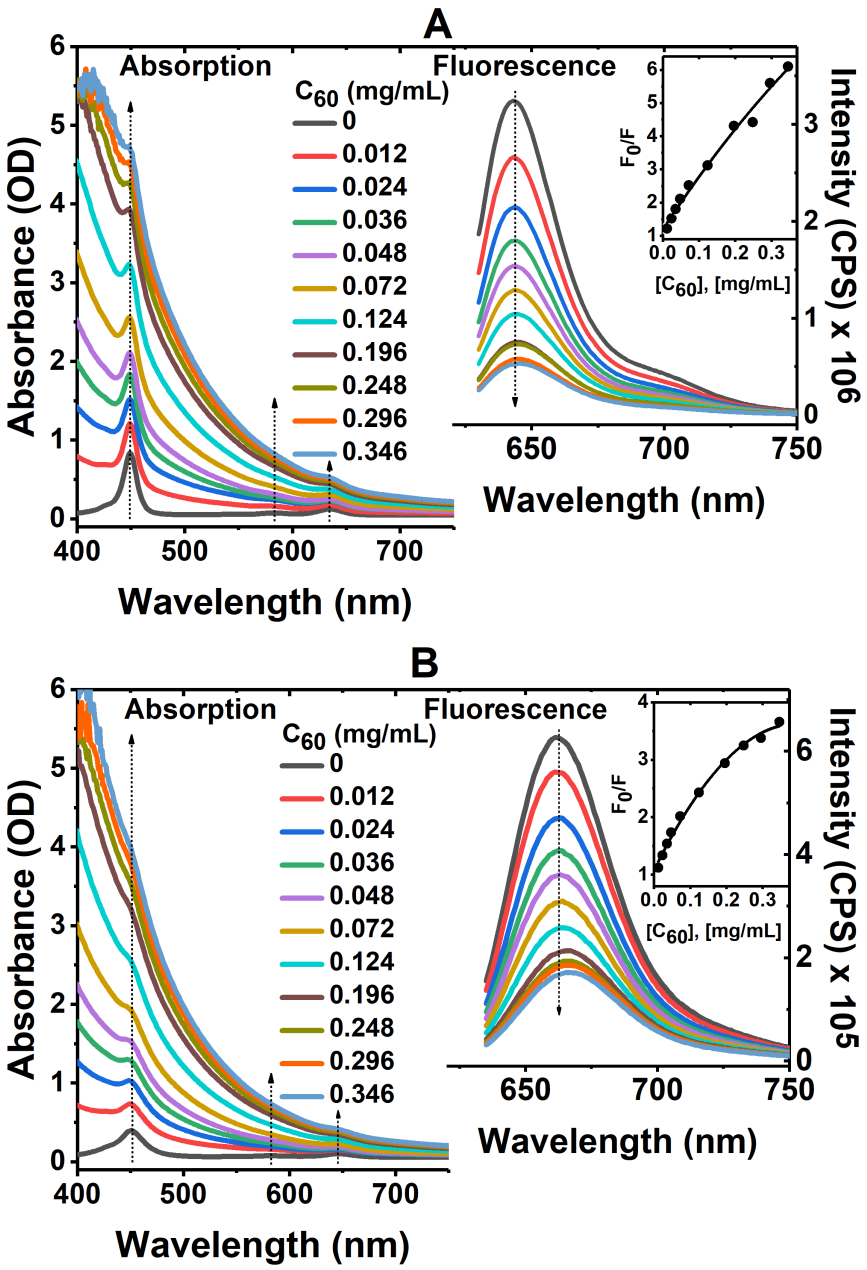

Figure 5.1: Steady-state absorption (left) and emission spectra (λ_{Ex}=625 nm) (right) of (A) Am1 5,15-1 and (B) SlpE026 recorded at different C_{60} concentrations (in mg/mL) as indicated. The Stern-Volmer plots as a function of the C_{60} concentration of each porphyrin are showed in the insets.

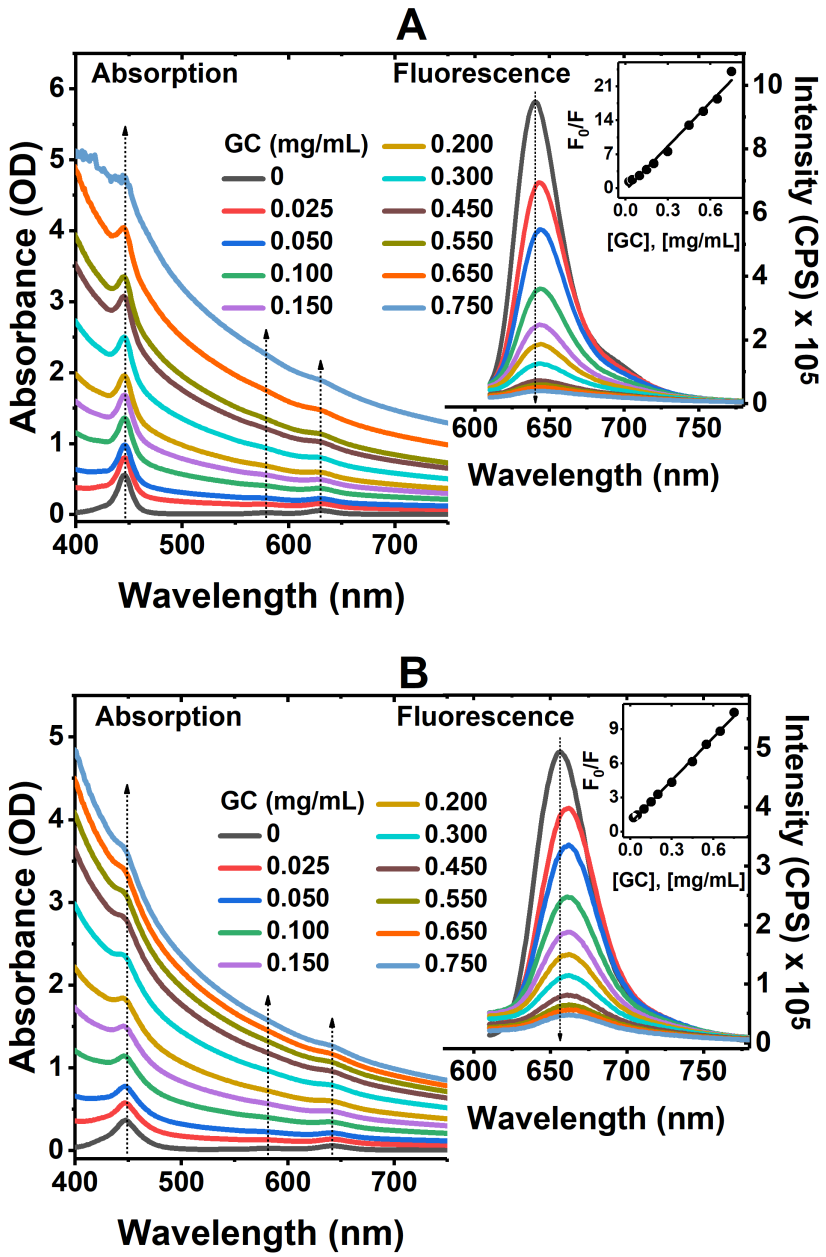

Figure 5.2: Absorption (left) and fluorescence after excitation at 600 nm (right) of (A) Am1 5,15-1 and (B) SlpE026 recorded at different GC concentrations (in mg/mL) as indicated. Insets show the respective Stern-Volmer plots.

To gain insight into the nature of quenching, we have constructed Stern-Volmer plots of the emission quenching of Am1 5,15-1 and SlpE026 upon association with C_{60} as illustrated in the insets of Fig. 5.1A and B, respectively. Each data plot shows an upward curvature with increasing C_{60} concentration, which demonstrates a combined effect from both diffusion-controlled (dynamic) and static mechanisms in the excited-state deactivation.[278]

Stern-Volmer plots were also used to investigate the quenching mechanism of Am1 5,15-1 and SlpE026, respectively by GC in the right panels of the insets in Fig. 5.2A and B. Based on a linear correlation with the increasing GC concentration, it is revealed that quenching progresses according to a static mechanism in porphyrin/GC mixture.[278, 279] The efficient PL quenching can be attributed due to electron and/or energy transfer from the photoexcited porphyrin to the nanocarbon. To evaluate this, we perform femtosecond and nanosecond transient absorption spectroscopy as demonstrated in the following section.

5.2.2 Excited-state Measurements

Direct and comprehensive knowledge about the excited-state dynamics such as excited-state charge transfer (CT), charge separation (CS), and charge recombination (CR)[280-283] of the non-covalent interactions of Am1 5,15-1 and SlpE026 with C_{60} and GC are provided by fs-TA spectroscopic measurements. Fig. 5.3 and Fig. 5.4 show the fs-TA spectra with broadband capabilities within a 120-fs temporal resolution for Am1 5,15-1 and SlpE026 in the absence and presence of C_{60} and GC, respectively after 640 nm optical excitation, which mainly excites the porphyrins. For clarity, the differential spectra against the reference of the 550 fs and 650 fs spectrum and the differential spectra against the reference of the 250 fs and 725 fs spectrum, respectively are displayed in Fig. A.5 and A.6. Upon analysing the TA spectra in different time domains, strong negative absorption bands, which related to the ground state bleach (GSB) of the Soret band, are observed at 449 and 451 nm, respectively for Am1 5,15-1 and SlpE026 in NMP. Immediate after GSB, a broad excited state absorption (ESA) is extending up to 550 nm (Fig. 5.3A and C). Similar to NMP, the fs-TA measurements of these newly synthesized porphyrins were performed in THF:H_2O mixture following 640 nm optical excitation as shown in Fig. 5.4A and C, respectively. The GSB and ESA bands are also associated with time delay in similar pattern like NMP. The TA spectra illustrate the characteristic peaks of the porphyrin molecule.[147-149, 284, 285] However, the spectral shift is due to the presence of different functional moieties. The ESA band of Am1 5,15-1 and SlpE026 shows long-lived, which can be attributed to the excited triplet state absorption.[148, 286] fs-TA study shows within 5.5 ns time scale (see Fig. A.7) the GSB recovers by <30% to its ground state and the excess photoexcited porphyrin

decays into the long-lived triplet state through intersystem crossing that is in good agreement in the literature. [148, 149, 285, 286] The excited triplet state lifetime was calculated from ns-TA measurements, which is demonstrated in next section.

To get into details charge transfer interaction between free porphyrin and porphyrin-nanocarbon, fs-TA measurement has been performed with identical experimental conditions, which are illustrated in Figure 5.3B and D (porphyrin/C_{60}) and Figure 5.4B and D (porphyrin/GC). Upon addition of C_{60} and GC no spectral deviation is noticed; however, GSB recovery and decay of ESA follow differently.

From Figure 5.3B and D, it is clear that the GSB and ESA of Am1 5,15-1/C_{60} and SlpE026/C_{60} recover and decay, respectively faster than only porphyrin, which can be attributed as electron transfer from the photoexcited porphyrin to the C_{60}.[147, 148, 287] The spectroscopic signature in the ESA region of the Am1 5,15-1/C60 and SlpE026/C60 in Fig. 5.3B and D is the signature of porphyrin cation radical. This clearly indicates that CT occur because of formation of the porphyrin$^{\bullet+}$ cation radical. During the electron transfer process, there is usually a fast change in GSB recovery, because of the recombination of the donor and acceptor systems. After photo-excitation, an electron transfer will be occurred from the porphyrin to the C_{60} to form a charge separated state, which will later combine to generate the neutral or the initial state[288]. In the case of Am1 5,15-1/C_{60} and SlpE026/C_{60}, we see that a separation is followed by an electron transfer. For this reason, we do not see an efficient change within this time for the GSB. Because, the electron is in the C_{60} propagates far from the surface and has not gone back yet to Am1 5,15-1 and also SlpE026 to see recovery[289]. Similar to C_{60} interaction, the bleach recovery of the porphyrin takes place a faster rate with GC; however, decay of ESA shows reversely. Further studies were conducted by comparing the kinetics traces of the porphyrins in the presence and absence of the nanocarbon.

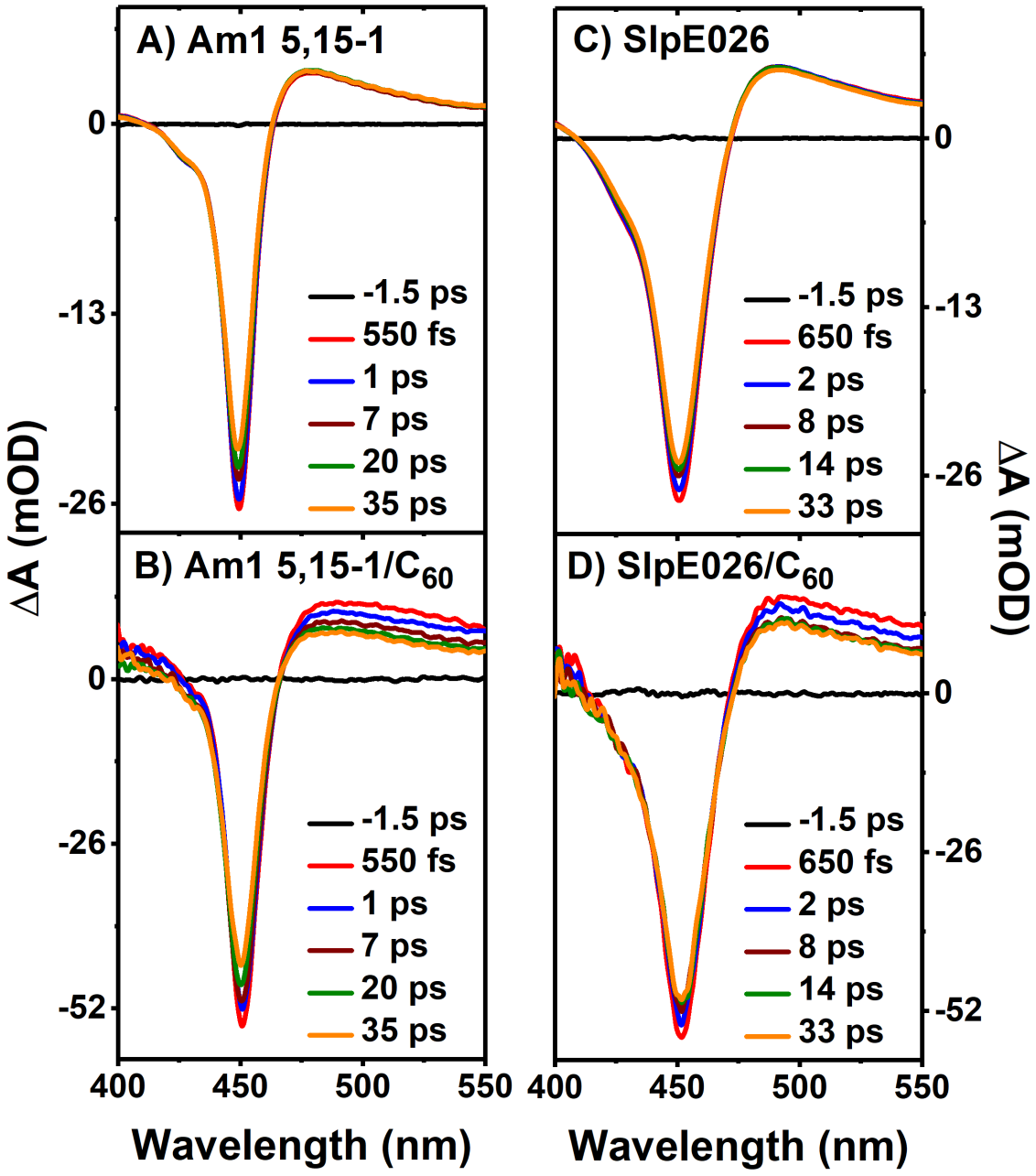

Figure 5.3: fs-TA spectra recorded after 640 nm optical excitation for (A) Am1 5,15-1, (B) Am1 5,15-1/C_{60}, (C) SlpE026, and (D) SlpE026/C_{60}.

Additionally, it is worth to mention here that the absorbance change of the porphyrins in the absence and presence of nanocarbons in the results of TA spectroscopy can be explained as the difference in the concentration or experimental condition. Here, we are not interested in the changes in the intensity. Because, the electron transfer process is monitored by comparing the dynamics.

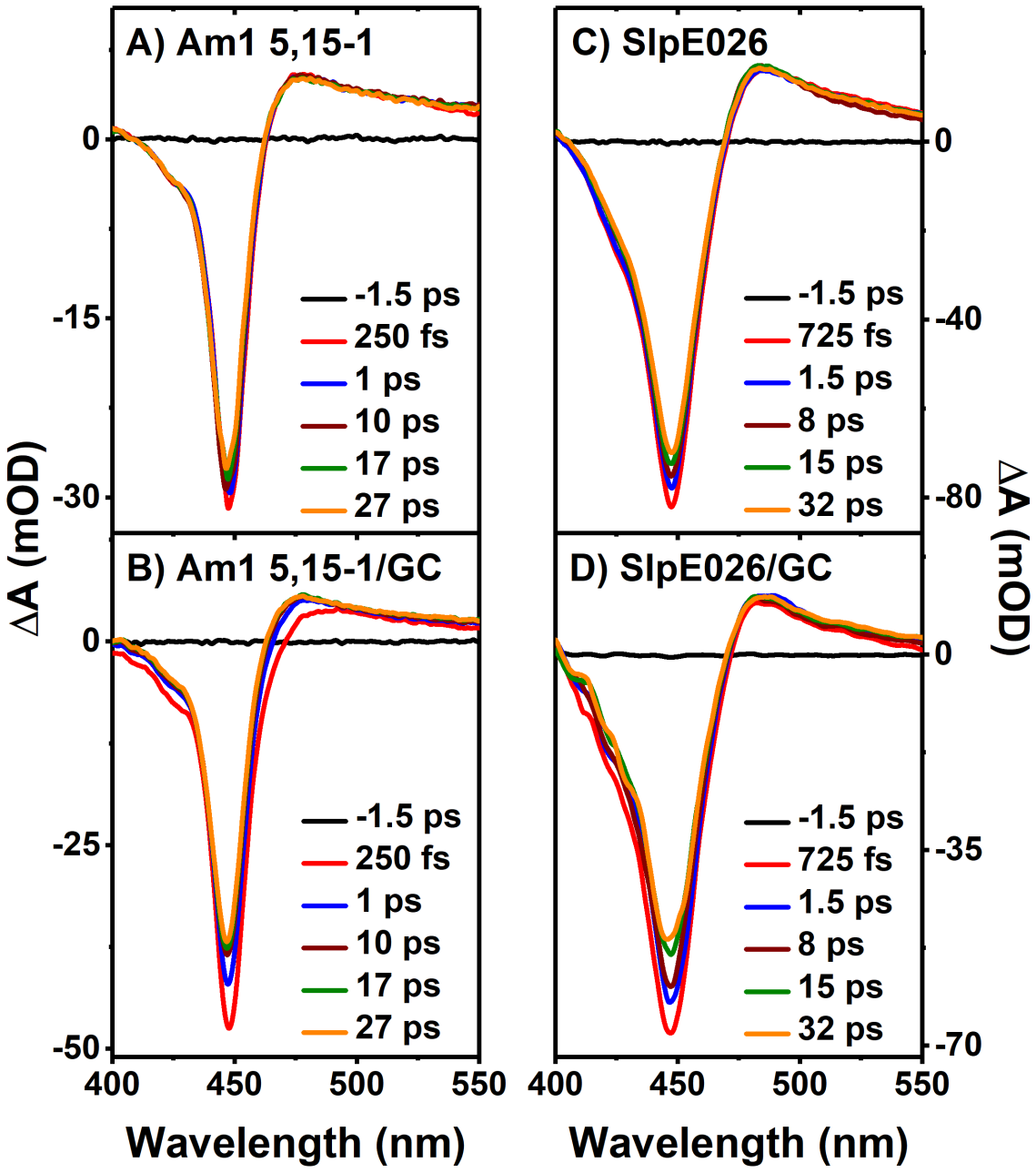

Figure 5.4: fs-TA spectra of (A) Am1 5,15-1, (B) Am1 5-15-1/GC, (C) SlpE026, and (D) SlpE026/GC recorded after 640 nm optical excitation.

Association of kinetics traces of Am1 5,15-1 and SlpE026 in the absence and presence of C_{60} in NMP is depicted in Figure 5.5. The kinetics are plotted up to 200 ps time window to visualize the change. The GSB of Am1 5,15-1 and SlpE026 probed at 450 nm can be fit using bi-exponential decay functions (see Table 5.1), which has a fast component of (20±1.5 ps in NMP and 3±0.2 ps in THF:H_2O mixture for Am1 5,15-1; 3±0.2 ps in NMP and 4±0.2 ps in THF:H_2O mixture for SlpE026) and a long time constant of (1.1±0.1 ns

in NMP and 509±50 ps in THF:H_2O mixture for Am1 5,15-1; 2±0.2 ns in NMP and 2±0.2 ns in THF:H_2O mixture for SlpE026). The short time component can be attributed to non-radiative de-excitation through intermolecular H-bonding through the carboxylate group, while the long components can be assigned to singlet excited state lifetime. On the other hand, the ESA of these newly synthesized porphyrins shows almost non-decaying single exponential kinetics. The long-lived state reflects the triplet state, which is populated through non-radiative decay channel (ISC; intersystem crossing). The calculated lifetimes from GSB and ESA kinetics show good agreement with the literature value.[147, 148, 287] The comparison of kinetics traces of Am1 5,15-1 and SlpE026 in the absence and presence of nanocarbon (with C_{60} in NMP; and with GC in THF:H_2O mixture) is depicted in Figure 5.5 and 5.6. Similar to the free porphyrin, in presence of C_{60} the GSB of Am1 5,15-1 and SlpE026 can be fitted with a bi-exponential exponential decay function having a short sub tens of ps and a long time component varied up to ns. However, in the presence of GC an additional time constant of ~0.2 ps noticed in the fitting parameter (Table 5.1). The short-lived time constant can be attributed to charge recombination between the donor-acceptor pair following the ultrafast electron transfer from the porphyrins to the nanocarbon, while the long-lived component may be assigned to ISC of the porphyrins that did not undergo ET. More importantly, the presence of very fast component on the GSB in presence of GC clearly indicates faster electron transfer rate as compared to the C_{60} analogue. This observation is in good agreement with our steady-state PL study (Figure 5.1 and 5.2). Surprisingly, the ESA of Am1 5,15-1 and SlpE026 with C_{60} shows decay while with GC it shows a rising in the ESA signal. The rise time ($\tau_{1(rise)}$ = ~20-23 ps) of the ESA signal with GC can be assigned as the time of formation of porphyrin$^{\bullet+}$ radical cation, which forms immediate after photoexcitation followed by electron injection (less than temporal resolution <120 fs). On the other hand, the porphyrin/C_{60} hybrid shows only a broad ESA feature over the range of 475−550 nm. Again, this band can be assigned to the excited state absorption of porphyrin radical cation.[273, 290] However, in case of C_{60} the ESA follows faster decay (recombination takes less than 100 ps) because of recombination between porphyrin$^{\bullet+}$ radical cation and C60$^{\bullet-}$, which is not noticed in case of GC (better charge separation). This is because of 2D layer structure of the GC, which promote electron

injection through π-π stacking interaction. Formation of cation radical and absence of spectral overlap between donor-acceptor pair are the evidence of electron transfer not energy transfer. From, the kinetics study it is clear that the quenching (ET) in presence of C_{60} takes place through long range diffusion control manner while in case of GC it occurs via a short range static mechanism. The long-range electron transfer process is further studied through ns-TA measurement which are shown in the following section.

Table 5.1: Ultrafast time constants of the exponential fitting of the experimental data. The parenthesis indicates percentage of amplitude.

	Life Time – fs TA		Life Time – ns TA	
Sample Name	**GSB**	**ESA**	**GSB**	**ESA**
Am1 5,15-1 in NMP	τ_1=20±1.5 (20%) ps τ_2=1.1±0.1 (80%) ns	τ=1.8±0.2 ns	τ=1.2±0.1μs	τ=1.2±0.1 μs
Am1 5,15-1/C_{60} in NMP	τ_1=9.5±1 (21%) ps τ_2=472±30 (79%) ps	τ_1=2.3±0.1 (31%) ps τ_2=55±4 (69%) ps	τ_1=1.8±0.1 (24%) ns τ_2=1±0.1 (76%) μs	τ_1=2±0.2 (24%) ns τ_2=1±0.1 (76%) μs
SlpE026 in NMP	τ_1=3±0.2 ps (15%) τ_2=2±0.2 (85%) ns	τ=2.4±0.2 ns	τ=1.8±0.2 μs	τ=1.8±0.1 μs
SlpE026/C_{60} in NMP	τ_1=11±1 (13%) ps τ_2=1.8±0.1 (87%) ns	τ_1=2.5±0.2 (42%) ps τ_2=90±8 (58%) ps	τ_1=2.5±0.2 (14%) ns τ_2=2±0.1 (86%) μs	τ_1=1.7±0.1 (32%) ns τ_2=2±0.2 (68%) μs
Am1 5,15-1 in THF:H_2O	τ_1=3±0.2 (10%) ps τ_2=509±50 (90%) ps	τ=3±0.2 ns	τ=0.65±0.04 μs	τ=0.7±0.04 μs
Am1 5,15-1/GC in THF:H_2O	τ_1=0.25±0.02 (14%) ps τ_2=5±0.5 (11%) ps τ_3=547±53 (75%) ps	τ_{1rise}=23±2.3 (21%) ps τ_2=3.4±0.03 (79%) ns	τ=0.7±0.03 μs	τ=0.7±0.04 μs
SlpE026 in THF:H_2O	τ_1=4±0.2 (14%) ps τ_2=2±0.2 (86%) ns	τ=1.1±0.1 ns	τ=1±0.04 μs	τ=1±0.06 μs
SlpE026/GC in THF:H_2O	τ_1=0.2±0.02 (12%) ps τ_2=13±1.3 (18%) ps τ_3=500±49 (70%) ps	τ_{1rise}=20±1 (25%) ps τ_2=819±17 (75%) ps	τ=1±0.04 μs	τ=1±0.06 μs

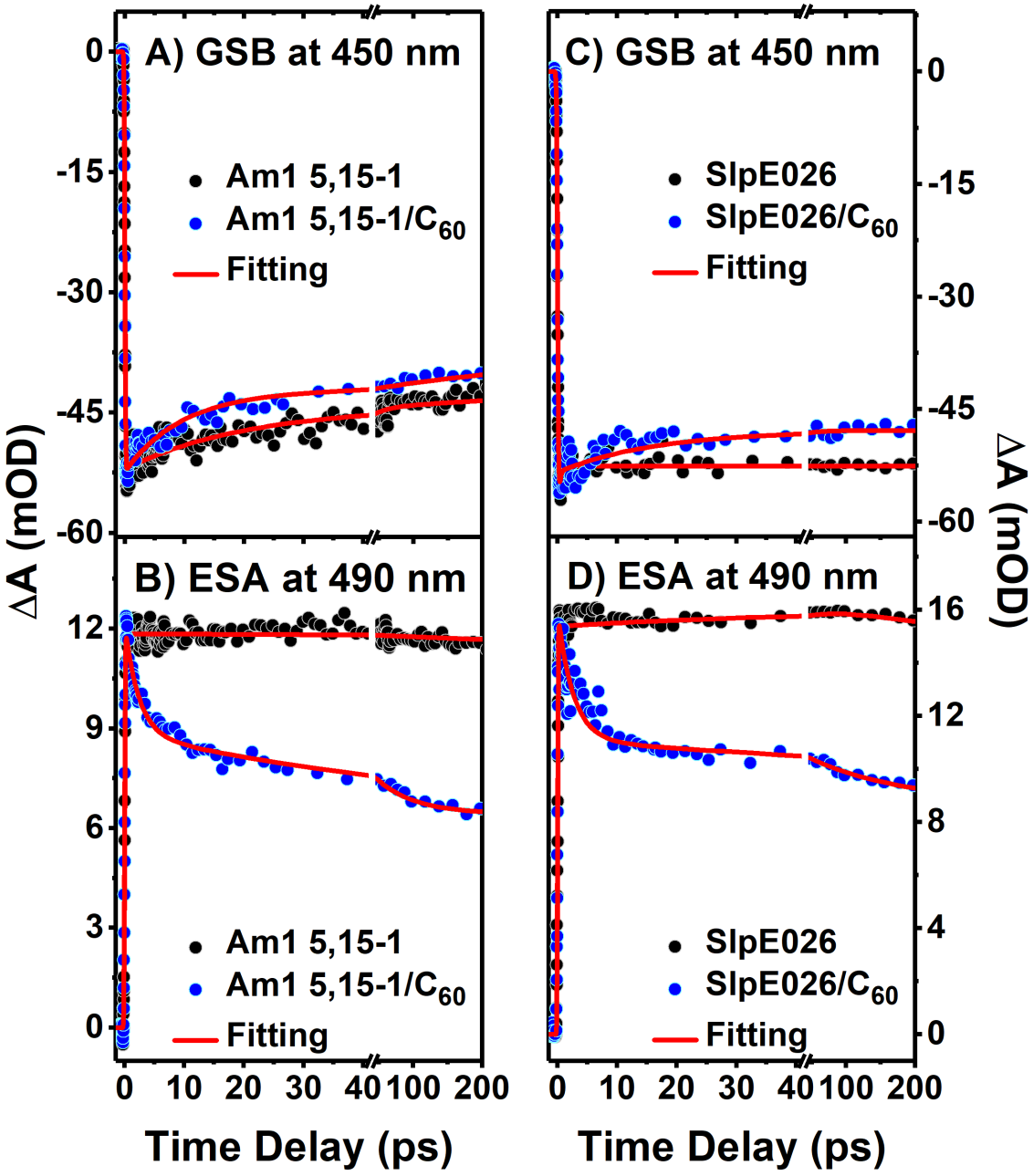

Figure 5.5: Normalized fs-TA kinetics of (A and C) GSB at 450 nm of the Am1 5,15-1 and SlpE026, respectively in the absence (black) and presence (blue) of C_{60}, and (B and D) ESA at 490 nm of the Am1 5,15-1 and SlpE026, respectively in the absence (black) and presence (blue) of C_{60}. The red solid lines show the exponential fit to the acquired data.

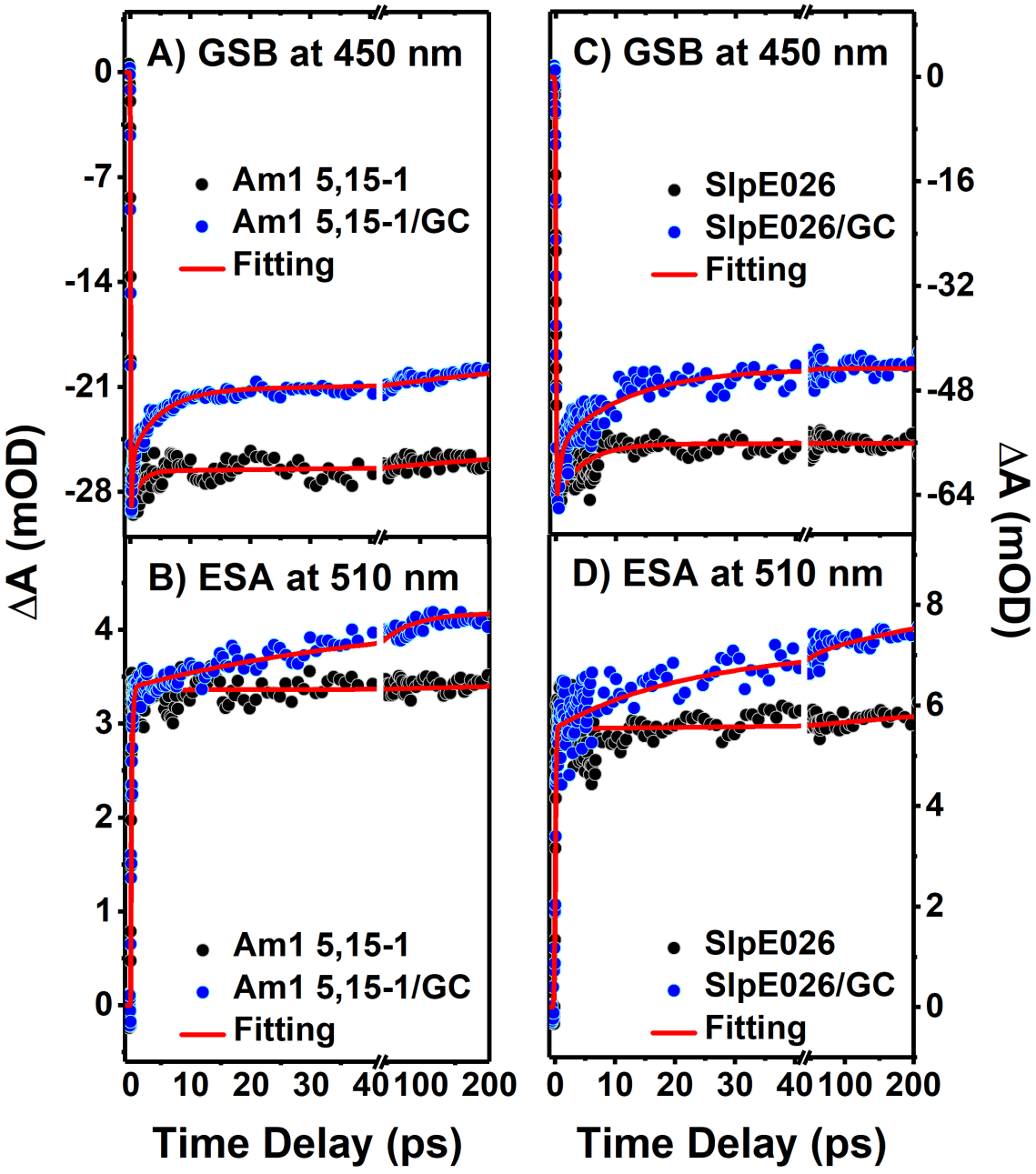

Figure 5.6: Normalized fs-TA kinetics of (A and C) GSB at 450 nm of the Am1 5,15-1 and SlpE026, respectively in the absence (black) and presence (blue) of GC, and (B and D) ESA at 490 nm of the Am1 5,15-1 and SlpE026, respectively in the absence (black) and presence (blue) of GC. The red solid lines show the exponential fit to the acquired data.

To explore whether the interaction between the porphyrins and the nanocarbons is effective via the triplet state as well, we operated nanosecond TA spectroscopy. The ns-TA spectra up to microseconds time scales for Am1 5,15-1 and SlpE026 in the absence and presence of C_{60} and GC are showed in Fig. A.8. Fig. 5.7 represents ns-TA kinetics of free

Am1 5,15-1 and SlpE026 as well as the mixture with C_{60}. It is worth to mention that we noticed from fs-TA that the bleach recovery of porphyrin/nanocarbon is slower with C_{60} as compared to the GC, while we observed more than 70% quenching in steady-state PL study. Also, non-linear pattern of the SV plot of porphyrin/C_{60} suggested dynamics in the quenching of the Am1 5,15-1 and SlpE026 with C_{60}. The ns-TA kinetics of porphyrin/nanocarbon has been shown up to 200 ns time window which reflects faster bleach recovery and decay of ESA with C_{60} (Fig. 5.7). Finally, our experimental researches continued with investigating ns-TA kinetics of the same porphyrins in the absence and presence of GC as can be seen in Fig. 5.8. However, no clear change for Am1 5,15-1/GC and SlpE026/GC were monitored in ns-TA, which confirms that diffusion-controlled electron transfer process was not observed in these cases. These results reveal that each porphyrin is just absorbed GC on the surface of the complexation and by this way, only static electron transfer process occur between them. Such ns-TA spectra and corresponding time constants elucidate unambiguously that long-lived species can be attributed to the triplet excited state of free porphyrin molecule. No change in the lifetime upon addition of GC, clearly indicates that ET does not take place through triplet state but rather it occurs via singlet excited state. We observed diffusion-controlled process (dynamic interaction) between each porphyrin and C_{60}. It means that each porphyrin and C_{60} hybrid is far from each other and they need to diffuse to form a reactive complex with the certain difference between porphyrin and C_{60}. They need longer time to interact with each other. Therefore, the change in the ns kinetics is observed for GSB at 450 nm and ESA at 490 nm. Two time constants (sub ns and μs) which refer to singlet state and triplet state lifetime respectively are given in Table 5.1.

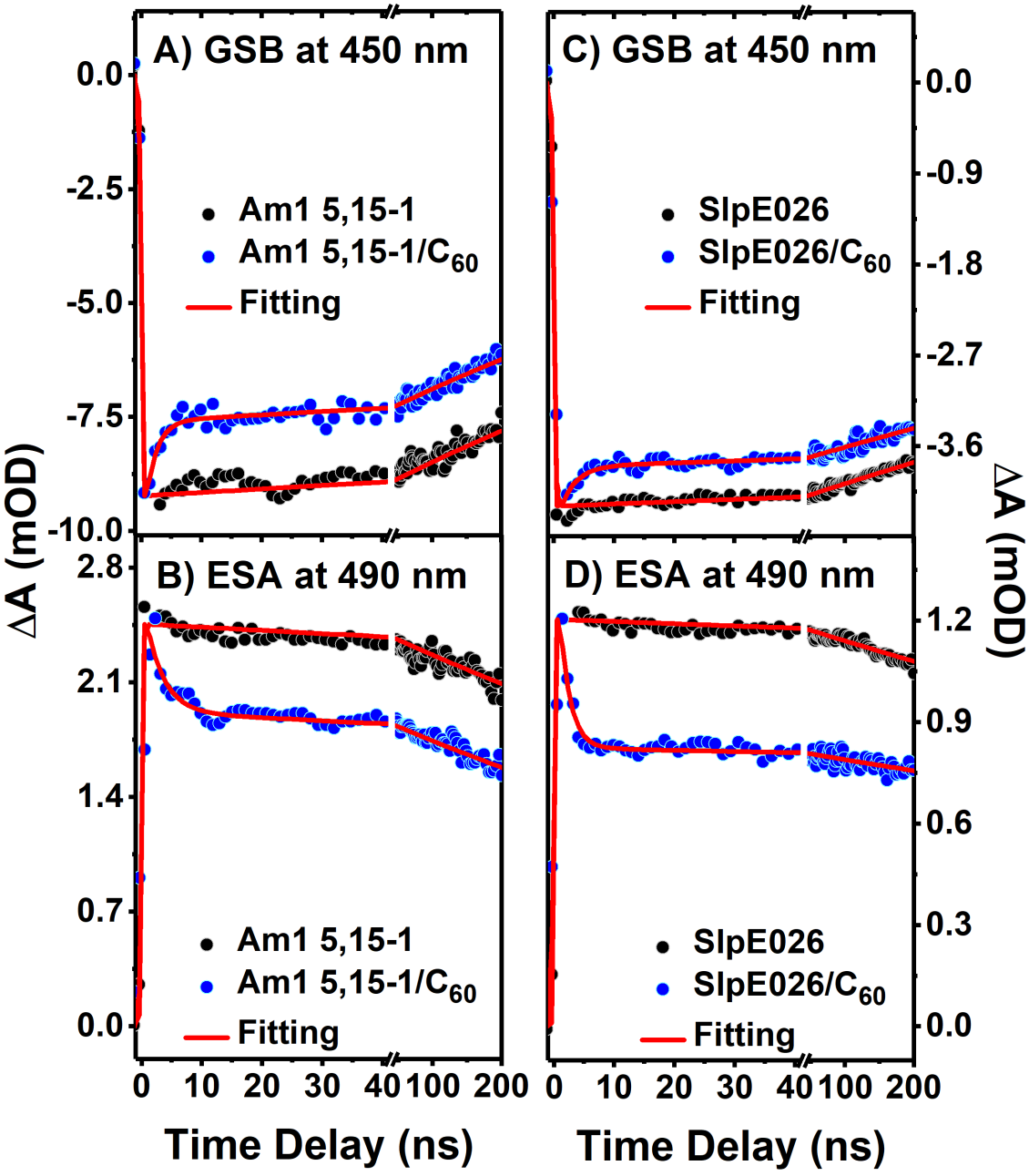

Figure 5.7: Normalized ns-TA kinetics of (A and C) GSB at 450 nm of the Am1 5,15-1 and SlpE026, respectively in the absence (black) and presence (blue) of C_{60}, and (B and D) ESA at 490 nm of the Am1 5,15-1 and SlpE026, respectively in the absence (black) and presence (blue) of C_{60} in NMP after 640 nm laser excitation. Fitted lines are represented in red.

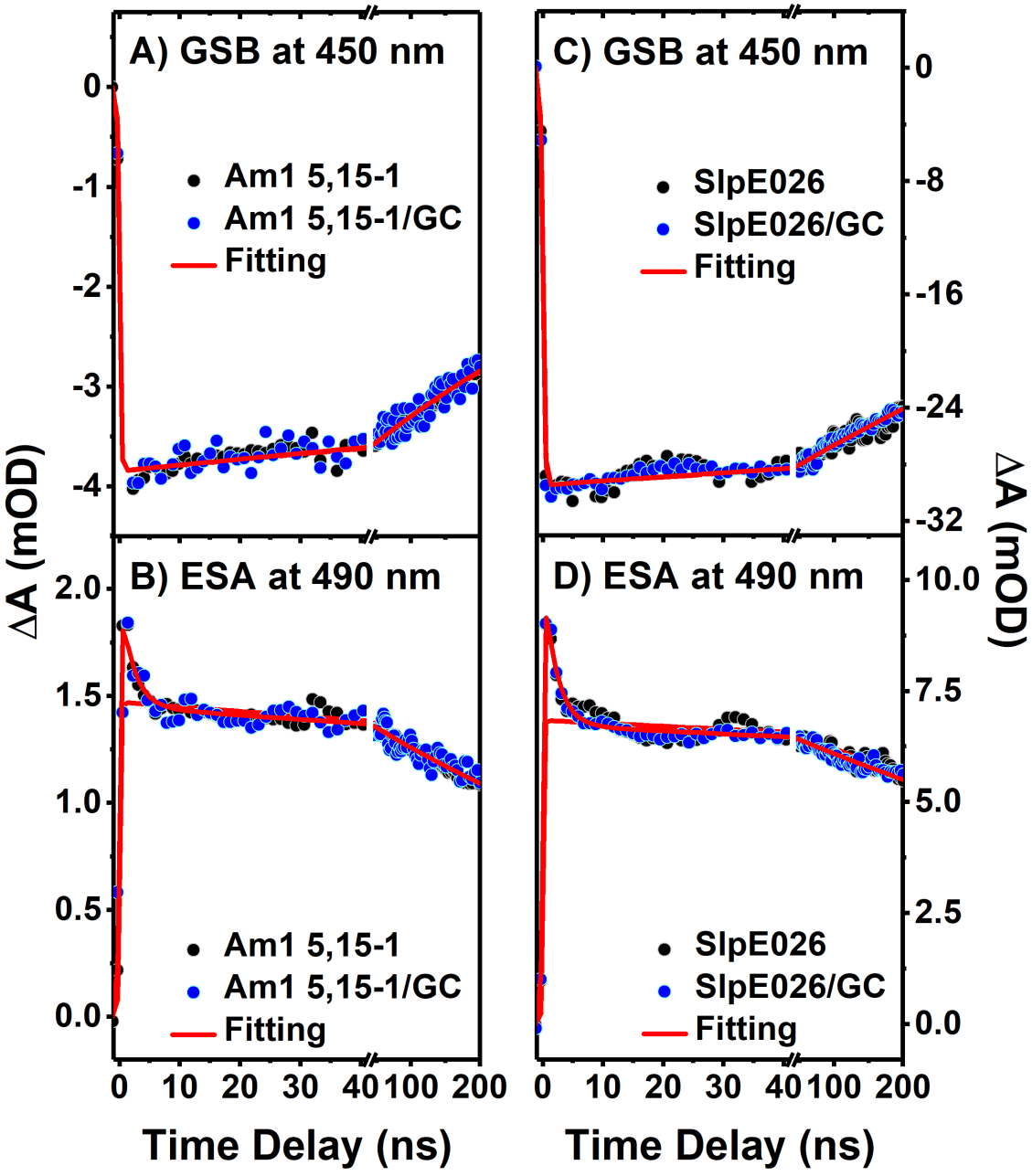

Figure 5.8: Normalized ns-TA kinetics of (A and C) GSB at 450 nm of the Am1 5,15-1 and SlpE026, respectively in the absence (black) and presence (blue) of GC, and (B and D) ESA at 490 nm of the Am1 5,15-1 and SlpE026, respectively in the absence (black) and presence (blue) of GC in (THF:H_2O) [1:1 v/v] after 640 nm laser excitation. Fitted lines are represented in red.

5.3 Conclusion

In conclusion, the photoinduced charge transfer process has been thoroughly investigated between two newly synthesized porphyrins and nanocarbons interface. Steady-state PL quenching is observed which illustrates that energy and/or electron transfer from the excited porphyrin to the nanocarbon. In addition, Stern-Volmer plots of porphyrin/GC varies linearly with increasing GC concentration while a deviation from linearity is found with cumulative addition of C_{60} into porphyrin. The static and a combination of static and dynamics quenching in presence of GC and C_{60}, respectively is further studied through fs and ns-TA. Faster GSB recovery in fs-TA and no change in ns-TA of these newly synthesized porphyrins in presence of GC reveals that the ET reactions occur via the non-covalent association of porphyrin/GC from the singlet excited porphyrin to the GC, resulting from the formation of porphyrin$^{\bullet+}$ radical cation. Importantly, faster GSB recovery of porphyrin/C_{60} in both fs and ns-TA is confirmed by the combination of static and diffusion-controlled electron quenching. Moreover, faster decay of ESA of porphyrin/C_{60} indicates strong recombination between porphyrin cation radical and C_{60} anion radical pairs. Our analysis suggest that ET is more efficient and faster in a porphyrin/GC interface.

CHAPTER 6: Summary and Outlook

6.1 Summary

In chapter 4, the photophysical investigation of different series of *push-pull* porphyrins are described due to their potential usefulness as an absorber layer in solar cell devices. Steady-state absorption and emission, time-resolved transient absorption spectroscopies indicate that the photophysical properties among the Am1 5,15-1 and Am1 5,10-1 isomers are almost the same, while the differences of photophysical properties among the SlpE029 and SlpE026 *push-pull* porphyrins are pronounced. Steady-state measurements and ns-TA spectroscopy results also indicate that the origin of the broadened and red-shifted spectral features, which are mostly observed in the SlpE029 and SlpE026 porphyrins can be attributed to the greater extent of intramolecular charge transfer between the D and A moieties, because aggregation effects can be neglected as a result of concentration dependent experiments. Although the singlet state lifetime of the porphyrins is almost the same as revealed by TRPL tests, the longest triplet state population is recorded in SlpE026 porphyrin, followed by SlpE029, and then Am1 5,15-1 and Am1 5,10-1 with almost the same triplet state lifetime as indicated by ns-TA kinetics. Additionally, a case study is done for the first time to present charge transfer interaction from the $MAPbI_3$ perovskite film to the SlpE026 porphyrin by using same spectroscopic techniques, motivated as these kinds of porphyrins also can act as an electron acceptor in photovoltaics or in any D-A systems.

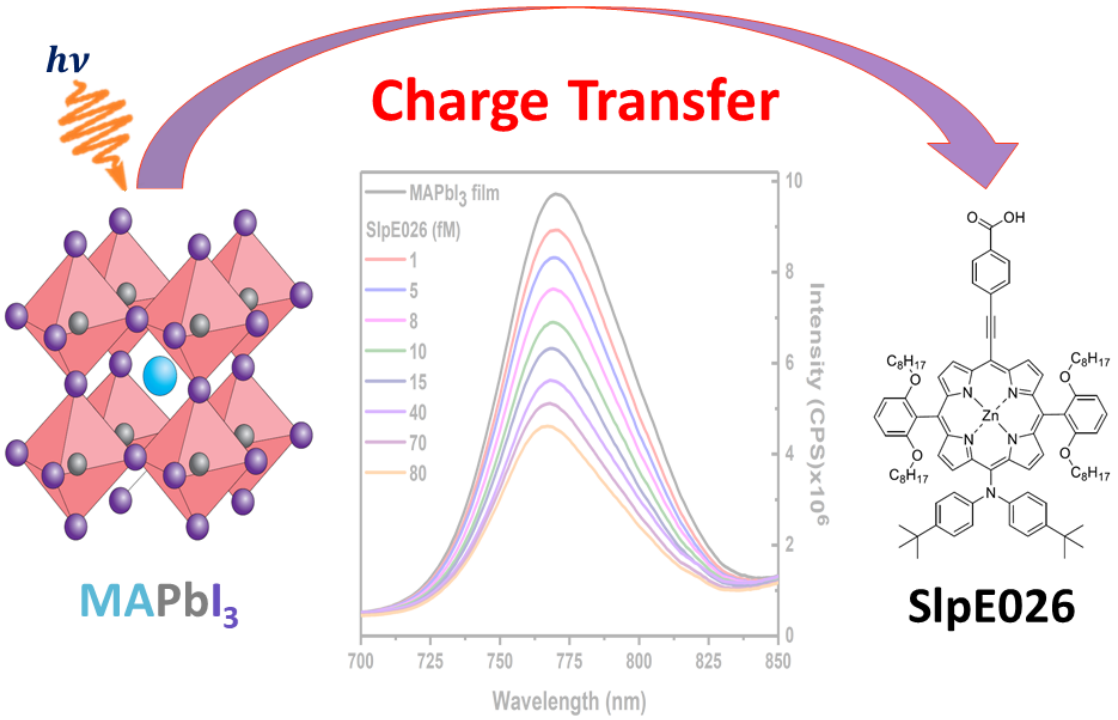

Figure 6.1: Schematic illustration of electron transfer at the $MAPbI_3$ film-SlpE026 porphyrin interface. (The $MAPbI_3$ perovskite structure was obtained from reference[291].

Controlling charge transfer, charge separation and charge recombination at interfaces in D-A systems is quite important to optimize the power conversion efficiency in photovoltaic cell devices. Electron transfer processes from newly synthesized 5,15-disubstituted porphyrins to nanocarbon interfaces are investigated using steady-state measurements and ns and fs-TA spectroscopies in chapter 5. Efficient PL quenching indicates energy and/or electron transfer from the donor porphyrins (Am1 5,15-1 and SlpE026) to the acceptor nanocarbons (C_{60} and GC). Stern-Volmer plots illustrate static quenching only in the case of porphyrin/GC hybrids and a combination of both static and dynamic quenching for the porphyrin/C_{60} hybrids. Both porphyrins show strong GSB corresponding to the depletion of the Soret band and ESA due to presence of a long-lived triplet state as revealed by fs-TA spectroscopy. The fast bleach recovery indicates ultrafast ET from singlet-excited porphyrin to the nanocarbon. The formation time of porphyrin cation radical is attributed by rising in the excited state decay kinetics in the case of porphyrin/GC hybrids. Moreover, in presence of C_{60} fast recovery and decay of GSB and ESA, respectively of the porphyrins, which attributed long distance diffusion control quenching process, are illustrated by ns-

TA results. As there is no change in ns-TA measurements of porphyrin/GC hybrids, the results indicate only static electron transfer process for these hybrid systems. Finally, slightly changing the structure of the porphyrins from the *meso*-units does not change much the interaction with nanocarbon materials.

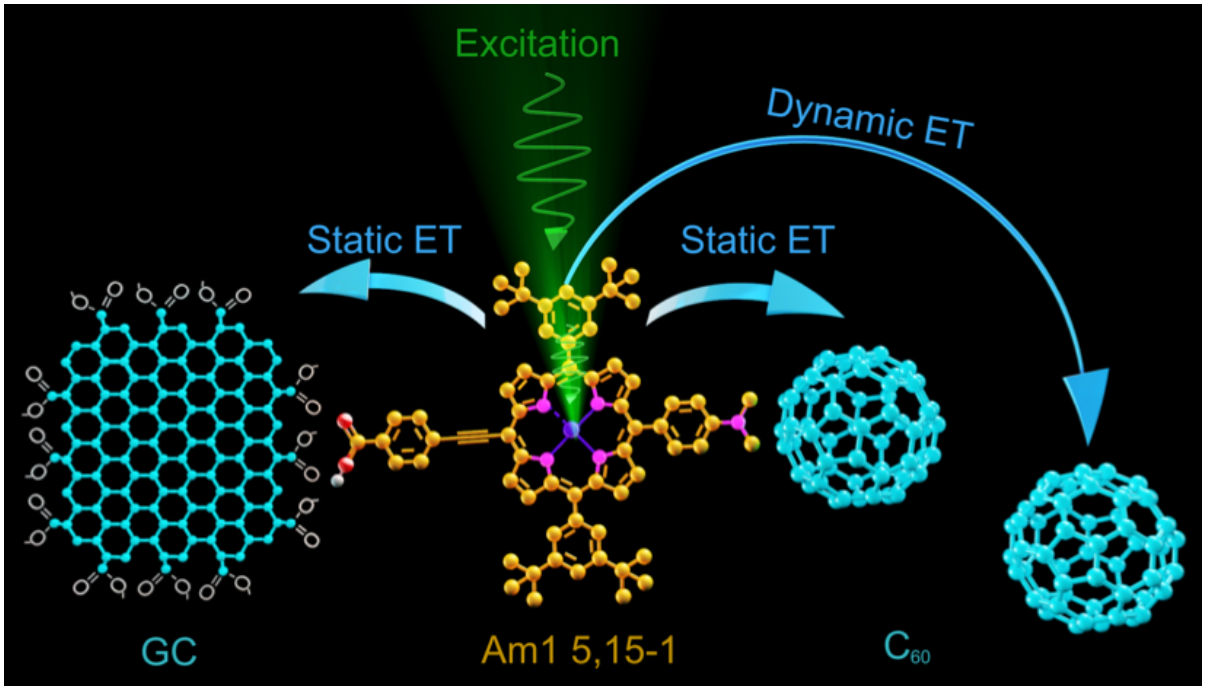

Figure 6.2: A diagram illustrates static and dynamic (diffusion-controlled) mechanisms of PET from porphyrin to C_{60} and static mechanism of PET from porphyrin to GC.

6.2 Outlook

In physical chemistry, material science and solar cells communities, photoinduced charge transfer is one of the most important phenomena at the D-A interfaces. Thus, the comprehensive understanding of such dynamical processes in D-A systems will be beneficial for ultimate optimization of solar cell devices. It is aimed to extend these measurements to various photoactive materials with a variety of different porphyrin structures and 2D layered materials (such as chalcogenides, oxides etc.) to evaluate the impact of changes in the energy level alignments on CT, CR and subsequently the device performance. The number of layers changes the band gap. Therefore, if the thickness of the monolayers can be controlled, then it is possible to match them to the energy structure of the porphyrin. In this way, CT can be optimized by minimizing the energetic barrier

between the porphyrin and nanomaterial. That leads to enhance the CT and PV efficiency. Another possibility is to investigate the porphyrins which are linked by conjugated bridges and therefore form an extended π-electron system. That way, the porphyrins can be matched with 2D materials. This leads to enhance CT and improve PV efficiency. The benefit of π-conjugated porphyrin arrays is that they can also absorb in near-infrared and therefore improve the energy harvesting.

Particularly, the main goals are to provide fundamental information on the mechanistic and kinetic details of the CT process and to find a clear way to promote it at the interfaces of donor-acceptor. In this way, main variable components to control the charge transfer dynamics and the transfer efficiency at such donor-acceptor systems may be provided.

Appendices

Fig. A.1 is used to show that a control experiment was also done with 0.02 mM porphyrin solutions. Therefore, the aggregation effects in these porphyrin solutions were minimized in 0.002 mM concentration as shown in Fig. 4.1.

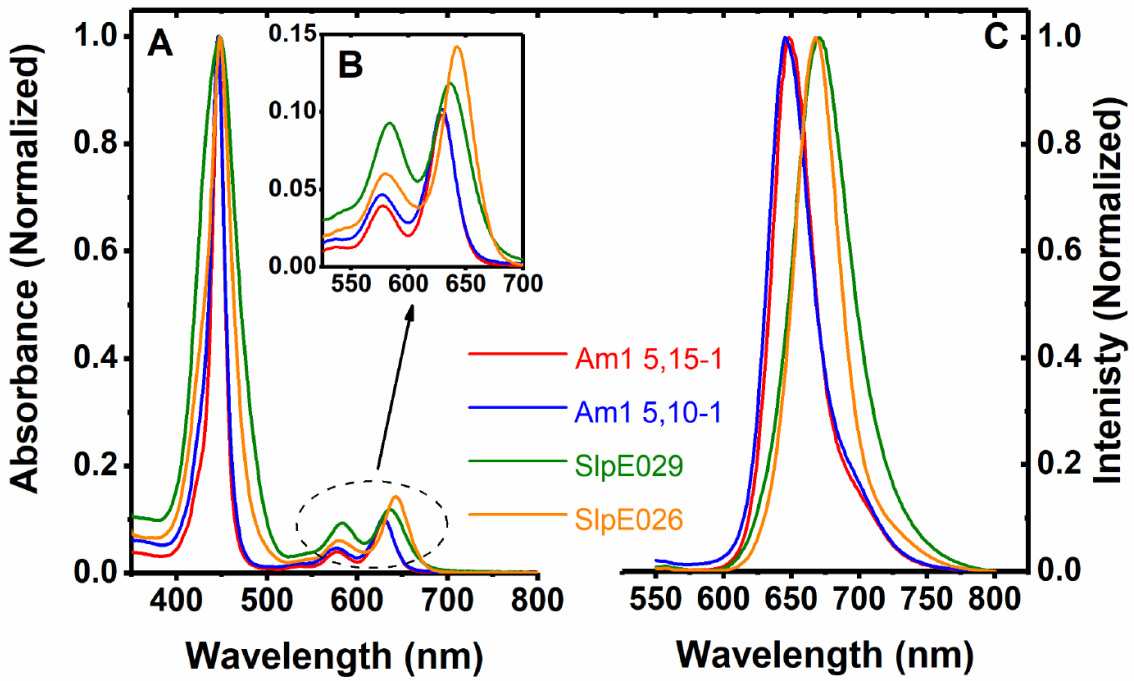

Figure A.1: Normalized steady-state (A) absorption, (C) emission (λ_{Ex}= 532 nm) spectrums of 0.02 mM Am1 5,15-1 (red), Am1 5,10-1 (blue), SlpE029 (green) and SlpE026 (orange) porphyrins in THF solution. The Q bands region of each porphyrin in the absorption spectrum is enlarged in (B).

The experiment in Fig. A.2 was done in the absent of oxygen. Fig. A.2 is used to show that the lifetime of the porphyrin is quenched (reduced) in the presence of oxygen (for comparison see Fig. 4.4).

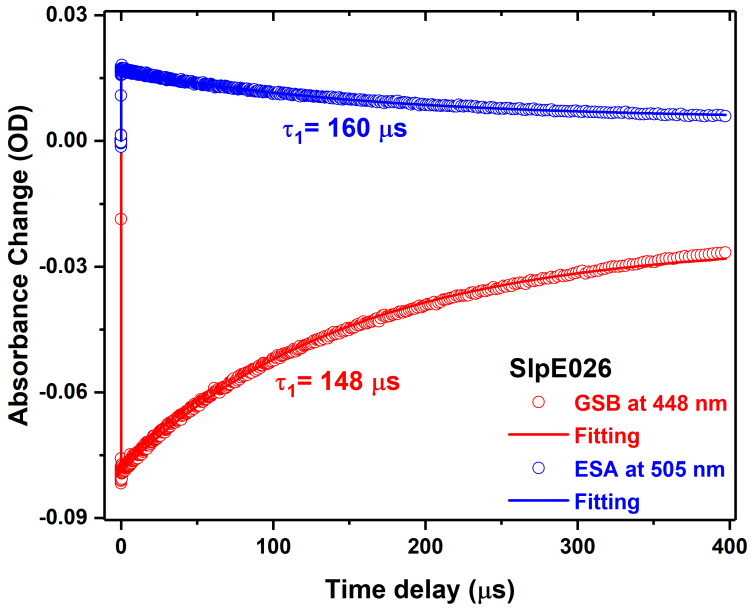

Figure A.2: Normalized time profile of nanosecond transient absorption kinetics of the SlpE026 porphyrin in the absent of oxygen. GSB at 448 nm (red) and ESA at 505 nm (blue). The solid lines show the exponential fit to the acquired data.

Fig. A.3 is used to show that there is no signal coming from the SlpE026 porphyrin (no intrinsic response of the porphyrin as the concentration of the porphyrin is very low) after 650 nm laser excitation (see Fig. 4.7).

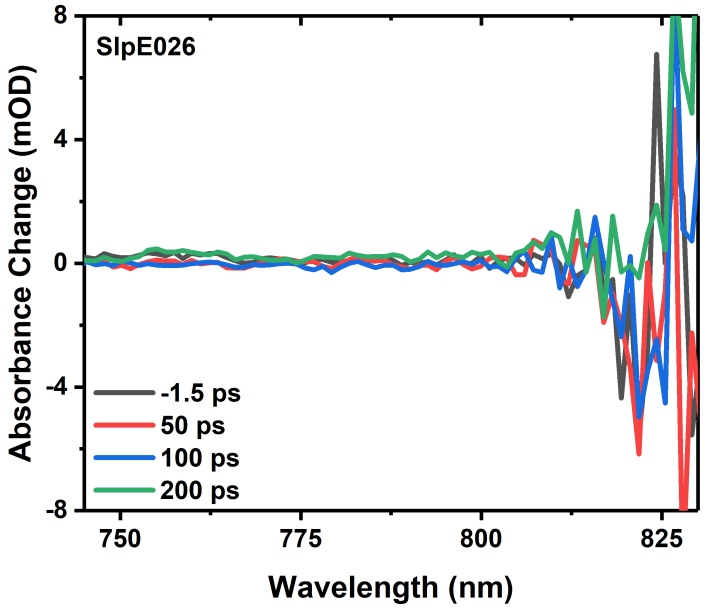

Figure A.3: Femtosecond transient absorption spectra of 80 fM SlpE026 porphyrin in chloroform solution onto the glass substrate recorded after 650 nm pulsed-laser 120 fs excitation.

Fig. A.4 is used to show a monotonically decreased broad signal from the UV to the visible region is observed which refers to the signal of the tested nanocarbons. (see the absorption graphs in Fig. 5.1 and 5.2)

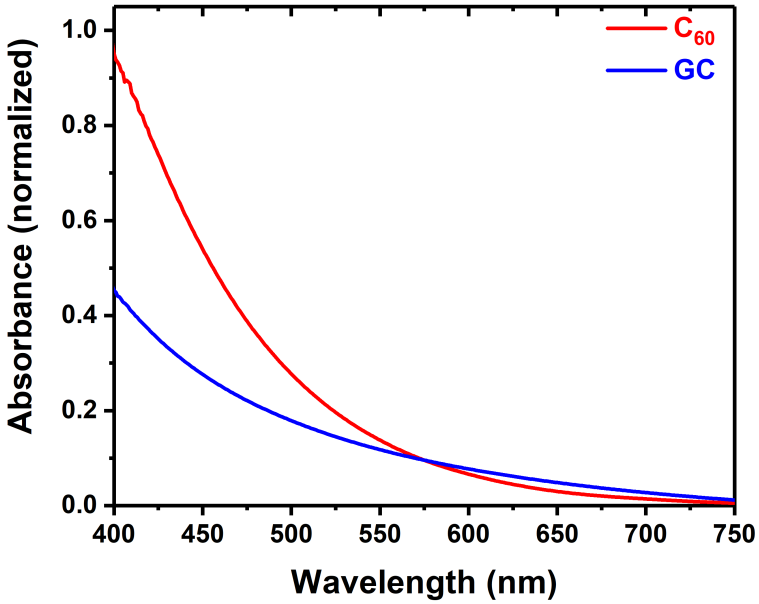

Figure A.4: Absorption spectrum of 0.346 mg/mL C_{60} in NMP and 0.750 mg/mL GC in THF:H_2O mixture [1:1 v/v].

To clarify the data shown in Fig. 5.3 and 5.4, the differential spectra against the reference of the 550 fs and 650 fs spectrum and the differential spectra against the reference of the 250 fs and 725 fs spectrum, respectively are displayed in Fig. A.5 and A.6.

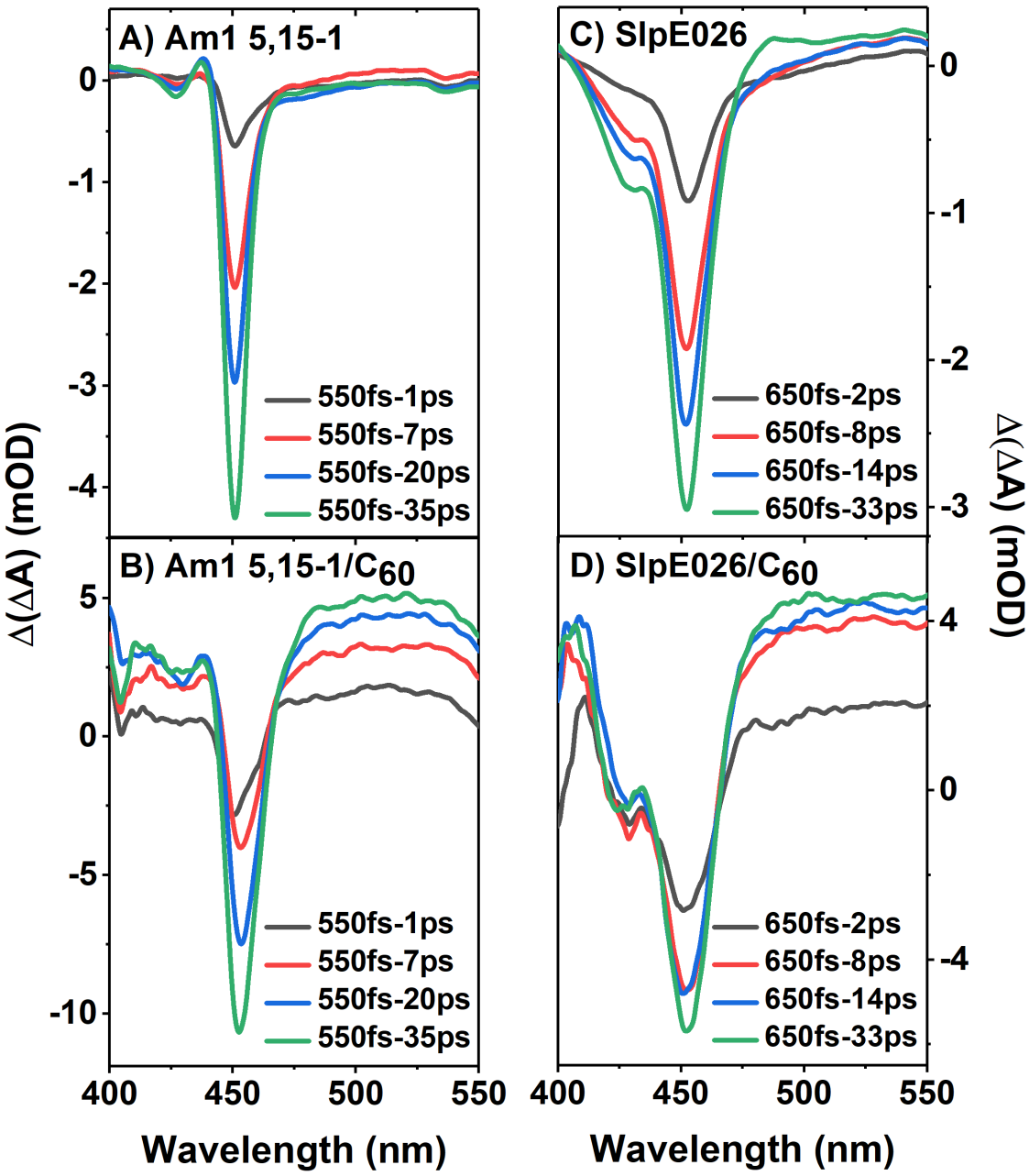

Figure A.5: Differential fs-TA spectra recorded after 640 nm optical excitation for (A) Am1 5,15-1, (B) Am1 5,15-1/C_{60}, (C) SlpE026, and (D) SlpE026/C_{60}.

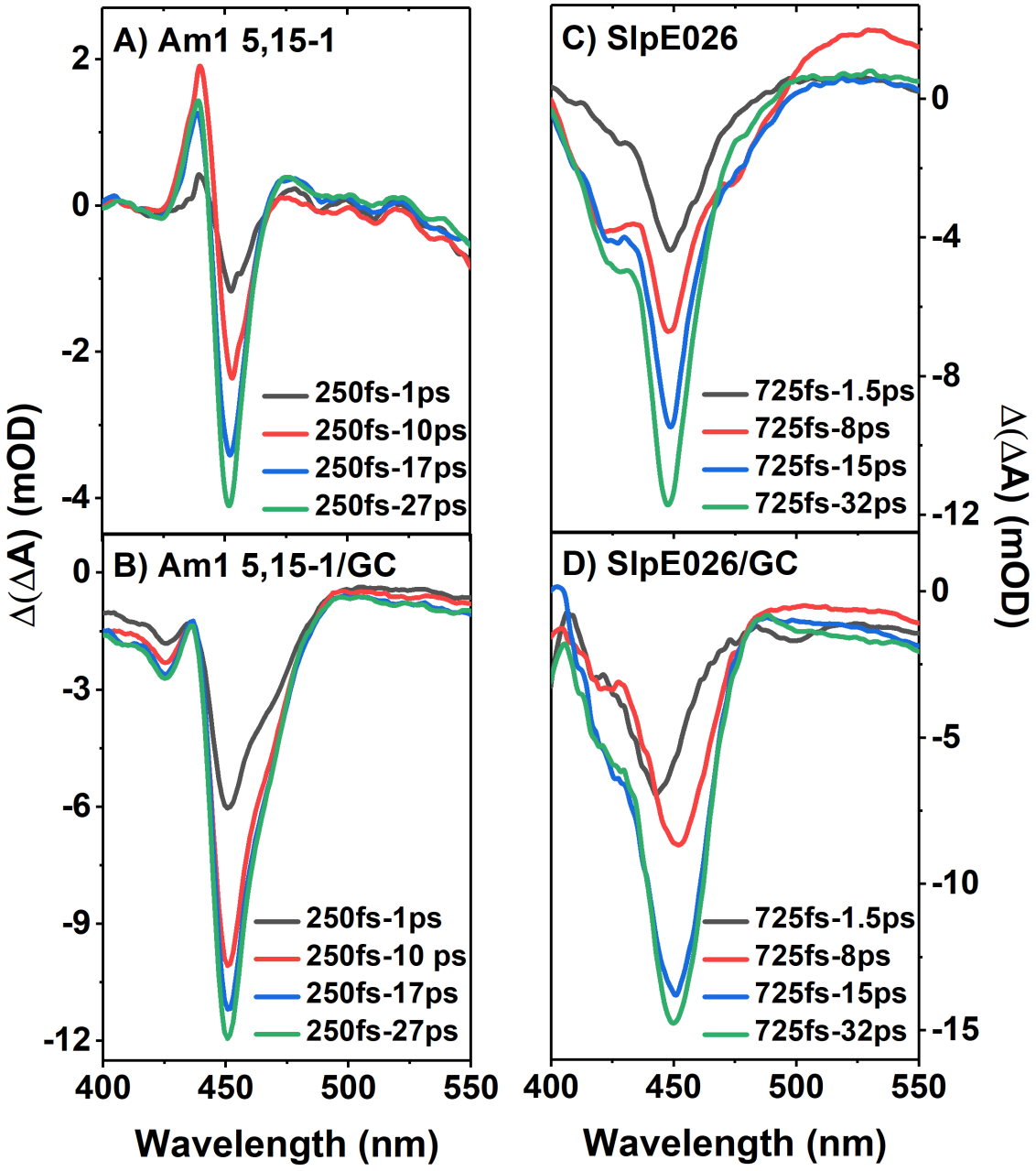

Figure A.6: Differential fs-TA spectra of (A) Am1 5,15-1, (B) Am1 5-15-1/GC, (C) SlpE026, and (D) SlpE026/GC recorded after 640 nm optical excitation.

Femtosecond TA spectroscopy study in Fig. A.7 shows within 5.5 ns time scale the GSB recovers by <30% to its ground state and the excess photoexcited porphyrin decays into the long-lived triplet state through intersystem crossing. This data is used to support the findings (fs-TA spectroscopy results) in chapter 5.

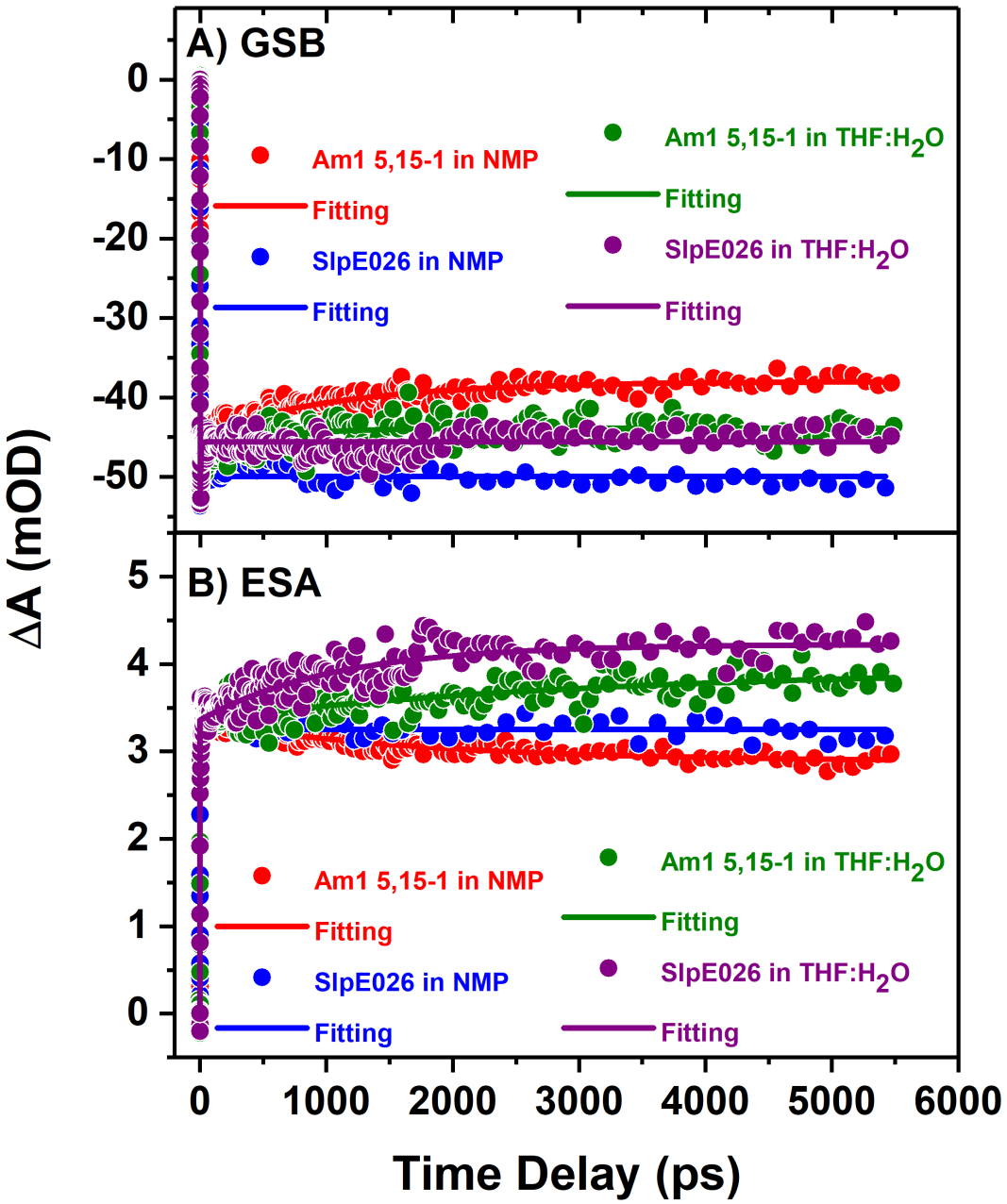

Figure A.7: Normalized fs-TA kinetics of (A) GSB at 450 nm of the Am1 5,15-1 in NMP, SlpE026 in NMP, Am1 5,15-1 in THF:H_2O and SlpE026 in THF:H_2O and (B) ESA at 490 nm of the Am1 5,15-1 in NMP, ESA at 490 nm the SlpE026 in NMP, ESA at 510 nm of the Am1 5,15-1 in THF:H_2O and ESA at 510 nm of the SlpE026 in THF:H_2O.

To explore whether the interaction between the porphyrins and the nanocarbons is effective via the triplet state as well, ns-TA spectroscopy was operated in chapter 5 and the ns-TA spectrums of the porphyrins are represented in Fig. A.8.

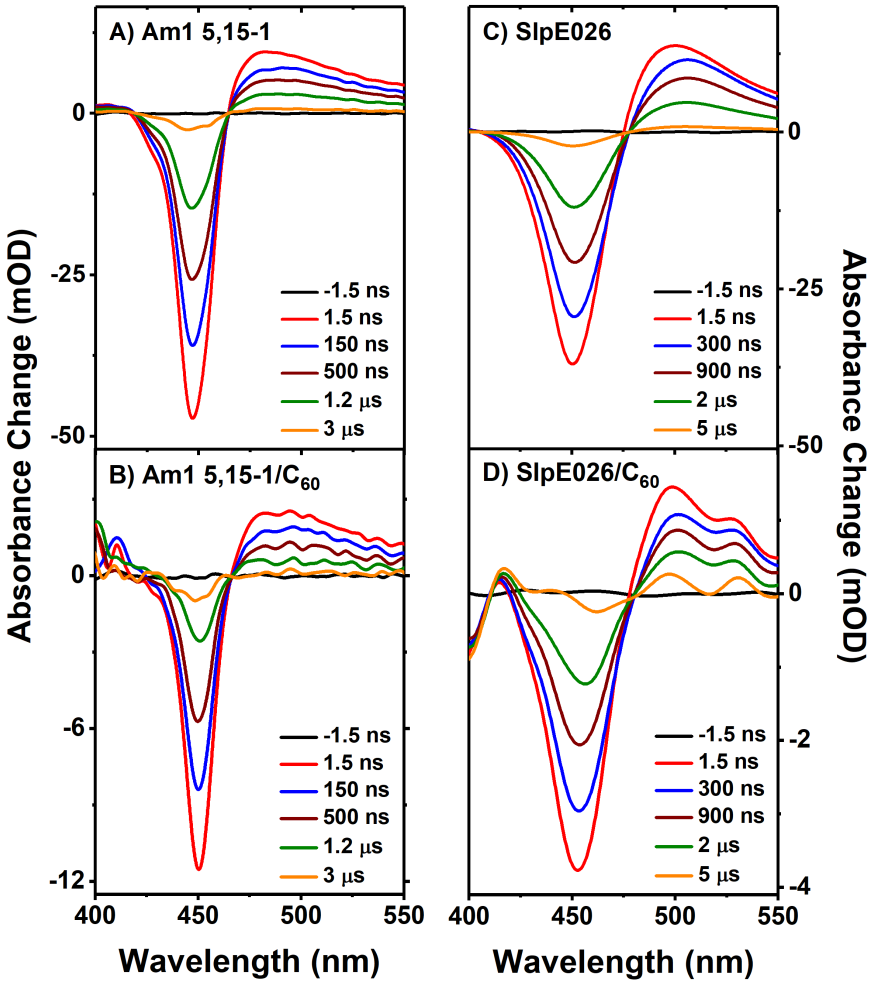

Figure A.8: ns-TA spectra recorded after 640 nm optical excitation for (A) Am1 5,15-1, (B) Am1 5-15-1/C_{60}, (C) SlpE026, and (D) SlpE026/C_{60}.

List of Presentations and Publications

Presentations

- NanoteC16 Conference, Carbon Nanoscience and Technology, 31 August-3 Sep 2016, Dublin, Ireland, Poster Presentation

- Nanotube (NT) NT16 Conference, 7-13 August 2016, Vienna, Austria, Poster Presentation

- European Membrane Society Summer School on "Membranes and Membrane Processes Design, Jun 26–1 July 2016, Bologna, Italy, Poster Presentation

- Graphene Week, 13–17 June 2016, Warsaw, Poland, Poster Presentation

- Wurzburg Summer School 2015 on Supramolecular Nanosystems, 27-31 July 2015, Germany, Poster Presentation

- Energy Materials Nanotechnology (EMN) Istanbul 2015 Conference, 1-4 July 2015, Turkey, Poster Presentation

Publications

- Charge Transfer Process at the Interface of Methylammonium Lead Triiodide Perovskite and Push-Pull Porphyrins *(Manuscript in preparation)*

- Ultrafast Charge Transfer Interaction between Nanocarbon Materials and Porphyrins *(Manuscript in preparation)*

References

1. Milgrom, L.R., *The Colours of Life. An Introduction to the Chemistry of Porphyrins and Related Compounds*. 1997, United States: Oxford University Press.
2. Dolphin, D., *The porphyrins*. 1978, New York: Academic Press.
3. Küster, W., *Beiträge zur Kenntnis des Bilirubins und Hämins*, in *Hoppe-Seyler´s Zeitschrift für physiologische Chemie*. 1912. p. 463-483.
4. *Handbook of Porphyrin Science*, ed. W. Kadish, K.M. Smith, and R. Guilard. Vol. 44. 2010-2016: World Scientific Publishing Co.:Singapore.
5. Moore, M.W., *An historical introduction to porphyrin and chlorophyll synthesis. In Tetrapyrroles: Birth, Life, and Death*, ed. M. Warren and A. Smith. 2009, Berlin, Germany: Landes Bioscience and Springer Science+Business Media.
6. Suslick, K.S., et al., *The materials chemistry of porphyrins and metalloporphyrins*. Journal of Porphyrins and Phthalocyanines, 2000. **4**(4): p. 407-413.
7. Cook, L.P., W. Wong-Ng, and G. Brewer, *Porphyrin-based chemistry for carbon capture and sequestration. In Advances in Materials Science for Environmental and Energy Technologies V*, ed. T. Ohji, et al. 2016: Wiley & Sons: Hoboken, NJ, USA.
8. Giovannetti, R., *The Use of Spectrophotometry UV-Vis for the Study of Porphyrins, Macro To Nano Spectroscopy*, ed. J. Uddin. 2012: INTECH Open Access Publisher. 87-108.
9. *International Union of Pure and Applied Chemistry. Nomenclature of Tetrapyrroles.* http://www.chem.qmul.ac.uk/iupac/tetrapyrrole/. [31/03/2017].
10. Cook, L.P., G. Brewer, and W. Wong-Ng, *Structural Aspects of Porphyrins for Functional Materials Applications*. Crystals, 2017. **7**: p. 223.
11. *Cambridge Crystallographic Data Center. The porphine structure.* https://www.ccdc.cam.ac.uk/. [31/03/2017].
12. Saltsman, I., et al., *Porphine and pyrrole-substituted porphyrin from cyclocondensation of tripyrrane with mono-substituted pyrroles*. Tetrahedron Letters, 2007. **48**(2): p. 239-244.
13. Jiao, L., *Synthesis and Functionalizations of Tetrapyrrole Derivatives*. 2007, Louisiana State University and Agricultural and Mechanical College.
14. Sessler, J.L. and M.C. Hoehner, *An Efficient, High-Yield Preparation of Substituted 2,2'-Bipyrroles*. SYNLETT, 1994(3): p. 211-212.
15. Notaras, E.G.A., et al., *A_2B_2-type push-pullporphyrins as reverse saturable and saturable absorbers*. Chemical Communications, 2007(21): p. 2166-2168.

16. Vicente, M.G.H. and M.S. Kevin, *Porphyrins and Derivatives Synthetic Strategies and Reactivity Profiles.* Current Organic Chemistry, 2000. **4**(2): p. 139-174.
17. Ravikanth, M. and T.K. Chandrashekar, *Nonplanar porphyrins and their biological relevance: Ground and excited state dynamics. Structure and Bonding*, in *Coordination Chemistry*. 1995, Springer Berlin Heidelberg: Berlin, Heidelberg. p. 105-188.
18. Senge, M.O., *Exercises in molecular gymnastics-bending, stretching and twisting porphyrins.* Chemical Communications, 2006(3): p. 243-256.
19. Gouterman, M., *Spectra of porphyrins.* Journal of Molecular Spectroscopy, 1961. **6**: p. 138-163.
20. Weiss, C., H. Kobayashi, and M. Gouterman, *Spectra of porphyrins: Part III. Self-consistent molecular orbital calculations of porphyrin and related ring systems.* Journal of Molecular Spectroscopy, 1965. **16**(2): p. 415-450.
21. Namuangruk, S., et al., *Theoretical investigation of the charge-transfer properties in different meso-linked zinc porphyrins for highly efficient dye-sensitized solar cells.* Dalton Transactions, 2014. **43**(24): p. 9166-9176.
22. Adar, F., *Electronic Absorption Spectra of Hemes and Hemoproteins*, in *The Porphyrins*, D. Dolphin, Editor. 1978, Academic Press. p. 167-209.
23. Li, B., et al., *Review of recent progress in solid-state dye-sensitized solar cells.* Solar Energy Materials and Solar Cells, 2006. **90**(5): p. 549-573.
24. *European Commission - Energy Strategy and Energy Union* https://ec.europa.eu/energy/en/topics/renewable-energy. [15/01/2018].
25. *Department of Energy: Successes of the Recovery Act - 2012* https://energy.gov/sites/prod/files/RecoveryActSuccess_Jan2012final.pdf. [15/01/2018].
26. Gong, J., et al., *Review on dye-sensitized solar cells (DSSCs): Advanced techniques and research trends.* Renewable and Sustainable Energy Reviews, 2017. **68**: p. 234-246.
27. O'Regan, B. and M. Grätzel, *A low-cost, high-efficiency solar cell based on dye-sensitized colloidal TiO_2 films.* Nature, 1991. **353**: p. 737-740.
28. Mathew, S., et al., *Dye-sensitized solar cells with 13% efficiency achieved through the molecular engineering of porphyrin sensitizers.* Nature Chemistry, 2014. **6**: p. 242-247.
29. Wang, H., R.G.W. Jinadasa, and S. Kumar, *Push-Pull Porphyrins: Synthesis, Properties and Applications*, in *Handbook of Porphyrin Science. Nanoorganization of Porphyrinoids*, K.M. Kadish, K.M. Smith, and R. Guilard, Editors. 2016, World Scientific Publishing Company. p. 105-200.

30. Imahori, H., Y. Mori, and Y. Matano, *Nanostructured artificial photosynthesis*. Journal of Photochemistry and Photobiology C: Photochemistry Reviews, 2003. **4**(1): p. 51-83.
31. Forneli, A., et al., *The role of para-alkyl substituents on meso-phenyl porphyrin sensitised TiO_2 solar cells: control of the e_{TiO2}/electrolyte+ recombination reaction*. Journal of Materials Chemistry, 2008. **18**(14): p. 1652-1658.
32. Deshpande, R., *A New Approach to the Benzoporphyrins: Towards Dye Sensitized Solar Cells*. 2010, Miami University.
33. Liang, G., et al., *Using enzymatic reactions to enhance the photodynamic therapy effect of porphyrin dityrosine phosphates*. Chemical Communications, 2006(48): p. 5021-5023.
34. Gu, H., et al., *Synthesis and cellular uptake of porphyrin decorated iron oxide nanoparticles-a potential candidate for bimodal anticancer therapy*. Chemical Communications, 2005(34): p. 4270-4272.
35. Huang, Z., *A Review of Progress in Clinical Photodynamic Therapy*. Technology in Cancer Research & Treatment, 2005. **4**(3): p. 283-293.
36. Obata, M., et al., *In Vitro Heavy-Atom Effect of Palladium(II) and Platinum(II) Complexes of Pyrrolidine-Fused Chlorin in Photodynamic Therapy*. Journal of Medicinal Chemistry, 2009. **52**(9): p. 2747-2753.
37. Allison, R.R., et al., *Photosensitizers in clinical PDT*. Photodiagnosis and Photodynamic Therapy, 2004. **1**(1): p. 27-42.
38. Sun, R.W.-Y. and C.-M. Che, *The anti-cancer properties of gold(III) compounds with dianionic porphyrin and tetradentate ligands*. Coordination Chemistry Reviews, 2009. **253**(11): p. 1682-1691.
39. Nam, W., *High-Valent Iron(IV)–Oxo Complexes of Heme and Non-Heme Ligands in Oxygenation Reactions*. Accounts of Chemical Research, 2007. **40**(7): p. 522-531.
40. Groves, J.T., et al., *High-valent iron-porphyrin complexes related to peroxidase and cytochrome P-450*. Journal of the American Chemical Society, 1981. **103**(10): p. 2884-2886.
41. Tani, F., et al., *Synthetic models for the active site of cytochrome P450*. Coordination Chemistry Reviews, 2002. **226**(1): p. 219-226.
42. Meunier, B., *Metalloporphyrins as versatile catalysts for oxidation reactions and oxidative DNA cleavage*. Chemical Reviews, 1992. **92**(6): p. 1411-1456.
43. Mansuy, D., *Activation of alkanes : the biomimetic approach*. Coordination Chemistry Reviews, 1993. **125**(1-2): p. 129-141.

44. Dolphin, D., T.G. Traylor, and L.Y. Xie, *Polyhaloporphyrins: Unusual Ligands for Metals and Metal-Catalyzed Oxidations.* Accounts of Chemical Research, 1997. **30**(6): p. 251-259.

45. Liu, H.-Y., et al., *A Bulky Bis-Pocket Manganese(V)−Oxo Corrole Complex: Observation of Oxygen Atom Transfer between Triply Bonded $Mn^{V}\equiv O$ and Alkene.* Journal of the American Chemical Society, 2009. **131**(36): p. 12890-12891.

46. Gorin, C.F., et al., *Interfacial Electric Field Effects on a Carbene Reaction Catalyzed by Rh Porphyrins.* Journal of the American Chemical Society, 2013. **135**(30): p. 11257-11265.

47. Wielopolski, M., et al., *Blending Through-Space and Through-Bond π–π-Coupling in [2,2']-Paracyclophane-oligophenylenevinylene Molecular Wires.* Journal of the American Chemical Society, 2013. **135**(28): p. 10372-10381.

48. Ying, X., et al., *Second order nonlinear optical properties of corroles: experimental and theoretical investigations.* Journal of Porphyrins and Phthalocyanines, 2012. **16**(12): p. 1276-1284.

49. Robertson, N., *Optimizing Dyes for Dye-Sensitized Solar Cells.* Angewandte Chemie International Edition, 2006. **45**(15): p. 2338-2345.

50. Imahori, H., T. Umeyama, and S. Ito, *Large π-Aromatic Molecules as Potential Sensitizers for Highly Efficient Dye-Sensitized Solar Cells.* Accounts of Chemical Research, 2009. **42**(11): p. 1809-1818.

51. Shi, Y., et al., *Synthesis and photophysical studies of self-assembled multicomponent supramolecular coordination prisms bearing porphyrin faces.* Proceedings of the National Academy of Sciences, 2014. **111**(26): p. 9390-9395.

52. Kay, A. and M. Graetzel, *Artificial photosynthesis. 1. Photosensitization of titania solar cells with chlorophyll derivatives and related natural porphyrins.* The Journal of Physical Chemistry, 1993. **97**(23): p. 6272-6277.

53. Bessho, T., et al., *Highly Efficient Mesoscopic Dye-Sensitized Solar Cells Based on Donor–Acceptor-Substituted Porphyrins.* Angewandte Chemie International Edition, 2010. **49**(37): p. 6646-6649.

54. Senge, M.O., et al., *Nonlinear Optical Properties of Porphyrins.* Advanced Materials, 2007. **19**(19): p. 2737-2774.

55. Di Carlo, G., et al., *Influence of Porphyrinic Structure on Electron Transfer Processes at the Electrolyte/Dye/TiO_2 Interface in PSSCs: a Comparison between meso Push–Pull and β-Pyrrolic Architectures.* ACS Applied Materials & Interfaces, 2014. **6**(18): p. 15841-15852.

56. Urbani, M., et al., *Meso-Substituted Porphyrins for Dye-Sensitized Solar Cells.* Chemical Reviews, 2014. **114**(24): p. 12330-12396.
57. Higashino, T. and H. Imahori, *Porphyrins as excellent dyes for dye-sensitized solar cells: recent developments and insights.* Dalton Transactions, 2015. **44**(2): p. 448-463.
58. Verbiest, T., et al., *Second-order nonlinear optical materials: recent advances in chromophore design.* Journal of Materials Chemistry, 1997. **7**(11): p. 2175-2189.
59. de la Torre, G., et al., *Phthalocyanines and related compounds:organic targets for nonlinear optical applications.* Journal of Materials Chemistry, 1998. **8**(8): p. 1671-1683.
60. Chaudhary, A., A. Srinivasan, and T.K. Chandrashekar, *Nonlinear Optical Properties of Porphyrins and Expanded Porphyrins*, in *Handbook of Porphyrin Science*, K.M. Kadish, K.M. Smith, and R. Guilard, Editors. 2014, World Scientific: Singapore. p. 271-336.
61. Li, L.-L. and E.W.-G. Diau, *Porphyrin-sensitized solar cells.* Chemical Society Reviews, 2013. **42**(1): p. 291-304.
62. Suslick, K.S., et al., *Push-pull porphyrins as nonlinear optical materials.* Journal of the American Chemical Society, 1992. **114**(17): p. 6928-6930.
63. Hayashi, H., et al., *Triarylamine-Substituted Imidazole- and Quinoxaline-Fused Push–Pull Porphyrins for Dye-Sensitized Solar Cells.* ChemSusChem, 2013. **6**(3): p. 508-517.
64. Chen, J., et al., *Design and synthesis of β-multi-substituted push-pull porphyrins.* RSC Advances, 2013. **3**(22): p. 8227-8231.
65. Di Carlo, G., et al., *Tetraaryl Zn^{II} Porphyrinates Substituted at β-Pyrrolic Positions as Sensitizers in Dye-Sensitized Solar Cells: A Comparison with meso-Disubstituted Push–Pull Zn^{II} Porphyrinates.* Chemistry – A European Journal, 2013. **19**(32): p. 10723-10740.
66. Ishida, M., et al., *β-(Ethynylbenzoic acid)-substituted push-pull porphyrins: DSSC dyes prepared by a direct palladium-catalyzed alkynylation reaction.* Chemical Communications, 2013. **49**(80): p. 9164-9166.
67. Ishida, M., et al., *β-Functionalized Push–Pull Porphyrin Sensitizers in Dye-Sensitized Solar Cells: Effect of π-Conjugated Spacers.* ChemSusChem, 2015. **8**(17): p. 2967-2977.
68. Ishida, M., et al., *Donor-Substituted β-Functionalized Porphyrin Dyes on Hierarchically Structured Mesoporous TiO_2 Spheres. Highly Efficient Dye-Sensitized Solar Cells.* The Journal of Physical Chemistry C, 2011. **115**(39): p. 19343-19354.
69. Lindsey, J.S., *Synthesis of meso-Substituted Porphyrins*, in *The Porphyrin Hanbook*, K.M. Kadish, K.M. Smith, and R. Guilard, Editors. 2000, Academic Press: San Diego. p. 45-118.

70. Lindsey, J.S., *Synthetic Routes to meso-Patterned Porphyrins.* Accounts of Chemical Research, 2010. **43**(2): p. 300-311.
71. Wallace, D.M., et al., *Rational tetraarylporphyrin syntheses: tetraarylporphyrins from the MacDonald route.* The Journal of Organic Chemistry, 1993. **58**(25): p. 7245-7257.
72. Lee, C.-H., et al., *Synthetic approaches to regioisomerically pure porphyrins bearing four different meso-substituents.* Tetrahedron, 1995. **51**(43): p. 11645-11672.
73. Senge, M.O., *Stirring the porphyrin alphabet soup-functionalization reactions for porphyrins.* Chemical Communications, 2011. **47**(7): p. 1943-1960.
74. Hyslop, A.G., et al., *Suzuki Porphyrins: New Synthons for the Fabrication of Porphyrin-Containing Supramolecular Assemblies.* Journal of the American Chemical Society, 1998. **120**(48): p. 12676-12677.
75. Senge, M.O., *Nucleophilic Substitution as a Tool for the Synthesis of Unsymmetrical Porphyrins.* Accounts of Chemical Research, 2005. **38**(9): p. 733-743.
76. Sergeeva, N.N., M.O. Senge, and A.A. Ryan, *Organometallic C-C Coupling Reactions for Porphyrins*, in *Handbook of Porphyrin Science*, K.M. Kadish, K.M. Smith, and R. Guilard, Editors. 2010, World Scientific: Singapore. p. 325-366.
77. Meindl, A., et al., *Comparative Synthetic Strategies for the Generation of 5,10- and 5,15-Substituted Push-Pull Porphyrins.* Eur. J. Org. Chem., 2017. **2017**(25): p. 3565–3583.
78. *NREL, Best Research-Cell Efficiencies* www.nrel.gov/pv/assets/images/efficiency-chart.png [cited 2017].
79. Khenkin, M.V., et al., *Reconsidering figures of merit for performance and stability of perovskite photovoltaics.* Energy & Environmental Science, 2018. **11**(4): p. 739-743.
80. Bakr, O.M. and O.F. Mohammed, *Powering up perovskite photoresponse.* Science, 2017. **355**(6331): p. 1260-1261.
81. Shi, D., et al., *Low trap-state density and long carrier diffusion in organolead trihalide perovskite single crystals.* Science, 2015. **347**(6221): p. 519-522.
82. Stranks, S.D., et al., *Electron-Hole Diffusion Lengths Exceeding 1 Micrometer in an Organometal Trihalide Perovskite Absorber.* Science, 2013. **342**(6156): p. 341-344.
83. Li, X., et al., *A vacuum flash–assisted solution process for high-efficiency large-area perovskite solar cells.* Science, 2016. **353**(6294): p. 58-62.
84. de Quilettes, D.W., et al., *Impact of microstructure on local carrier lifetime in perovskite solar cells.* Science, 2015. **348**(6235): p. 683-686.

85. Roy, J.N. and D.N. Bose, *Photovoltaic Science and Technology*. 2017, Cambridge: Cambridge University Press.
86. Ku, Z., et al., *Full Printable Processed Mesoscopic $CH_3NH_3PbI_3/TiO_2$ Heterojunction Solar Cells with Carbon Counter Electrode*. Scientific Reports, 2013. **3**: p. 3132.
87. Kojima, A., et al., *Organometal Halide Perovskites as Visible-Light Sensitizers for Photovoltaic Cells*. Journal of the American Chemical Society, 2009. **131**(17): p. 6050-6051.
88. Savenije, T.J., et al., *Thermally Activated Exciton Dissociation and Recombination Control the Carrier Dynamics in Organometal Halide Perovskite*. The Journal of Physical Chemistry Letters, 2014. **5**(13): p. 2189-2194.
89. Dong, Q., et al., *Electron-hole diffusion lengths > 175 μm in solution-grown $CH_3NH_3PbI_3$ single crystals*. Science, 2015. **347**(6225): p. 967-970.
90. Wetzelaer, G.-J.A.H., et al., *Trap-Assisted Non-Radiative Recombination in Organic–Inorganic Perovskite Solar Cells*. Advanced Materials, 2015. **27**(11): p. 1837-1841.
91. Lee, M.M., et al., *Efficient Hybrid Solar Cells Based on Meso-Superstructured Organometal Halide Perovskites*. Science, 2012. **338**(6107): p. 643-647.
92. Kim, H.-S., et al., *Lead Iodide Perovskite Sensitized All-Solid-State Submicron Thin Film Mesoscopic Solar Cell with Efficiency Exceeding 9%*. Scientific Reports, 2012. **2**: p. 591.
93. Burschka, J., et al., *Sequential deposition as a route to high-performance perovskite-sensitized solar cells*. Nature, 2013. **499**: p. 316-319.
94. Chen, Q., et al., *Planar Heterojunction Perovskite Solar Cells via Vapor-Assisted Solution Process*. Journal of the American Chemical Society, 2014. **136**(2): p. 622-625.
95. Rudmann, D., et al., *Efficiency enhancement of $Cu(In,Ga)Se_2$ solar cells due to post-deposition Na incorporation*. Applied Physics Letters, 2004. **84**(7): p. 1129-1131.
96. Durose, K., P.R. Edwards, and D.P. Halliday, *Materials aspects of CdTe/CdS solar cells*. Journal of Crystal Growth, 1999. **197**(3): p. 733-742.
97. Chen, Y., et al., *Large-area perovskite solar cells - a review of recent progress and issues*. RSC Advances, 2018. **8**(19): p. 10489-10508.
98. Saran, R., V. Stolojan, and R.J. Curry, *Ultrahigh Performance C_{60} Nanorod Large Area Flexible Photoconductor Devices via Ultralow Organic and Inorganic Photodoping*. Scientific Reports, 2014. **4**: p. 5041.
99. Zakharian, T.Y., et al., *A Fullerene−Paclitaxel Chemotherapeutic: Synthesis, Characterization, and Study of Biological Activity in Tissue Culture*. Journal of the American Chemical Society, 2005. **127**(36): p. 12508-12509.

100. Brown, P. and P.V. Kamat, *Quantum Dot Solar Cells. Electrophoretic Deposition of CdSe−C_{60} Composite Films and Capture of Photogenerated Electrons with nC_{60} Cluster Shell.* Journal of the American Chemical Society, 2008. **130**(28): p. 8890-8891.
101. Kroto, H.W., et al., *C_{60}: Buckminsterfullerene.* Nature, 1985. **318**: p. 162-163.
102. Iijima, S., *Helical microtubules of graphitic carbon.* Nature, 1991. **354**: p. 56-58.
103. Novoselov, K.S., et al., *Electric Field Effect in Atomically Thin Carbon Films.* Science, 2004. **306**(5696): p. 666-669.
104. Wallace, P.R., *The Band Theory of Graphite.* Physical Review, 1947. **71**(9): p. 622-634.
105. Shrestha, L.K., *Self-Assembled Fullerene Nanostructures at Liquid Interface.* Austin J Nanomed Nanotechnol., 2014. **2**(5): p. 1031.
106. Suzuki, A., K. Nishimura, and T. Oku, *Effects of Germanium Tetrabromide Addition to Zinc Tetraphenyl Porphyrin / Fullerene Bulk Heterojunction Solar Cells.* Electronics, 2014. **3**(1): p. 112-121.
107. Smerdon, J.A., et al., *Chiral "Pinwheel" Heterojunctions Self-Assembled from C_{60} and Pentacene.* ACS Nano, 2013. **7**(4): p. 3086-3094.
108. Oku, T., et al., *Fabrication and characterization of fullerene/porphyrin bulk heterojunction solar cells.* Journal of Physics and Chemistry of Solids, 2010. **71**(4): p. 551-555.
109. Armaroli, N., et al., *Charge-transfer interactions in face-to-face porphyrin-fullerene systems: solvent-dependent luminescence in the infrared spectral region.* Chem. Eur. J., 2000. **6**(9): p. 1629-1645.
110. Yoshimoto, S. and K. Itaya, *Advances in supramolecularly assembled nanostructures of fullerenes and porphyrins at surfaces.* Journal of Porphyrins and Phthalocyanines, 2007. **11**(05): p. 313-333.
111. Garg, V., et al., *Conformationally Constrained Macrocyclic Diporphyrin−Fullerene Artificial Photosynthetic Reaction Center.* Journal of the American Chemical Society, 2011. **133**(9): p. 2944-2954.
112. Al-Subi, A.H., et al., *Effect of Anion Ligation on Electron Transfer of Double-Linked Zinc Porphyrin−Fullerene Dyad.* The Journal of Physical Chemistry A, 2011. **115**(15): p. 3263-3271.
113. Cárdenas-Jirón, G., et al., *Excited States of Light-Harvesting Systems Based on Fullerene/Graphene Oxide and Porphyrin/Smaragdyrin.* The Journal of Physical Chemistry C, 2017. **121**(9): p. 4859-4872.

114. Saegusa, Y., et al., *Supramolecular Interaction of Fullerenes with a Curved π-Surface of a Monomeric Quadruply Ring-Fused Porphyrin.* Chemistry – A European Journal, 2015. **21**(14): p. 5302-5306.

115. Da Ros, T., et al., *A noncovalently linked, dynamic fullerene porphyrin dyad. Efficient formation of long-lived charge separated states through complex dissociation.* Chemical Communications, 1999(7): p. 635-636.

116. Da Ros, T., et al., *Efficient Charge Separation in Porphyrin-Fullerene-Ligand Complexes.* Chemistry – A European Journal, 2001. **7**(4): p. 816-827.

117. D'Souza, F., et al., *Structural studies of a non-covalently linked porphyrin-fullerene dyad.* Chemical Communications, 2001(3): p. 267-268.

118. D'Souza, F., et al., *Self-Assembled Porphyrin−C_{60} and Porphycene−C_{60} Complexes via Metal Axial Coordination.* Inorganic Chemistry, 1999. **38**(9): p. 2157-2160.

119. Wilson, S.R., et al., *Synthesis and photophysics of a linear non-covalently linked porphyrin-fullerene dyad.* Chemical Communications, 2003(2): p. 226-227.

120. Tagmatarchis, N. and M. Prato, *Organofullerene Materials*, in *Fullerene-Based Materials: Structures and Properties*, K. Prassides, Editor. 2004, Springer Berlin Heidelberg: Berlin, Heidelberg. p. 1-39.

121. Sugunan, S.K., et al., *Photophysics of Untethered ZnTPP–Fullerene Complexes in Solution.* The Journal of Physical Chemistry A, 2011. **115**(44): p. 12217-12227.

122. Stangel, C., et al., *Case Study for Artificial Photosynthesis: Noncovalent Interactions between C_{60}-Dipyridyl and Zinc Porphyrin Dimer.* The Journal of Physical Chemistry C, 2017. **121**(9): p. 4850-4858.

123. Geim, A.K., *Graphene: Status and Prospects.* Science, 2009. **324**(5934): p. 1530-1534.

124. Yang, M., Y. Hou, and N.A. Kotov, *Graphene-based multilayers: Critical evaluation of materials assembly techniques.* Nano Today, 2012. **7**(5): p. 430-447.

125. Liu, Z., et al., *Improving photovoltaic properties by incorporating both SPFGraphene and functionalized multiwalled carbon nanotubes.* Solar Energy Materials and Solar Cells, 2010. **94**(12): p. 2148-2153.

126. Stankovich, S., et al., *Graphene-based composite materials.* Nature, 2006. **442**: p. 282-286.

127. Jo, G., et al., *Large-scale patterned multi-layer graphene films as transparent conducting electrodes for GaN light-emitting diodes.* Nanotechnology, 2010. **21**: p. 175201.

128. Zhu, Y., et al., *Graphene and Graphene Oxide: Synthesis, Properties, and Applications.* Advanced Materials, 2010. **22**(35): p. 3906-3924.

129. Jo, G., et al., *Tuning of a graphene-electrode work function to enhance the efficiency of organic bulk heterojunction photovoltaic cells with an inverted structure.* Applied Physics Letters, 2010. **97**(21): p. 213301-213303.

130. Dubacheva, G.V., C.-K. Liang, and D.M. Bassani, *Functional monolayers from carbon nanostructures – fullerenes, carbon nanotubes, and graphene – as novel materials for solar energy conversion.* Coordination Chemistry Reviews, 2012. **256**(21): p. 2628-2639.

131. Iwan, A. and A. Chuchmała, *Perspectives of applied graphene: Polymer solar cells.* Progress in Polymer Science, 2012. **37**(12): p. 1805-1828.

132. Du, X., et al., *Approaching ballistic transport in suspended graphene.* Nature Nanotechnology, 2008. **3**: p. 491-495.

133. Lotya, M., et al., *Liquid Phase Production of Graphene by Exfoliation of Graphite in Surfactant/Water Solutions.* Journal of the American Chemical Society, 2009. **131**(10): p. 3611-3620.

134. Kim, K.S., et al., *Large-scale pattern growth of graphene films for stretchable transparent electrodes.* Nature, 2009. **457**: p. 706-710.

135. Li, X., et al., *Large-Area Synthesis of High-Quality and Uniform Graphene Films on Copper Foils.* Science, 2009. **324**(5932): p. 1312-1314.

136. Bae, S., et al., *Roll-to-roll production of 30-inch graphene films for transparent electrodes.* Nature Nanotechnology, 2010. **5**: p. 574-578.

137. Park, S. and R.S. Ruoff, *Chemical methods for the production of graphenes.* Nature Nanotechnology, 2009. **4**: p. 217-224.

138. Shao, Y., et al., *Facile and controllable electrochemical reduction of graphene oxide and its applications.* Journal of Materials Chemistry, 2010. **20**(4): p. 743-748.

139. Zhu, Y., et al., *Exfoliation of Graphite Oxide in Propylene Carbonate and Thermal Reduction of the Resulting Graphene Oxide Platelets.* ACS Nano, 2010. **4**(2): p. 1227-1233.

140. Williams, G., B. Seger, and P.V. Kamat, *TiO_2-Graphene Nanocomposites. UV-Assisted Photocatalytic Reduction of Graphene Oxide.* ACS Nano, 2008. **2**(7): p. 1487-1491.

141. Wang, Y., et al., *Graphene and graphene oxide: biofunctionalization and applications in biotechnology.* Trends in Biotechnology, 2011. **29**(5): p. 205-212.

142. Kiessling, D., et al., *Novel nanographene/porphyrin hybrids - preparation, characterization, and application in solar energy conversion schemes.* Chemical Science, 2013. **4**(8): p. 3085-3098.

143. Georgakilas, V., et al., *Functionalization of Graphene: Covalent and Non-Covalent Approaches, Derivatives and Applications*. Chemical Reviews, 2012. **112**(11): p. 6156-6214.

144. Malig, J., N. Jux, and D.M. Guldi, *Toward Multifunctional Wet Chemically Functionalized Graphene—Integration of Oligomeric, Molecular, and Particulate Building Blocks that Reveal Photoactivity and Redox Activity*. Accounts of Chemical Research, 2013. **46**(1): p. 53-64.

145. Hirsch, A., J.M. Englert, and F. Hauke, *Wet Chemical Functionalization of Graphene*. Accounts of Chemical Research, 2013. **46**(1): p. 87-96.

146. Zhang, X., et al., *One-Pot Functionalization of Graphene with Porphyrin through Cycloaddition Reactions*. Chemistry – A European Journal, 2011. **17**(32): p. 8957-8964.

147. Aly, S.M., et al., *Ultrafast electron injection at the cationic porphyrin-graphene interface assisted by molecular flattening*. Chemical Communications, 2014. **50**(72): p. 10452-10455.

148. Masih, D., et al., *Real-time observation of ultrafast electron injection at graphene-Zn porphyrin interfaces*. Physical Chemistry Chemical Physics, 2015. **17**(14): p. 9015-9019.

149. Parida, M.R., et al., *To What Extent Can Charge Localization Influence Electron Injection Efficiency at Graphene–Porphyrin Interfaces?*. Phys. Chem. Chem. Phys., 2015. **17**: p. 14513-14517.

150. Aly, S.M., C.E.C. Jr., and P.D. Harvey, *Photophysics and Photochemistry of Metal-Containing Polymers*. Introduction to Photophysics and Photochemistry. Vol. 10. 2010, Canada: John Wiley & Sons, Inc., Hoboken, New Jersey.

151. Jaffe, H.H. and A.L. Miller, *The fates of electronic excitation energy*. Journal of Chemical Education, 1966. **43**(9): p. 469.

152. Universitat Basel. *Fluorescence and Phosphorescence. March 27, 2006. 15 pp web tutorial.* https://fp.physik.unibas.ch/documents/Fluorescence_and_Phosphorescence%20(2).pdf. [01/04/2015].

153. Priestley, E.B. and A. Haug, *Phosphorescence Spectrum of Pure Crystalline Naphthalene*. The Journal of Chemical Physics, 1968. **49**(2): p. 622-629.

154. Tress, W., *Organic Solar Cells - Theory, Experiment, and Device Simulation*. Vol. 208. 2014: Springer.

155. Beer, A., *Determination of the absorption of red light in colored liquids*. Annalen der Physik und Chemie, 1852. **86**: p. 78-88.

156. Thermo Spectronic. *Basic UV-Vis Theory, Concepts and Applications.* http://www.uni-salzburg.at/fileadmin/oracle_file_imports/359201.PDF. [01/07/2018]; [1-28].
157. Valeur, B., *Molecular Fluorescence: Principles and Applications*. 2001: Wiley-VCH.
158. Noomnarm, U. and R.M. Clegg, *Fluorescence lifetimes: fundamentals and interpretations.* Photosynthesis Research, 2009. **101**(2): p. 181-194.
159. Atkins, P.W. and J. de Paula, *Kurzlehrbuch Physikalische Chemie*. 2006, Weinheim: Wiley-VCH.
160. Atkins, P.W., *Physical Chemistry*. 1994: Oxford University Press.
161. Michl, J. and V. Bonacic-Koutechy, *Electronic Aspects of Organic Photochemistry*. 1990: Wiley Interscience, New York.
162. Universitat Zurich. *Physikalisch-chemisches Praktikum I. Fluorescence Quenching - 2017*. https://www.chem.uzh.ch/dam/jcr:6031b93c-7a09-48e7-8544-3081dab39c11/FluorescenceQuenching_HS17.pdf. [01/07/2018].
163. Strobl, M., *Covalent Coupling of Fluorescent pH Indicators in a Polymeric Matrix*. 2013, University of Technology, Graz.
164. Hutter, L., *On covalent immobilization of Indicators in Optical sensors*. 2012, Graz University of Technology.
165. Marcus, R.A. and N. Sutin, *Electron transfers in chemistry and biology.* Biochimica et Biophysica Acta (BBA) - Reviews on Bioenergetics, 1985. **811**: p. 265-322.
166. Williams, R.M., *Fullerenes as Electron Accepting Components in Supramolecular and Covalently Linked Electron Transfer Systems*. 1996, University of Amsterdam.
167. Escudero, D., *Revising Intramolecular Photoinduced Electron Transfer (PET) from First-Principles.* Accounts of Chemical Research, 2016. **49**(9): p. 1816-1824.
168. Blankenship, R.E., *Molecular Mechanisms of Photosynthesis*. 2002: Blackwell Science Ltd.
169. Gray, H.B. and J.R. Winkler, *Electron Transfer in Proteins.* Annu Rev. Biochem., 1996. **65**: p. 537-561.
170. Weber, S., *Light-driven enzymatic catalysis of DNA repair: a review of recent biophysical studies on photolyase.* Biochimica et Biophysica Acta, 2005. **1707**: p. 1-23.
171. Noy, D., C.C. Moser, and P.L. Dutton, *Design and engineering of photosynthetic light-harvesting and electron transfer using length, time, and energy scales.* Biochimica et Biophysica Acta, 2006. **1757**(2): p. 90-105.

172. Chan, W.-L., J.R. Tritsch, and X.-Y. Zhu, *Harvesting Singlet Fission for Solar Energy Conversion: One- versus Two-Electron Transfer from the Quantum Mechanical Superposition.* J. Am. Chem. Soc., 2012. **134**: p. 18295−18302.

173. Krishnamurthy, S. and P.V. Kamat, *CdSe–Graphene Oxide Light-Harvesting Assembly: Size-Dependent Electron Transfer and Light Energy Conversion Aspects.* ChemPhysChem 2014. **15**: p. 2129 – 2135

174. Mattay, J., *Photoinduced Electron Transfer IV*. Vol. 163. 1992: Springer Verlag: Berlin.

175. Balzani, V., *Electron Transfer in Chemistry*. 2001: WILEY-VCH

176. Petty, M.C., *Molecular Electronics From Principles to Practice*. 2007: John Wiley & Sons Ltd.

177. Marcus, R.A., *Electron Transfer Reactions in Chemistry: Theory and Experiment (Nobel Lecture)*. Angewandte Chemie International Edition in English, 1993. **32**(8): p. 1111-1121.

178. Closs, G.L. and J.R. Miller, *Intramolecular Long-Distance Electron Transfer in Organic Molecules*. Science, 1988. **240**(4851): p. 440-447.

179. Weller, A., *Photoinduced Electron Transfer in Solution: Exciplex and Radical Ion Pair Formation Free Enthalpies and their Solvent Dependence*, in *Zeitschrift für Physikalische Chemie*. 1982. p. 93-98.

180. Williams, R.M. and S.E. Braslavsky, *Triggering of Photomovement − Molecular Basis. In Photomovement*. Comprehensive Series in Photosciences, ed. D.-P. Häder and M. Lebert, Eds. Vol. 1. 2001, The Netherlands: Elsevier Science B.V. 15-50.

181. Orzeł, Ł., et al., *New trends in the application of laser flash photolysis – case studies.* Journal of Coordination Chemistry, 2010. **63**(14-16): p. 2695-2714.

182. Miura, T., et al., *Rational Design Principle for Modulating Fluorescence Properties of Fluorescein-Based Probes by Photoinduced Electron Transfer.* Journal of the American Chemical Society, 2003. **125**(28): p. 8666-8671.

183. Fukuzumi, S., K. Ohkubo, and T. Suenobu, *Long-Lived Charge Separation and Applications in Artificial Photosynthesis.* Accounts of Chemical Research, 2014. **47**(5): p. 1455-1464.

184. Vlček, A., et al., *Electron-Transfer Acceleration Investigated by Time Resolved Infrared Spectroscopy.* Accounts of Chemical Research, 2015. **48**(3): p. 868-876.

185. Delor, M., et al., *Toward control of electron transfer in donor-acceptor molecules by bond-specific infrared excitation.* Science, 2014. **346**(6216): p. 1492-1495.

186. Batat, P., et al., *Dynamics of ion-regulated photoinduced electron transfer in BODIPY-BAPTA conjugates*. Photochemical & Photobiological Sciences, 2012. **11**(11): p. 1666-1674.

187. Ceroni, P. and V. Balzani, *Photoinduced Energy and Electron Transfer Processes*. The Exploration of Supramolecular Systems and Nanostructures by Photochemical Techniques, ed. P. Ceroni. Vol. 78. 2012: Springer, Dordrecht.

188. Vengris, M. *Introduction to time-resolved spectroscopy. With applications in biophysics and physical chemistry*. http://web.vu.lt/ff/m.vengris/images/TR_spectroscopy02.pdf. [02/01/2018].

189. Norrish, R.G.W. and G. Porter, *Chemical Reactions Produced by Very High Light Intensities*. Nature, 1949. **164**: p. 658-658.

190. Porter, G., *Flash Photolysis and Spectroscopy a New Method for the Study of Free Radical Reactions*. Proceedings of the Royal Society of London Series a-Mathematical and Physical Sciences, 1950. **200**: p. 284-308.

191. Norrish, R.G.W., *Some Fast Reactions in Gases Studied by Flash Photolysis and Kinetic Spectroscopy. In Spectroscopy of the Excited State*, ed. B. Di Bartolo, D. Pacheco, and V. Goldberg. 1976: Springer US. 117-160.

192. Zewail, A.H., *Femtochemistry: Atomic-Scale Dynamics of the Chemical Bond Using Ultrafast Lasers (Nobel Lecture)*. Angewandte Chemie International Edition, 2000. **39**(15): p. 2586-2631.

193. Lourenço, M.A., et al., *Efficient silicon light emitting diodes made by dislocation engineering*. Physica E: Low-dimensional Systems and Nanostructures, 2003. **16**(3): p. 376-381.

194. HORIBA-Scientific;. *Macro Photoluminescence and Electroluminescence. Lifetime Measurements in PV Material Characterization*. http://www.horiba.com/fileadmin/uploads/Scientific/Documents/OSD/OSD-AppNote-Macro_Photo_and_Electroluminescence.pdf. [04/01/2018].

195. CAPPA;. *Time-Resolved Photoluminescence*. http://www.cappa.ie/advanced-research/techniques/time-resolved-photoluminescence/. [04/01/2018].

196. Takahashi, A., et al. *New femtosecond streak camera with temporal resolution of 180 fs*. in *OE/LASE '94*. 1994. SPIE.

197. Selinsky, R.S., et al., *Quantum dot nanoscale heterostructures for solar energy conversion*. Chemical Society Reviews, 2013. **42**(7): p. 2963-2985.

198. Aly, S.M., et al., *Ultrafast Photoinduced Electron Transfer in a π-Conjugated Oligomer/Porphyrin Complex*. J. Phys. Chem. Lett., 2014. **5**: p. 3386−3390.

199. Mohammed, O.F., et al., *Excited-State Intramolecular Hydrogen Transfer (ESIHT) of 1,8-Dihydroxy-9,10-anthraquinone (DHAQ) Characterized by Ultrafast Electronic and Vibrational Spectroscopy and Computational Modeling.* The Journal of Physical Chemistry A, 2014. **118**(17): p. 3090-3099.

200. Alsulami, Q.A., *Ultrafast Photoinduced Electron Transfer in Bimolecular Donor-Acceptor Systems*. 2016, King Abdullah University of Science and Technology (KAUST).

201. Berera, R., R. van Grondelle, and J.T.M. Kennis, *Ultrafast transient absorption spectroscopy: principles and application to photosynthetic systems.* Photosynthesis Research, 2009. **101**(2): p. 105-118.

202. Alsulami, Q.A., et al., *Ultrafast Excited-State Dynamics of Diketopyrrolopyrrole (DPP)-Based Materials: Static versus Diffusion-Controlled Electron Transfer Process.* The Journal of Physical Chemistry C, 2015. **119**(28): p. 15919-15925.

203. Ohkita, H., et al., *Transient Absorption Spectroscopy for Polymer Solar Cells.* IEEE Journal of Selected Topics in Quantum Electronics, 2016. **22**(1): p. 100-111.

204. Ahn, N., et al., *Highly Reproducible Perovskite Solar Cells with Average Efficiency of 18.3% and Best Efficiency of 19.7% Fabricated via Lewis Base Adduct of Lead(II) Iodide.* J. Am. Chem. Soc., 2015. **137**: p. 8696−8699.

205. Sun, J., et al., *Generation of Multiple Excitons in Ag_2S Quantum Dots: Single High-Energy versus Multiple-Photon Excitation.* J. Phys. Chem. Lett., 2014. **5**: p. 659−665.

206. Begum, R., et al., *Engineering Interfacial Charge Transfer in CsPbBr3 Perovskite Nanocrystals by Heterovalent Doping.* Journal of the American Chemical Society, 2017. **139**(2): p. 731-737.

207. Murali, B., et al., *The Surface of Hybrid Perovskite Crystals: A Boon or Bane.* ACS Energy Letters, 2017. **2**(4): p. 846-856.

208. Ahmed, G.H., et al., *Pyridine-Induced Dimensionality Change in Hybrid Perovskite Nanocrystals.* Chemistry of Materials, 2017. **29**(10): p. 4393-4400.

209. Sarmah, S.P., et al., *Double Charged Surface Layers in Lead Halide Perovskite Crystals.* Nano Letters, 2017. **17**(3): p. 2021-2027.

210. Hamamatsu. *Universal streak camera C10910 series* https://www.hamamatsu.com/resources/pdf/sys/SHSS0016E_C10910s.pdf. [08/07/2018].

211. Lu, J., et al., *Novel porphyrin-preparation, characterization, and applications in solar energy conversion.* Physical Chemistry Chemical Physics, 2016. **18**(9): p. 6885-6892.

212. Kuimova, M.K., et al., *Photophysical properties and intracellular imaging of water-soluble porphyrin dimers for two-photon excited photodynamic therapy.* Organic & Biomolecular Chemistry, 2009. **7**(5): p. 889-896.

213. Arunkumar, C., et al., *Fluorinated meso-tetraaryl Pt(ii)-porphyrins: structure, photophysical, electrochemical, and phosphorescent oxygen sensing studies.* New Journal of Chemistry, 2017. **41**(12): p. 4908-4917.

214. Dong, Q., et al., *Porphyrin-based metallopolymers: synthesis, characterization and pyrolytic study for the generation of magnetic metal nanoparticles.* Journal of Materials Chemistry C, 2016. **4**(22): p. 5010-5018.

215. Maximiano, R.V., et al., *Excited-state absorption investigation of a cationic porphyrin derivative.* Journal of Photochemistry and Photobiology A: Chemistry, 2010. **214**(2): p. 115-120.

216. *The Porphyrin Handbook*, ed. K.M. Kadish, K.M. Smith, and R. Guilard. 2000, San Diego, CA: Academic Press.

217. Chen, J., et al., *Push-pull porphyrins with different anchoring group orientations for fully printable monolithic dye-sensitized solar cells with mesoscopic carbon counter electrodes.* New Journal of Chemistry, 2015. **39**(7): p. 5231-5239.

218. Lin, C.-Y., et al., *Design and Characterization of Novel Porphyrins with Oligo(phenylethylnyl) Links of Varied Length for Dye-Sensitized Solar Cells: Synthesis and Optical, Electrochemical, and Photovoltaic Investigation.* The Journal of Physical Chemistry C, 2009. **113**(2): p. 755-764.

219. Yella, A., et al., *Porphyrin-Sensitized Solar Cells with Cobalt (II/III)–Based Redox Electrolyte Exceed 12 Percent Efficiency.* Science, 2011. **334**(6056): p. 629-634.

220. Yella, A., et al., *Molecular Engineering of Push–Pull Porphyrin Dyes for Highly Efficient Dye-Sensitized Solar Cells: The Role of Benzene Spacers.* Angewandte Chemie International Edition, 2014. **53**(11): p. 2973-2977.

221. Wang, C.-L., et al., *Highly efficient porphyrin-sensitized solar cells with enhanced light harvesting ability beyond 800 nm and efficiency exceeding 10%.* Energy & Environmental Science, 2014. **7**(4): p. 1392-1396.

222. Hill, J.P., *Molecular Engineering Combined with Cosensitization Leads to Record Photovoltaic Efficiency for Non-ruthenium Solar Cells.* Angewandte Chemie International Edition, 2016. **55**(9): p. 2976-2978.

223. Obraztsov, I., W. Kunter, and F. D'Souza, *Metalloporphyrins in Solar Energy Conversion.* Electrochemistry of N4 Macrocylic Metal Complexes, ed. J.H. Zagal and F. Bedioui. Vol. 1. 2016, Switzerland: Springer. 171–262.

224. Grätzel, M., *Dye-sensitized solar cells.* Journal of Photochemistry and Photobiology C: Photochemistry Reviews, 2003. **4**(2): p. 145-153.

225. Bessho, T., et al., *Highly Efficient Mesoscopic Dye-Sensitized Solar Cells Based on Donor–Acceptor-Substituted Porphyrins.* Angewandte Chemie, 2010. **122**(37): p. 6796-6799.

226. Kurotobi, K., et al., *Highly Asymmetrical Porphyrins with Enhanced Push–Pull Character for Dye-Sensitized Solar Cells.* Chemistry – A European Journal, 2013. **19**(50): p. 17075-17081.

227. Higashino, T., et al., *Effects of Bulky Substituents of Push–Pull Porphyrins on Photovoltaic Properties of Dye-Sensitized Solar Cells.* ACS Applied Materials & Interfaces, 2016. **8**(24): p. 15379-15390.

228. Higashino, T., et al., *Synthesis of Push-Pull Type Porphyrin with Two Electron-Donating and Two Electron-Withdrawing Groups and Its Application to Dye-Sensitized Solar Cell.* J. Porphyrins Phthalocyanines, 2014. **18**: p. 1-10.

229. Sampaio, R.N., et al., *Investigation of Ground- and Excited-State Photophysical Properties of 5,10,15,20-Tetra(4-pyridyl)-21H,23H-porphyrin with Ruthenium Outlying Complexes.* The Journal of Physical Chemistry A, 2012. **116**(1): p. 18-26.

230. Alarousu, E., et al., *Ultralong Radiative States in Hybrid Perovskite Crystals: Compositions for Submillimeter Diffusion Lengths.* The Journal of Physical Chemistry Letters, 2017. **8**(18): p. 4386-4390.

231. Zhumekenov, A.A., et al., *Formamidinium Lead Halide Perovskite Crystals with Unprecedented Long Carrier Dynamics and Diffusion Length.* ACS Energy Letters, 2016. **1**(1): p. 32-37.

232. *National Renewable Energy Laboratory (NREL). Best Research-Cell Efficiencies. http://www.nrel.gov/ncpv/images/efficiency_chart.jpg. (accessed January 1, 2016).*

233. Subbaiyan, N.K., C.A. Wijesinghe, and F. D'Souza, *Supramolecular Solar Cells: Surface Modification of Nanocrytalline TiO_2 with Coordinating Ligands To Immobilize Sensitizers and Dyads via Metal−Ligand Coordination for Enhanced Photocurrent Generation.* Journal of the American Chemical Society, 2009. **131**(41): p. 14646-14647.

234. Wang, J.C., I.A. Murphy, and K. Hanson, *Modulating Electron Transfer Dynamics at Dye–Semiconductor Interfaces via Self-Assembled Bilayers.* The Journal of Physical Chemistry C, 2015. **119**(7): p. 3502-3508.

235. Buchalska, M., et al., *Photoinduced hole injection in semiconductor-coordination compound systems.* Coordination Chemistry Reviews, 2013. **257**(3): p. 767-775.

236. Bignozzi, C.A., R. Argazzi, and C.J. Kleverlaan, *Molecular and supramolecular sensitization of nanocrystalline wide band-gap semiconductors with mononuclear and polynuclear metal complexes.* Chemical Society Reviews, 2000. **29**(2): p. 87-96.

237. Xu, J., et al., *A Strong Donor–Acceptor System Based on a Metal Chalcogenide Cluster and Porphyrin.* Inorganic Chemistry, 2017. **56**(14): p. 8036-8044.

238. Xue, L.-J., et al., *An ionic charge-transfer dyad prepared cost-effectively from a tetrathiafulvalene carboxylate anion and a TMPyP cation.* Physical Chemistry Chemical Physics, 2016. **18**(4): p. 2940-2948.

239. Albinsson, B. and H.L. Anderson, *Multiporphyrin Arrays: Fundamentals and Applications*, ed. D. Kim. 2012: Pan Stanford.

240. Kadish, K.M., K.M. Smith, and R. Guilard, *The Porphyrin Handbook: Inorganic, organometallic and coordination chemistry*. 2000, USA: Academic Press.

241. Yadav, P., et al., *β -Trisubstituted "Push–Pull" Porphyrins – Synthesis and Structural, Photophysical, and Electrochemical Redox Properties.* Eur. J. Inorg. Chem., 2017(26): p. 3269–3274.

242. Lin, V.S., S.G. DiMagno, and M.J. Therien, *Highly conjugated, acetylenyl bridged porphyrins: new models for light-harvesting antenna systems.* Science, 1994. **264**(5162): p. 1105-1111.

243. *The Porphyrin Handbook Volume 8 Electron Transfer*, ed. K.M. Kadish, K.M. Smith, and R. Guilard. 2000, USA: Academic Press.

244. Orbelli Biroli, A., et al., *A Multitechnique Physicochemical Investigation of Various Factors Controlling the Photoaction Spectra and of Some Aspects of the Electron Transfer for a Series of Push–Pull Zn(II) Porphyrins Acting as Dyes in DSSCs.* The Journal of Physical Chemistry C, 2011. **115**(46): p. 23170-23182.

245. Ubbink, R. and E.G. Mik, *Probing Tissue Oxygenation by Delayed Fluorescence of Protoporphyrin IX*, in *Quenched-phosphorescence Detection of Molecular Oxygen: Applications in Life Sciences*, D.B. Papkovsky and R.I. Dmitriev, Editors. 2018, The Royal Society of Chemistry. p. 259-277.

246. Lee, S., et al., *Electron Transfer from Triplet State of TIPS-Pentacene Generated by Singlet Fission Processes to $CH_3NH_3PbI_3$ Perovskite.* The Journal of Physical Chemistry Letters, 2017. **8**(4): p. 884-888.

247. Chang, J., et al., *Enhancing the photovoltaic performance of planar heterojunction perovskite solar cells by doping the perovskite layer with alkali metal ions.* Journal of Materials Chemistry A, 2016. **4**: p. 16546–16552.

248. Zhang, W., et al., *Enhanced optoelectronic quality of perovskite thin films with hypophosphorous acid for planar heterojunction solar cells.* Nature Communications, 2015. **6**(10030): p. 1-9.

249. Wang, L., et al., *Femtosecond Time-Resolved Transient Absorption Spectroscopy of $CH_3NH_3PbI_3$ Perovskite Films: Evidence for Passivation Effect of PbI_2.* Journal of the American Chemical Society, 2014. **136**(35): p. 12205-12208.

250. Kira, A., et al., *Supramolecular Donor−Acceptor Heterojunctions by Vectorial Stepwise Assembly of Porphyrins and Coordination-Bonded Fullerene Arrays for Photocurrent Generation.* Journal of the American Chemical Society, 2009. **131**(9): p. 3198-3200.

251. Wang, M., et al., *High efficiency solid-state sensitized heterojunction photovoltaic device.* Nano Today, 2010. **5**(3): p. 169-174.

252. Deibel, C., T. Strobel, and V. Dyakonov, *Role of the Charge Transfer State in Organic Donor–Acceptor Solar Cells.* Advanced Materials, 2010. **22**(37): p. 4097-4111.

253. Sykora, M., et al., *Photoinduced Charge Transfer between CdSe Nanocrystal Quantum Dots and Ru−Polypyridine Complexes.* Journal of the American Chemical Society, 2006. **128**(31): p. 9984-9985.

254. Tseng, T.-C., et al., *Charge-transfer-induced structural rearrangements at both sides of organic/metal interfaces.* Nature Chemistry, 2010. **2**: p. 374-379.

255. Braun, T., A.P. Schubert, and R.N. Kostoff, *Growth and Trends of Fullerene Research as Reflected in Its Journal Literature.* Chemical Reviews, 2000. **100**(1): p. 23-38.

256. Bettencourt, L.M.A., et al., *Population modeling of the emergence and development of scientific fields.* Scientometrics, 2008. **75**(3): p. 495-518.

257. *Advances in Carbon Nanomaterials: Science and Applications*, ed. N. Tagmatarchis. 2012, Singapore: Pan Stanford Publishing Pte. Ltd.

258. Georgakilas, V., et al., *Broad Family of Carbon Nanoallotropes: Classification, Chemistry, and Applications of Fullerenes, Carbon Dots, Nanotubes, Graphene, Nanodiamonds, and Combined Superstructures.* Chemical Reviews, 2015. **115**(11): p. 4744-4822.

259. Vilatela, J.J. and D. Eder, *Nanocarbon Composites and Hybrids in Sustainability: A Review.* ChemSusChem, 2012. **5**(3): p. 456-478.

260. Yan, L., et al., *Low-toxic and safe nanomaterials by surface-chemical design, carbon nanotubes, fullerenes, metallofullerenes, and graphenes.* Nanoscale, 2011. **3**(2): p. 362-382.

261. Titirici, M.-M., et al., *Sustainable carbon materials.* Chemical Society Reviews, 2015. **44**(1): p. 250-290.

262. Jariwala, D., et al., *Carbon nanomaterials for electronics, optoelectronics, photovoltaics, and sensing.* Chemical Society Reviews, 2013. **42**(7): p. 2824-2860.

263. Zhong, Q., et al., *Fused Porphyrin–Single-Walled Carbon Nanotube Hybrids: Efficient Formation and Photophysical Characterization.* ACS Nano, 2013. **7**(4): p. 3466-3475.

264. K. C, C.B., et al., *Ultrafast charge separation in supramolecular tetrapyrrole-graphene hybrids.* Chemical Communications, 2012. **48**(97): p. 11859-11861.

265. Otsuki, J., *STM studies on porphyrins.* Coordination Chemistry Reviews, 2010. **254**(19): p. 2311-2341.

266. Bernal, M.M. and E.M. Pérez, *One-Pot Exfoliation of Graphite and Synthesis of Nanographene/Dimesitylporphyrin Hybrids.* International Journal of Molecular Sciences, 2015. **16**(5): p. 10704-10714.

267. Guo, Z., et al., *Covalently porphyrin-functionalized single-walled carbon nanotubes: a novel photoactive and optical limiting donor-acceptor nanohybrid.* Journal of Materials Chemistry, 2006. **16**(29): p. 3021-3030.

268. Xu, H., et al., *Controlling the morphology and optoelectronic properties of graphene hybrid materials by porphyrin interactions.* Chemical Communications, 2014. **50**(64): p. 8951-8954.

269. Malig, J., et al., *Direct exfoliation of graphite with a porphyrin - creating functionalizable nanographene hybrids.* Chemical Communications, 2012. **48**(70): p. 8745-8747.

270. Camus, J.-M., et al., *Design of Triads for Probing the Direct Through Space Energy Transfers in Closely Spaced Assemblies.* Inorganic Chemistry, 2013. **52**(15): p. 8360-8368.

271. Yang, E., et al., *Probing Electronic Communication for Efficient Light-Harvesting Functionality: Dyads Containing a Common Perylene and a Porphyrin, Chlorin, or Bacteriochlorin.* The Journal of Physical Chemistry B, 2014. **118**(6): p. 1630-1647.

272. Brennan, B.J., et al., *Hole Mobility in Porphyrin- and Porphyrin-Fullerene Electropolymers.* The Journal of Physical Chemistry B, 2013. **117**(1): p. 426-432.

273. Wojcik, A. and P.V. Kamat, *Reduced Graphene Oxide and Porphyrin. An Interactive Affair in 2-D.* ACS Nano, 2010. **4**(11): p. 6697-6706.

274. Geng, J. and H.-T. Jung, *Porphyrin Functionalized Graphene Sheets in Aqueous Suspensions: From the Preparation of Graphene Sheets to Highly Conductive Graphene Films.* The Journal of Physical Chemistry C, 2010. **114**(18): p. 8227-8234.

275. Xu, Y., et al., *Flexible Graphene Films via the Filtration of Water-Soluble Noncovalent Functionalized Graphene Sheets.* Journal of the American Chemical Society, 2008. **130**(18): p. 5856-5857.

276. Ye, T.-x., et al., *Spectroscopic characterization of tetracationic porphyrins and their noncovalent functionalization with graphene.* Spectrochimica Acta Part A: Molecular and Biomolecular Spectroscopy, 2012. **86**: p. 467-471.

277. Wang, A., et al., *A 1,3-Dipolar Cycloaddition Protocol to Porphyrin-functionalized Reduced Graphene Oxide with a Push–pull Motif.* Nano Research, 2015. **8**(3): p. 870-886.

278. Lakowicz, J.R., *Principles of Fluorescence Spectroscopy*. 3rd edn ed. 2006, Singapore: Springer Science + Business Media, LLC,.

279. Keizer, J., *Nonlinear Fluorescence Quenching and the Origin of Positive Curvature in Stern-Volmer Plots.* J. Am. Chem. Soc., 1983. **105**: p. 1494-1498.

280. Zhong, D. and A.H. Zewail, *Femtosecond Dynamics of Dative Bonding: Concepts of Reversible and Dissociative Electron Transfer Reactions.* Proc. Natl. Acad. Sci. USA, 1999. **96**: p. 2602–2607.

281. Zhong, D., T.M. Bernhardt, and A.H. Zewail, *Femtosecond Real-Time Probing of Reactions. 24. Time, Velocity, and Orientation Mapping of the Dynamics of Dative Bonding in Bimolecular Electron Transfer Reactions.* J. Phys. Chem. A, 1999. **103**: p. 10093-10117.

282. Lang, B., et al., *Broadband Ultraviolet-Visible Transient Absorption Spectroscopy in the Nanosecond to Microsecond Time Domain with sub-nanosecond Time Resolution.* Rev Sci Instrum., 2013. **84**(7): p. 073107.

283. Banerji, N., et al., *Exciton Formation, Relaxation, and Decay in PCDTBT.* J. Am. Chem. Soc., 2010. **132**(49): p. 17459–17470.

284. Enescu, M., et al., *Femtosecond relaxation processes from upper excited states of tetrakis(N-methyl-4-pyridyl)porphyrins studied by transient absorption spectroscopy.* Physical Chemistry Chemical Physics, 2002. **4**(24): p. 6092-6099.

285. Keane, P.M., et al., *Photophysical studies of CdTe quantum dots in the presence of a zinc cationic porphyrin.* Dalton Transactions, 2012. **41**(42): p. 13159-13166.

286. Kalyanasundaram, K. and M. Neumann-Spallart, *Photophysical and redox properties of water-soluble porphyrins in aqueous media.* The Journal of Physical Chemistry, 1982. **86**(26): p. 5163-5169.

287. Aly, S.M., et al., *Molecular-structure Control of Ultrafast Electron Injection at Cationic Porphyrin–CdTe Quantum Dot Interfaces.* The Journal of Physical Chemistry Letters, 2015. **6**(5): p. 791-795.

288. Solomon, G.C., *Charge Transfer: Interfering with Interference.* Nature Chemistry, 2015. **7**: p. 621–622.

289. Simon, J.D., *Ultrafast Dynamics of Chemical Systems*. 1994, Netherlands: Kluwer Academic Publishers.

290. El-Khouly, M.E., et al., *Intermolecular and supramolecular photoinduced electron transfer processes of fullerene–porphyrin/phthalocyanine systems.* Journal of Photochemistry and Photobiology C: Photochemistry Reviews, 2004. **5**(1): p. 79-104.

291. Green, M.A., A. Ho-Baillie, and H.J. Snaith, *The emergence of perovskite solar cells.* Nature Photonics, 2014. **8**: p. 506-514.